THE UNIVERSITY OF CHICAGO

THE ROLE OF DEVELOPMENTAL CONSTRAINTS IN SHAPING MACROEVOLUTIONARY PATTERNS OF DISPARITY IN AGNOSTINE ARTHROPODS

A DISSERTATION SUBMITTED TO

THE FACULTY OF THE DIVISION OF THE PHYSICAL SCIENCES

IN CANDIDACY FOR THE DEGREE OF

DOCTOR OF PHILOSOPHY

DEPARTMENT OF GEOPHYSICAL SCIENCES

BY

RHIANNON JUNE LAVINE

CHICAGO, ILLINOIS

MARCH 2020

TABLE OF CONTENTS

LIST OF TABLES

LIST OF FIGURES

ACKNOWLEDGEMENTS

The process of completing a dissertation is not a light undertaking and without the support of several people, I may not have been successful. The names that appear in this section represent only a fraction of those who have had a profound impact on me over the years—this list is far from exhaustive. First and foremost, I would like express endless gratitude to my advisor, Mark Webster, for his guidance, patience, and compassion throughout everything that life has thrown at me during this process. The meticulous attention to detail and rigorous methods of scientific inquiry that I have come to know as standard practice have prepared me for a career characterized by high quality work. I extend thanks to my committee members, Michael Foote and David Jablonski, for their support and guidance. I regret not taking advantage of their open doors as much as I could have. I would also like to thank my lab mate, Matt Witte, for being my "trilobite twin", accountabili-buddy, and the wall for me to bounce off crazy research ideas. Much of the paleo group, past and present, have earned my gratitude as well for listening to me throughout the years. In particular, I am grateful for Graham Slater and Susan Kidwell always taking the time to work through problems with me. There is far too much to admire about the residents of the second floor of Hinds, and I am truly humbled to have had the opportunity to be among their ranks.

Beyond the brick walls of Hinds, I have immense support from friends and family. I owe much of my current trajectory to my undergraduate advisor, Rex Hanger, who saw potential in an art major in a Bauhaus shirt who took his earth history course for fun. I can trace my initial spark of interest in paleontology directly to Rex's mentorship. I thank Julien Kimmig and L.J. Krumenacker (a.k.a. "Team Unfunk the Spence") for looking out for me in the field and helping me keep busy with a project that will keep me grounded in the Cambrian. My longtime friends,

Nica Wilson, Rachel Svetlik, Nicole Zwifelhofer, and Sara Metcalf have served as my tether to the world outside of academia, for which I am grateful. The staff and volunteers at PAWS Chicago gave me a space to do something good and impactful when I needed to take a break. I am in awe of their devotion to the mission of a no-kill Chicago and I will always be honored to be included in the PAWS family. My own family, including my in-laws Diana and Alan Zimmer, have never shied away from letting me know how proud of me they are —such simple affirmations were indispensable through this trial and even though I may not have shown it, I was appreciative. Finally, it is not possible to truly express the extent of my gratitude to my husband, Brooks Zimmer. He is my partner, my love, my vice on the ice, my home.

I dedicate the spirit of my work to the memory of my dad, Jeffrey LaVine. I am and always will be my father's daughter.

INTRODUCTION

Phenotypic integration and the associated concept of modularity have long been of interest to those seeking to understand the mechanics of evolvability. Since the publication of the pioneering work by Olson and Miller (1958), the study of patterns of trait covariances has itself evolved into a dynamic field that has its roots in ideas that were beginning to take shape as early as the nineteenth century. Cuvier's "principle of correlated parts" was such an observation, despite his flawed claim that the seeming perfection in the fit of each component to form a functional whole opposed evolutionary thought as change in one part would cause the entire system to fail (Mayr, 1982). The idea that organisms are composed of correlated sets of parts lends itself well to methods that utilize morphometric data. Because of this, the study of integration and modularity can be extended into the fossil record, where oftentimes the only data available is that relating to morphology. The fossil record also allows for an investigation of these patterns in deep time, which is an opportunity that is not afforded by the study of extant organisms alone.

Of particular interest is the idea that integration serves as a constraint on clade disparification. The term "constraint" is intuitively thought of as a limiting factor in terms of evolvability, but it is perhaps better thought of as a factor that can channel evolutionary variation in certain directions (e.g. Gould 1989, 2002). In order to investigate how phenotypic integration affects patterns of morphological diversity, one must first determine if it does, in fact, serve as a long-term constraint. The following studies aim to address that question within the framework of a fossil study system.

Chapter 1 presents the phylogenetic framework for the clade of interest, the Agnostina. These small, blind arthropods have been notoriously problematic in terms of systematic

classification given their conserved morphologies and their lack of reliable diagnostic characters. Using Bayesian inference and parismony methods, trees were recovered that support much of the existing rank-based systematics of the Agnostina, Chapter 2 explores the structure of integration in a middle Cambrian agnostine, *Pentagnostus brighamensis* (Resser, 1939) using geometric morphometric methods. The aim of this study was achieved by determining that the integration structure of this agnostine is driven by direct interactions among developmental pathways, thus potentially serving as a long-term constraint. The final chapter, Chapter 3, compares the structure and level of integration in the sister taxon of *P. brighamensis*, *Pentagnostus segmenta* (Robison, 1964), as determined by the phylogenetic analyses in Chapter 1. A phylomorphospace was constructed, highlighting Peronopsidae Westergård, 1936 as a morphologically conserved clade relative to other agnostines. It was shown that while Peronopsidae is conserved, that conservation is not due to phenotypic integration acting as a constraint on the clade as the degree of integration in both species is weak and the structure of integration is not conserved among sister taxa.

These studies are among the first to investigate the role of integration as a constraint on morphological evolution in fossil arthropods, and they are the first to do so focusing on agnostine arthropods. These are still the first steps into a rich field of study that remains disproportionately represented by research into extant organisms. The methods used herein are part of a toolkit allowing one to interrogate the fossil record and take advantage of its opportunities to pursue questions that can only be answered by observing patterns through time.

CHAPTER ONE:

TOWARD A PHYLOGENETIC FRAMEWORK FOR THE AGNOSTINA SALTER, 1864

ABSTRACT—Agnostina, the subclade of Agnostida that excludes Eodiscina, is a moderately diverse group of arthropods comprising at least twelve recognized families and over 100 genera that span the early Cambrian to the Late Ordovician. The conserved morphologies of these enigmatic organisms and their lack of reliable diagnostic characters result in an unstable systematic classification and difficulty in testing phylogenetic relationships among ingroup taxa. Herein, 51 taxa from 11 agnostine families, including some taxa that currently lack formal classification, were coded for a set of 79 characters and subjected to phylogenetic analysis using Bayesian and parsimony-based methods. While Bayesian methods are becoming commonplace in paleontological investigations, there is a dearth of studies that use these probabilistic methods to explore relationships in entirely extinct clades. The fossilized birth-death (FBD) process allows for a tree model that incorporates aspects of paleontological data such as estimates of speciation and extinction dynamics, preservation, and sampling as a set of priors. In this study, a maximum clade credibility (MCC) tree is proposed for Agnostina that shows strong crownward posterior support, reaffirming the majority of currently recognized taxonomic families with the notable exception of Pseudagnostidae. This tree provides a framework for continuing research into developmental constraints that may have shaped macroevolutionary patterns in this conservative group of arthropods.

INTRODUCTION—The small, blind, and historically perplexing arthropods of the Agnostina Salter, 1864 are found globally in rocks of Cambrian Series 2 to the Upper Ordovician. The

group is moderately diverse, traditionally comprised of two superfamilies, at least twelve recognized families, and over 100 genera (Naimark and Pegel, 2017). Seemingly cosmopolitan distributions and geologically rapid species turnover make these animals ideal for use as index fossils in regional and global biostratigraphic subdivisions during their peak abundance in the middle and upper Cambrian. Due to their biostratigraphic significance, agnostines continue to receive modern systematic study (e.g., Zhou and Zhen, 2008; Westrop and Eoff, 2012; Westrop and Landing, 2016; Naimark and Pegel, 2017). However, despite more than 150 years of intense collecting and systematic study, there is a dearth of studies exploring the phylogenetic affinities within Agnostina such that ingroup composition and relationships remain uncertain.

One phylogenetic study (Cotton and Fortey, 2005) has explored Agnostida Salter, 1864, the group that has historically included both the Agnostina and the Eodiscina Kobayashi, 1939; and only two cladistic analyses have focused solely on ingroup relationships of Agnostina and both were restricted to the Family Ptychagnostidae Kobayashi, 1939 (Westrop et al., 1996; Laurie, 2008). There have been no cladistic studies that investigate agnostine relationships above the family level. This may be, in part, due to difficulty in identifying a sufficient number of characters for any such analysis. The conserved morphologies of these organisms and their lack of reliable diagnostic characters have resulted in an unstable systematic classification and difficulty in testing phylogenetic relationships between ingroup taxa. Agnostine families are defined by broad and variable characteristics (Appendix A, Table A.2 and Table A.3). For example, the Agnostidae M'Coy, 1849 has been defined as being "en grande tenue to effaced, with nondeliquiate to deliquiate border furrows," (Shergold et al., 1990, p. 32; Shergold and Laurie, 1997, p. 339), illustrating the highly variable nature of traits that supposedly unite the family. The lack of adequate diagnostic criteria results in taxon classification being potentially

based on plesiomorphic and/or homoplastic traits, which would create uninformative "wastebasket taxa" that can distort metrics and analyses used in macroevolutionary studies, such as biasing diversity indices toward more commonly-occurring groups and dampening patterns or origination and extinction (Plotnick and Wagner, 2006).

In recent years, there has been an influx of paleontological studies using probabilistic approaches to reconstruct phylogenetic relationships with character matrices comprised of solely morphological data (e.g., Wagner, 1999; Pyron, 2011; Ronquist et al., 2012; Slater, 2013, 2015; Lee et al., 2014; Wright and Stigall, 2013; Wright, 2017; Wright et al., 2017). Of those, there have been few to use these methods to estimate phylogenies using only extinct taxa (Lee et al., 2014, Wright, 2017; Moysiuk and Caron, 2019b). It has been demonstrated that Bayesian inference using the Mk model performs better than any other method in recovering the true topology in simulations (Wright and Hillis, 2014) and it has been suggested that should be the default method when inferring phylogenetic relationships with morphological data (Puttick et al., 2017). However, the implementation of a single method remains controversial and it is advised that careful consideration should be given to the methods and models used (Brown et al., 2017).

The present paper conducts a phylogenetic analysis of the Agnostina in order to determine ingroup relationships and assess support for the systematic ranks currently recognized within the group. Bayesian methods are used to estimate the phylogeny, and cladograms are generated with parsimony methods in order to assess topological agreement between approaches. This study is the most expansive investigation of agnostine relationships, and utilizes the largest character matrix of agnostine-specific traits, to date. The phylogenetic reconstruction provided here offers a framework for research involving the Agnostina including, but certainly not limited

to, continuing studies on developmental constraints that may shape macroevolutionary patterns in this biostratigraphically important group of arthropods.

BACKGROUND—

Broader Affinities of Agnostina—Historically, the Agnostina has been considered to be nested within a paraphyletic Eodiscina, together comprising the trilobite Order Agnostida (Shergold and Laurie, 1997; Fortey and Theron, 1994; Jell, 1997; Cotton and Fortey 2005). To test this hypothesis, Cotton and Fortey (2005) subjected a matrix of 123 characters 82 taxa (of which 79 were eodiscines and three were agnostines) to cladistic analysis. Consistent with historical classification, the resulting cladogram showed agnostines nested deeply within Eodiscina. However, that topology can be questioned due to an outgroup selection consisting of the eodiscine family Tsunyidiscidae, which makes the implicit assumption of a monophyletic Agnostina + Eodiscina, and debatable homology of eodiscine traits in agnostine arthropods.

A close relationship between agnostines and eodiscines, and the systematic placement of agnostines within Trilobita Walch, 1771 have been questioned with the discovery of non-trilobite-like appendages in a juvenile *Agnostus pisiformis* (Linnaeus, 1747) (Müller and Walossek, 1987) and, more recently, in adults of *Peronopsis* Hawle and Corda, 1847 and *Ptychagnostus* Jaekel, 1909 agnostine species (Moysiuk and Caron, 2019a). Recent studies contend that Eodiscina is a clade within the class Trilobita (Adrain, 2011; Paterson and Edgecombe, 2019) while agnostines are excluded, either as a sister clade to polymerid trilobites (Moysiuk and Caron, 2019a) or as part of a mandibulate stem group with marrellomorphs and other taxa (Legg et al., 2013). This structure would follow the taxonomic hierarchy suggested by Rasetti (1945, 1948, 1952) and recognized by Moore (1959), Rushton (1966), Öpik (1961, 1967,

1975, 1979), Robison (1984), and Shergold et al. (1990) in which Agnostida includes only the Suborder Agnostina and is exclusive of Eodiscina. Any reference herein to the Order Agnostida refers to the group of agnostines, as defined in the Suborder Agnostina, excluding Eodiscina.

Traditional Ingroups Within Agnostina—The families included in the present analyses reflect the most stable diagnoses currently in use. Naimark and Pegel (2017) presented the most current agnostine classification, revising much of the previous accepted standard (e.g. Shergold and Laurie, 1997). The set of families that comprise ingroup Agnostina in this study is based on the revisions of Naimark and Pegel (2017), with the exclusion of Phalacromidae Hawle and Corda, 1847 (Table 1.1). This provides a systematic framework that will be tested by the phylogenetic analyses conducted herein.

Table 1.1—The 11 taxonomic families (+uncertain/unassigned) and constituent taxa of Agnostina included in phylogenetic analyses. Family assignments follow Naimark and Pegel (2017) and are tested using phylogenetic approaches herein. Asterisks denote type species.

Agnostidae M'Coy, 1849	**Ammagnostidae Öpik, 1967**	**Clavagnostidae Howell, 1937**
**Agnostus pisiformis* (Wahlenberg, 1818)	*Ammagnostus simplexiformis* (Rozova, 1964)	*Aspidagnostus laevis* Palmer, 1962
**Barrandagnostus barrandei* Ivshin, 1960	*Hadragnostus modestus* (Lochman, 1944)	**Clavagnostus repandus* (Westergård, 1930)
**Eurudagnostus grandis* Lermontova 1951	**Kormagnostus simplex* Resser, 1938	*Utagnostus songae* Peng & Robison, 2000
Homagnostus captiosus (Lazarenko, 1966)	**Proagnostus bulbus* Butts, 1926	**Utagnostus trispinulus* Robison, 1964
**Lotagnostus americanus* (Billings, 1860)		
Condylopygidae Raymond, 1913	**Diplagnostidae Whitehouse, 1936**	**Doryagnostidae Shergold, Laurie, & Sun, 1990**
Condylopyge carinata (Westergård, 1936)	**Diplagnostus planicauda* (Angelin, 1851)	**Doryagnostus incertus* (Brögger, 1878)
**Condylopyge rex* (Barrande, 1846)	**Linguagnostus kjerulfi* (Brögger, 1878)	*Doryagnostus wasatchensis* Robison, 1978
**Pleuroctenium granulatum* (Barrande, 1846)	**Oedorhachis typicalis* Resser , 1938	**Euagnostus opimus* Whitehouse, 1936
	**Oidalagnostus trispinifer* Westergård, 1946	**Rhodotypiscus nasonis* Öpik, 1979
Metagnostidae Jaekel, 1909	**Peronopsidae Westergård, 1836**	**Pseudagnostidae Whitehouse, 1936**
**Arthrorhachis tarda* (Barrande, 1846)	**Eoagnostus roddyi* Resser and Howell, 1938	**Acmarhachis typicalis* Resser, 1938
**Corrugatagnostus morea* (Salter, 1864)	*Itagnostus interstricta* (White, 1874)	*Agnostotes orientalis* (Kobayashi, 1935)
**Galbagnostus galba* (Whittington, 1965)	*Pentagnostus brighamensis* (Resser, 1939)	*Neoagnostus bilobus* (Shaw, 1951)
**Geragnostus sidenbladhi* (Linnarsson, 1869)	*Pentagnostus segmenta* (Robison, 1964)	**Sulcatagnostus securiger* (Lake, 1906)
Trinodus elspethi (Raymond, 1925)	**Peronopsis integer* (Beyrich, 1845)	
	Quadragnostus clarus (Pokrovskaya & Egorova, 1982)	
Ptychagnostidae Kobayashi, 1939	**Spinagnostidae Howell, 1935**	**Unassigned**
**Goniagnostus nathorsti* (Brögger, 1878)	**Cotalagnostus lens* (Grönwall, 1902)	**Agnostardis amplinatis* Öpik, 1963
**Lejopyge laevigata* (Dalman, 1828)	*Hypagnostus brevifrons* (Angelin, 1851)	**Glyptagnostus reticulatus* (Angelin, 1851)
Ptychagnostus atavus (Tullberg, 1880)	**Hypagnostus parvifrons* (Linnarsson, 1869)	**Quadrahomagnostus subquadratus* (Chu, 1959)
Ptychagnostus praecurrens (Westergård, 1936)	*Peratagnostus orientalis* (Lazarenko, 1966)	
**Triplagnostus gibbus* (Linnarsson, 1869)		

METHODS—

Taxon Selection and Material Examined—A total of 51 taxa were included in the final analyses. This includes representatives from all but one of the families within Agnostoidea M'Coy, 1849, the superfamily Condylopygoidea Raymond, 1913, and species of uncertain familial affiliation (Table 1.1). Phalacromidae Hawle and Corda, 1847 was excluded because these taxa are typically strongly effaced and lack most diagnostic dorsal features. In order to provide reasonable coverage of agnostine morphotypes, at least three exemplar species were selected from each family.

Morphological data were primarily sourced from type specimens as figured in published literature, supplemented by first-hand examination of specimens and latex replicas of type material housed in the collections of the Institute for Cambrian Studies (ICS), University of Chicago. Published non–type material was also examined to assist in character coding. A table of specimen references can be found in Appendix A (Table A.4).

Character Selection—Each species was coded for 79 morphological characters (Appendix A), of which 38 are cephalic characters and 41 describe the pygidium. Thoracic and ventral characters (such as the hypostome) were excluded as these sclerites are either unknown or not figured for most species.

The set of characters used in this analysis are based on dorsally-expressed cephalic and pygidial traits as observed in dorsal view. Characters relating to the degree of dorsal convexity or the relative height of features were not included, because lateral views of specimens were not always available in the published literature. This is unfortunate, because the three-dimensional

relief of anatomical features is thought to contain phylogenetic information. For example, Laurie (2008) noted the importance of the height of the pygidial axis and degree of convexity as diagnostic traits when exploring the affinities of ingroup Ptychagnostidae, and argued that exclusion of such characters could produce inaccurate results.

Öpik (1967) specified seven major traits identifiable on the external agnostine morphology that aid in broad categorization. Six of the seven have been included in these analyses. The seventh is the articulating device, a structure on the agnostine pygidium that joins the sclerite with the thorax, consisting of the articulating half ring, articulating furrow, and the recess in front of the axial lobe (Öpik, 1963, 1967). Öpik (1967) contended that the articulating device is a reliable diagnostic feature, but it is often neglected due to the paucity of published illustrations that show the structure. The form of the articulating device has not been included as a character in these analyses for that reason.

The majority of characters in the present study relates to pygidial morphology. The pygidium is a character-rich sclerite that shows considerable disparity across agnostine taxa. Combinations of pygidial characters have been used in recent studies to delineate morphogroups that aid in species diagnoses (Naimark, 2012, 2014; Naimark and Pegel, 2017) and it has been shown that pygidial character states often represent synapomorphies (Naimark, 2006, 2007, 2008, 2012). However, agnostine literature is muddied with conflicting terminology, commonly reflecting an author's taxonomic opinion. Terminology employed herein is clarified in the Appendix.

Character Coding—Seventeen traits with continuous variation were included in one version of the matrix and were transformed into discrete, ordered states in a second version (Appendix A,

Table A.1). Characters derived from quantitative data are useful as they increase the number of phylogenetically informative characters in a dataset (Baum, 1988; Chappill, 1989; Stevens, 1991; Thiele, 1993; Rae, 1998). Gap-weighting (Thiele, 1993), in which taxa are assigned states based on range-standardized mean values of a continuous trait, was the method used for discretization of states:

$$state_i = n\text{-}1\ x_i - min(x)/max(x) - min(x) \quad (1.1)$$

...where n is the number of states and x is the continuous variable (Equation 1.1). There are several methods of transforming quantitative data into discrete character states, with no agreement on which is the most appropriate or useful. Gap-weighting was chosen over other discretization methods as it retains information on the distance between states and performs better than several other methods in terms of retrieving the most phylogenetically-informative and variable characters (Garcia-Cruz and Sosa, 2006). More complex methods of discretization, such as Finite Mixture Coding (Strait et al., 1996), were not used given the reliance on either large sample sizes or the assumption of the data conforming to a normal distribution in order to appropriately identify character codes. Gap-weighted states were treated as ordered and additive. Reductive coding (Strong and Lipscomb, 1999) was used to code inapplicable characters.

Stratigraphic Occurrence Data—Tip dates were specified based on stratigraphic occurrence data that were collected from the primary literature for each taxon (Appendix A, Table A.4). Regional biozones and stages were correlated with the 2012 timescales for the Cambrian and Ordovician (Gradstein et al., 2012) and subsequent updates to the International Chronostratigraphic Chart

(Cohen et al., 2013) in order to obtain numerical tip dates that were used in the Bayesian tree search. This method of tip-dating is coarse, with resolution to the lowest international stage boundary for each taxon. In the absence of absolute dates or finely resolved global correlation, this method has been used in previous studies of extinct taxa (Paterson and Edgecombe, 2019).

Bayesian Inference—In paleontological studies, phylogenies are often reconstructed using morphological characters, and using solely morphological characters when there are no extant representatives of the clade of interest. For this reason, the most common options for resolving relationships of groups of extinct taxa have been parsimony methods which can lead to problems in recovering true relationships if rates are heterogenous. To avoid this, molecular phylogeneticists have used methods of tree inference that use probabilistic models of sequence evolution. One such model, the Jukes-Cantor model (1969), was modified for morphological data (Pagel, 1994; Lewis, 2001), which allowed character data from fossil taxa to be coded and used in phylogenetic studies. The Lewis Mk model (Lewis, 2001) applies to a discrete, morphological character having *k* unordered states. Evolution involves changing between these *k* states following a Markov process. The Lewis Mk model of morphological trait evolution as implemented in Bayesian inference has been shown to perform well relative to other phylogenetic methods when encountering some common problems in real data sets, including missing characters and homoplasy (Wright and Hillis, 2014; O'Reilly et al., 2016).

The fully discretized matrix (Appendix A, Table A.5) was loaded into BEAUti 2.5.2 (Bouckaert et al. 2019) for parameterization, then used in a Bayesian tree search conducted using BEAST 2.5.2 (Bouckaert et al. 2019) employing the Mk model (Lewis, 2001) of morphological trait evolution. Characters were subject to default partitioning based on number of states. Bayes

Factors (Kass and Raferty, 1995) were calculated for each of four different clock models, with marginal likelihood estimates generated from path sampling (Table 1.2). In this case, the uncorrelated lognormal relaxed clock was found to be the preferred model and used in the final tree search. This model allows rates to vary independently across branches with values drawn from a lognormal distribution, the variance of which is estimated from the data and for each partition of character states.

Table 1.2— Comparison of clock models using Bayes Factors (Kass and Raferty, 1995). Diagonal contains marginal likelihoods. Values >2 indicate the row model is favored over the column model. The relaxed lognormal clock model is favored over all models with the exception of the relaxed exponential clock; however, the relaxed exponential clock is not favored over the strict clock. Therefore, the relaxed lognormal clock model was chosen over the relaxed exponential clock model.

	Random Local	Strict	Relaxed Exp.	Relaxed Log.
Random Local	-2559.86			
Strict	6.70	-2531.31		
Relaxed Exp.	6.86	1.73	-2528.93	
Relaxed Log.	6.95	2.65	0.66	-2527.54

The tree prior chosen for this analysis is the fossilized birth–death (FBD) model. This model describes the probability of the tree topology and fossils given a set of parameters. It is a stochastic branching model with parameters that describe speciation rate (λ), extinction rate (μ), fossil recovery rate (ψ), and the probability of sampling extant species (ρ) (Stadler, 2010; Heath et al., 2014). Gavryushkina et al. (2014) modified this model in the SA ("Sampled Ancestors") package in BEAST2, allowing a version of FBD to be used as a tree prior with new parameters for Markov Chain Monte Carlo (MCMC) optimization: net diversification rate (λ-μ), turnover (μ/λ), and sampling proportion ($\psi/(\mu + \psi)$). In this analysis, the net diversification prior was set as an Exponential (1), the turnover prior as a Beta(2,1), and sampling proportion as a Beta(2,2) prior following the methodology of previous studies (e.g., Wright, 2017), modified for an extinct

clade. The ρ parameter was excluded because there are no extant representatives of this clade. As recommended by Gavryushkina (personal communication, 2019), the analysis was conditioned on the origin of the clade: the numerical age for the oldest taxon, with a uniform, and thus uninformative, prior. MCMC analyses consisted of independent runs sampling every 2,500 generations for 50 million generations per run with a burn-in of 20%. A total of 100,000 MCMC repetitions were sufficient for convergence, which was assessed by visual confirmation of log-likelihood plots in Tracer v.1.6.0 (Rambaut et al., 2014) and effective sample sizes greater than 300 (effective sample size for all traces is greater than 800). Tree Annotator (Rambaut and Drummond, 2015) was used to generate a maximum clade credibility (MCC) tree. Each clade within the tree was given a score based on its frequency within the sampled posterior trees, and the product of these scores within a tree is its score. The tree with the highest score is the MCC tree—a fully resolved tree that summarizes the posterior distribution of tree topologies.

Parsimony Analyses—For methodological comparison, cladograms were also generated with parsimony methods. A heuristic search in PAUP*4.0a build 164 (Swofford, 2002) was performed to find the most parsimonious cladogram, with branch swapping performed using tree bisection reconnection (TBR) and taxa added by random sequence addition with 100 replicates. TNT version 1.5 (Goloboff and Catalano, 2016) was used to analyze the data matrix consisting of 63 discrete characters and 17 continuous characters. The most parsimonious cladograms were determined using a heuristic search algorithm similar to that of the PAUP* analysis. Branch swapping was done with TBR and taxa added by random sequence addition with 1000 replicates. In both analyses, all characters were weighted equally and, with the exception of gap-weighted

characters, all multistate characters were treated as unordered. Strict consensus trees and consistency indices were computed for each of these methods.

Cladogram polarity was determined by outgroup comparison. Outgroup selection for Agnostina is difficult given the uncertain relationship between agnostines and eodiscines and to the Trilobita as a whole (see above). Moysiuk and Caron (2019a) proposed that in the future a more complete knowledge of artiopodan soft tissue traits and cephalic character polarity may aid in the resolution of these relationships. Such work lies beyond the scope of the present study. Herein, relationships among agnostines must be resolved without reference to non-agnostine outgroups.

Within the Agnostina, Condylopygoidea has been considered to represent a sister taxon to the Agnostoidea (Shergold and Laurie, 1997). However, the present study seeks to assess support for that relationship and so condylopygoids cannot be designated a priori as an agnostoid outgroup. For parsimony analyses in this study (below), *Eoagnostus roddyi* Resser and Howell, 1938 was therefore selected as the outgroup taxon because it is the stratigraphically oldest agnostine.

RESULTS—

Bayesian Inference—The BEAST2 analysis yielded 32,002 trees post burn-in with a total of 26,258 unique clades generated and analyzed. The MCC tree generated has a log clade credibility of -61.387 (Figure 1.1). A strongly-supported basal divergence separates a clade of diplagnostine taxa, *Glyptagnostus reticulatus*, and the pseudagnostid *Agnostotes orientalis* from the remaining agnostine taxa. The strongly cohesive Spinagnostidae forms a clade with a weakly cohesive Peronopsidae, the structure of which is moderately supported. While the node that

unites Peronopsidae as historically defined is weak, the relationships of the constituent taxa are well supported. Similarly, the Clavagnostidae is recovered with a weakly supported node and well supported relationships of component taxa. Condylopygidae (posterior = 0.94) is recovered as a derived sister clade to [Peronopsidae + Spinagnostidae]. Metagnostidae (posterior = 1.00) is similarly strongly-supported as monophyletic and derived. *Neoagnostus bilobus* (usually assigned to Pseudagnostidae) is included in Metagnostidae. The historically problematic family Agnostidae is recovered as paraphyletic, grading up to a monophyletic Doryagnostidae. Within the "Agnostidae" grade, *Barrandagnostus barrandei*, *Homagnostus captiosus*, and *Lotagnostus americanus* form a small clade with support that varies from strong (between *B. barrandei* and *H. captiosus*) to weak at the basal node. Ammagnostidae is monophyletic, containing all taxa traditionally assigned to that family. Ptychagnostidae, as historically defined, is recovered with weak-to-moderate support, excluding *Lejopyge laevigata* which occurs in the spinagnostine clade with strong support (posterior = 0.76). The remaining taxa representative of the traditional Family Pseudagnostidae (*Acmarhachis typicalis*, *Agnostotes orientalis*, and *Sulcatagnostus securiger*) do not coalesce into a single supported clade, nor do they have strong affinities within any other clade.

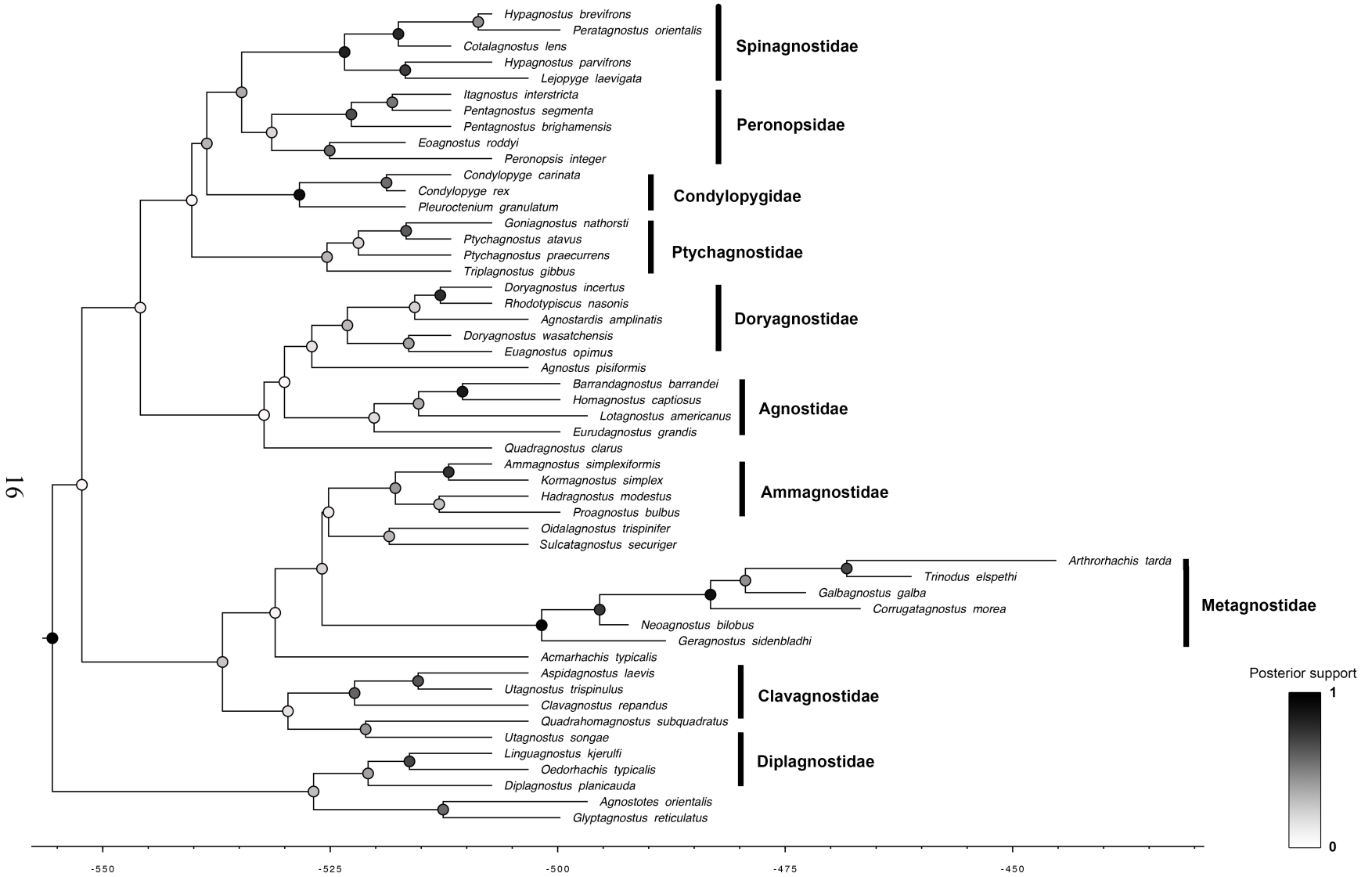

Figure 1.1—Bayesian maximum clade credibility (MCC) tree. Horizontal axis represents time in millions of years. Node symbols indicate posterior support, with darker values indicative of stronger support and lighter values showing weaker support. Black vertical bars indicate traditional familial classification. Posterior values are provided in Figure A.4.

Parsimony Analyses—The PAUP* analysis yielded six most parsimonious trees with a length of 638, CI 0.19, RC 0.10, and RI 0.53. The topology of the strict consensus tree (Figure 1.2) shows several nested clades that mostly reflect current taxonomy and largely agree with the results of the Bayesian analysis. Clades corresponding to the traditional families Ammagnostidae, Clavagnostidae, Metagnostidae, and Spinagnostidae are recovered. The metagnostid clade includes *N. bilobus* as in the MCC tree. Condylopygidae is recovered as a sister clade to Metagnostidae containing all traditionally assigned condylopygoid taxa, and highly derived relative to [Peronopsidae + Spinagnostidae]. The peronopsid outgroup, *E. roddyi*, pulls *Peronopsis integer* and [Peronopsidae + Spinagnostidae] into a clade toward the base of the tree contrary to its derived position in the MCC tree. Most currently recognized families are partially recovered as defined in rank-based systematics, as cohesive groups or with a single taxon on a neighboring branch. Exceptions include *Agnostus pisiformis*, *Euagnostus opimus, Eurudagnostus grandis*, *Oidalagnostus trispinifer*, and *Quadragnostus clarus*. Pseudagnostidae is again not recovered in this analysis.

The TNT analysis using the matrix of discrete and quantitative characters produced 12 optimal trees with a score of 404.43, CI 0.21, RI 0.59, RC: 0.12. The resulting cladogram is shown in Figure 1.3. The within-group topology is similar to that of the PAUP* cladogram, but the between-group relationships are quite different. The traditionally recognized Ammagnostidae, Condylopygidae, and Spinagnostidae are well-supported. Metagnostidae is again recovered as traditionally defined with the inclusion of *N. bilobus*. Doryagnostidae and Ptychagnostidae each contain nearly all taxa that are traditionally assigned to those families; the former losing *E. opimus* to the base of the tree and the latter without *L. laevigata*, which again appears within the Spinagnostidae. The peronopsids occur as a paraphyletic grade toward the

base of the tree. The taxa that were placed well outside of their traditional group assignments in the PAUP* analysis behave similarly in the TNT analysis.

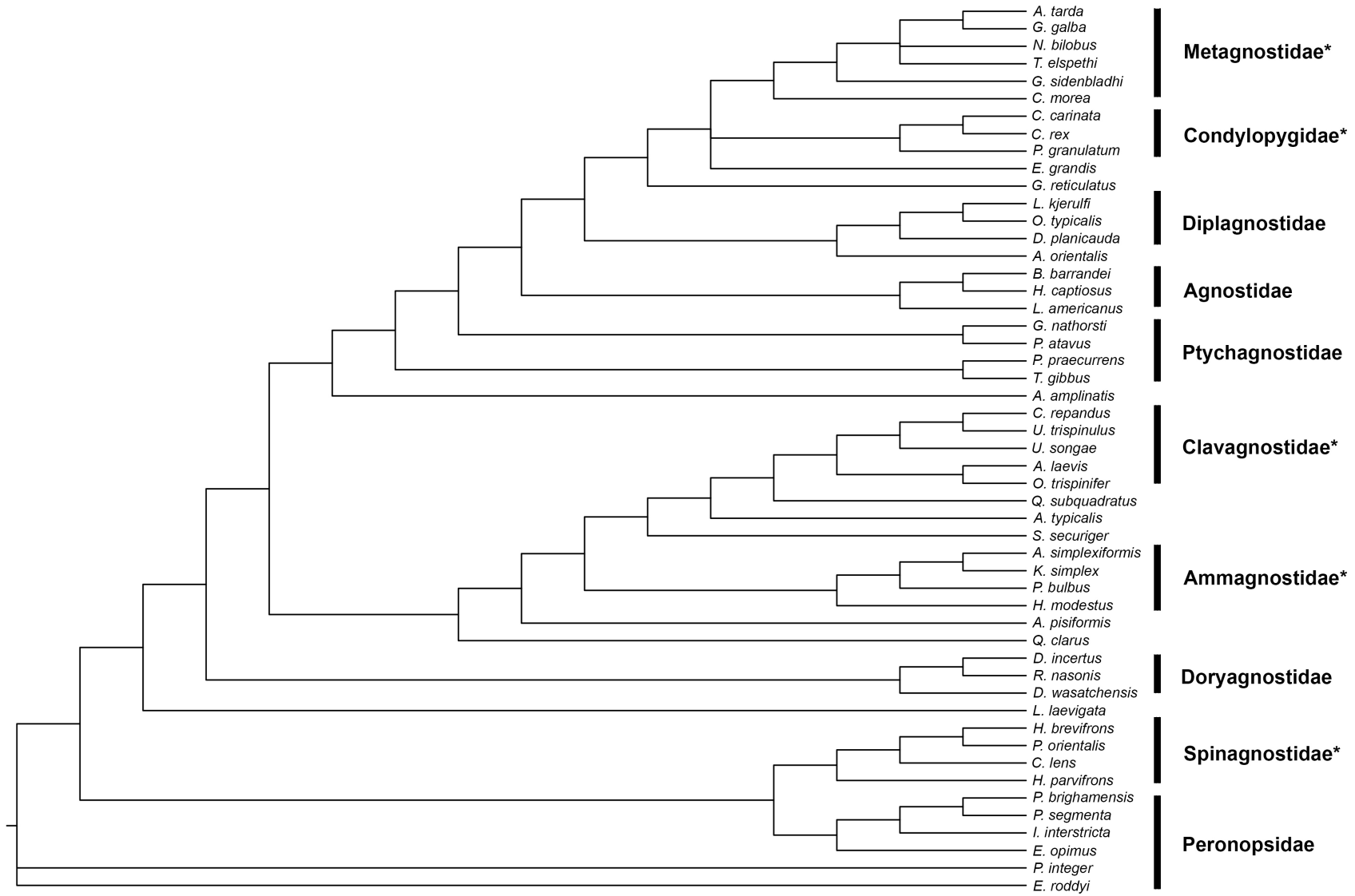

Figure 1.2—Strict consensus tree (PAUP*) from six most parsimonious trees with a length of 638, CI 0.19, RC 0.10, and RI 0.53. Black vertical bars indicate traditional familial classification and asterisks (*) indicate clades comprised of all taxa that are historically classified within that family.

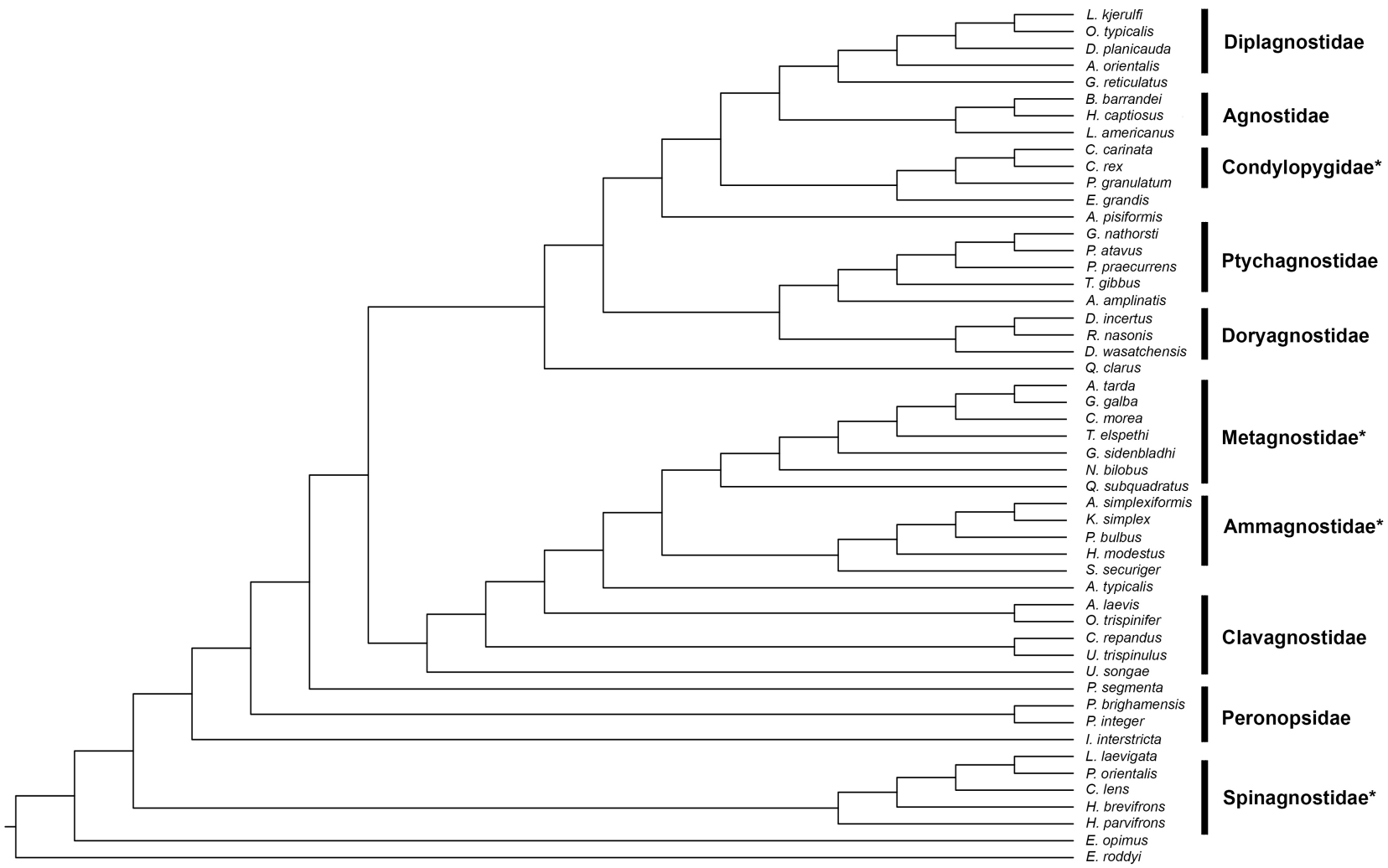

Figure 1.3—Strict consensus tree (TNT) of 12 optimal trees with a score of 404.43, CI 0.21, RI 0.59, RC: 0.12. Black vertical bars indicate traditional familial classification and asterisks (*) indicate clades comprised of all taxa that are historically classified within that family.

DISCUSSION—

Recovered clades—Of the eleven traditionally recognized families that were included in this study, ten were repeatedly recovered as clades. In all analyses, taxon membership within each of the Ammagnostidae, Condylopygidae, Metagnostidae, and Spinagnostidae clades was entirely consistent with traditional taxonomic assignments, suggesting that current classification is a reasonable first-order proxy for phylogeny. The peronopsids occur as a weakly-supported group or as paraphyletic with taxa pulled stemward, which may arise from the outgroup, *E. roddyi*, being an ingroup peronopsid and thus affecting the placement of sister taxa. The MCC tree, calculated without defining an outgroup, shows [Peronopsidae + Spinagnostidae] occurring as a more derived clade whereas the Diplagnostidae diverge basally. For comparison, cladistic analyses rooted on diplagnostine taxa instead of *E. roddyi*, result in the [Peronopsidae + Spinagnostidae] clade being recovered as derived (Appendix A, Figure A.5).

Of note is the recovery of Condylopygidae as a strongly derived clade in every analysis. Historically, members of this group have been considered to be a distinct taxonomic Superfamily sister to the whole of Agnostoidea, These results call into question that designation with the consistent recovery of condylopygids within the traditional Agnostoidea. However, this pattern may be driven by issues of character polarity and the autapomorphy of an inflated anterior glabella. The former is likely as there is moderate support for an association between condylopygids and [Peronopsidae + Spinagnostidae] in the MCC tree, all of which represent the oldest agnostines.

Inconsistencies—The inconsistent occurrences of several individual taxa affected the cohesion of several traditionally recognized families. In the parsimony-based cladograms, *O. trispinifer* is

pulled into a clade with clavagnostids, namely as sister to *A. laevis*, due to the apparent synapomorphy of a transverse axial sulcus (character 55). While a close affinity between diplagnostids and clavagnostids is not a new interpretation (e.g., Öpik, 1967), the present study suggests that *O. trispinifer* possesses an axial character state that is autapomorphic: an expanded and highly zonate axis and is not shown in other taxa that are assigned to Diplagnostidae or in other species of *Oidalagnostus* (Appendix A, Terminology, Figure A.3). The removal of character 55 from the data matrix places *O. trispinifer* within a pectinate arrangement of diplagnostine taxa (Appendix A, Figure A.6), reflecting the lack of characters that sufficiently describe diplagnostine variation for cladistic purposes. This lack of resolution for Diplagnostidae in the parsimony analyses is echoed by the relatively weak support (posterior 0.25) of the diplagnostine clade in the MCC tree. Consistent cohesion among the diplagnostine taxa between analyses, despite lack of internal resolution, suggests monophyly of the Diplagnostidae. The positions of *E. opimus* and *L. laevigata* are similarly influenced by characters that have been suggested to represent a convergent trait: characters 25 and 37 describe glabellar definition, which has previously been discussed as likely representing retention of a plesiomorphy as it occurs throughout Agnostida (Westrop et al., 1996) and has been noted to appear in parallel in several different lineages (Naimark, 2012). The removal of those characters collapses the node that defined the clade, causing *E. opimus* and *L. laevigata* to move to a pectinate arrangement with the other ptychagnostine taxa similarly unresolved (Appendix A, Figure A.7). In a previous cladistic analysis of the Ptychagnostidae, all included species of *Lejopyge* formed a clade with ingroup ptychagnostines relative to outgroup taxa of *A. pisiformis* and *P. brighamensis* (Westrop et al., 1996). The lack of resolution again indicates that characters defined in the current study

are adequate to resolve monophyly of some families, but studies conducted on a finer scale may be required in order to explore within-family relationships.

Wastebasket and Uncertain Taxa—Taxonomic families that may be considered to be wastebaskets, namely Agnostidae and Pseudagnostidae, did not coalesce into monophyletic groups. Instead their assigned taxa are typically problematic, often with inconsistent placement between trees. Of the Agnostidae, the type species (*A. pisiformis*) and *E. grandis* are inconsistent in their phylogenetic placements while *H. captiosus*, *B. barrandei*, and *L. americanus* form a distinct clade in all trees. In the MCC tree, *A. pisiformis* occurs within a clade that unites the Agnostidae and Doryagnostidae; however, in the PAUP* cladogram it is recovered as a sister taxon to a nested group of ammagnostids and clavagnostids, and in the tree produced by TNT it is recovered as a sister taxon to the other members of Agnostidae, condylopygids, and diplagnostids. The agnostine *E. grandis* occurs with other ingroup taxa of Agnostidae in the MCC tree, but occurs outside of that group and as a sister taxon to the condylopygids in both parsimony-based cladograms. The discrepancies arise from the treatment of character 14, a quantitative character that describes the size of the basal lobes. Removal of that character collapses the clade of ingroup Agnostidae, *A. pisiformis*, and *E. grandis* into a pectinate arrangement (Appendix A, Figure A.8). The Agnostidae are perhaps the most poorly defined group of all of Agnostina, being comprised of remnant taxa that happen to lack diagnostic traits of other agnostine groups. Indeed, virtually all agnostoids were historically assigned to the genus *Agnostus* Brongniart, 1822; attempts to subdivide that genus did not become widely recognized until nearly 100 years after its initial description (e.g., M'Coy, 1846; Hawle and Corda, 1847; Tullberg, 1880; Shergold et al., 1990). The sole uniting feature of the Agnostidae, as noted by

Öpik (1967), is the possession of what he termed the "agnostoid" type of articulating device. It is possible that the inclusion of thoracic characters such as the articulating device may yield a cohesive Agnostidae exclusive of remnant taxa.

The Problem of Pseudagnostidae—The most striking, but perhaps unsurprising, finding of the phylogenetic analyses is the lack of a clade that equates to the traditionally defined Pseudagnostidae. The Pseudagnostidae has a problematic history, being initially defined as a generic assignment by Jaekel (1909) for any agnostine species possessing a short pygidial axis and possession of a structure that was later termed a deuterolobe (see Appendix A, Terminology, Figure A.2). The deuterolobate condition is problematic in terms of classification because the definition of the structure is not clear. Shergold (1977) recognized the high disparity in the Pseudagnostidae and suggested subdivision into two broad groups—the speculate group and the papillonate group—based solely on the position of the anterior node. That disparity has been claimed to represent differences in underlying musculature structure, internal organ support, or perhaps as having a relation to interconnected nervous and photosensitive systems that aid in orientation, as was interpreted in early studies using experimentally-blinded cladocerans (Harris and Mason, 1956). Regardless of the significance of the axial node, its position is highly variable within Agnostina and is not an appropriate trait for taxonomic diagnosis.

It is expected that taxa that are assigned to Pseudagnostidae based on such loose criteria would not form a clade; instead, they either occur inconsistently between analyses as seen in *S. securiger* and *A. typicalis*, or form a strong association with another group, such as *A. orientalis* showing affinity to Diplagnostidae because of pygidial similarities, and *N. bilobus* consistently occurring within the metagnostid clade with the synapomorphy of a short pygidial axis. Given

the lack of any phylogenetic support of the Pseudagnostidae, or any synapomorphies defining this group, careful examination of all taxa currently assigned to this family is warranted. In 2017, Naimark and Pegel also acknowledged the difficulties in diagnosing pseudagnostine taxa and suggested a need for bottom-up phylogenetic analyses in order determine taxonomic placement, noting the potential reliability of unique border structures for generic assignment. The present analysis suggests a revised diagnosis for one of the taxa included herein (*N. bilobus*); however the inclusion of other species of *Neoagnostus* would be required to determine if a species revision is required or if it is necessary to reclassify the genus *Neoagnostus* in its entirety. Future phylogenetic analyses must resolve the affinities of other pseudagnostine species.

Caveats—While the investigation presented here is the most comprehensive exploration of agnostine ingroup relationships to date, it is not without its shortcomings. Several agnostine taxa remain unassigned to any particular taxonomic group in the literature due to the absence of synapomorphies with other taxa. *Agnostardis amplinatis*, *Glyptagnostus reticulatus*, and *Quadrahomagnostus subquadratus* show no consistent placement and cannot be unambiguously assigned in this study. Additionally, as discussed above, several taxa do not occur within the expected groups, and at least one family that does not coalesce at all (Pseudagnostidae). The inclusion of characters that describe the articulating device may provide insight into the placement of unassigned taxa, such as *Glyptagnostus*, or may lend support to the monophyly of Agnostidae and Pseudagnostidae.

Additional traits that have not been considered for this analysis include those that describe soft tissue and juvenile stages. Reliance on published type material when coding character states means that intraspecific variation might have been underestimated.

Ideally, a bottom-up process to estimating phylogenies, namely exploring affinities at the species level and working up to the genus- and family- level, would be pursued in order to reconstruct ingroup relationships within Agnostina; however this is a time-consuming approach to phylogenetic reconstruction and has not yet been implemented for the Agnostina on a large scale. Instead, top-down studies such as the one presented here, provide a foundation for testing the robustness of existing taxonomic classification and for generating a phylogenetic hypothesis for future studies.

CONCLUSION—Given the biostratigraphic importance of the Agnostina and several investigations into the group's affinities to various arthropod lineages, it is surprising that within-group relationships of agnostine taxa have received little attention using phylogenetic methods. Inadequate diagnostic criteria have led to discrepancies in taxonomic classification, with many taxa being assigned to higher taxonomic groups based on sets of plesiomorphic or homoplastic traits. This study has attempted a large-scale exploration of the Agnostina through Bayesian and parsimony-based methods to determine the phylogenetic support for the existing taxonomic framework of this group. It has been determined that several agnostine rank-based groups are supported, including the Ammagnostidae, Clavagnostidae, Metagnostidae, and Spinagnostidae. Furthermore, the Condylopygidae is supported in all analyses as a derived ingroup agnostine clade. There is moderate support, despite some topological inconsistencies, for Diplagnostidae, Doryagnostidae, Peronopsidae, and Ptychagnostidae. Taxa representative of Agnostidae and Pseudagnostidae failed to consistently coalesce into corresponding clades, reflective of a lack of synapomorphies defining those groups.

Future phylogenetic analyses that include thoracic, ventral, and soft tissue characters may help to further resolve ingroup agnostine relationships and aid in the polarization of characters when resolving affinities to other arthropod groups. This study found relatively weak support for deep branching patterns among agnostine clades. In order to resolve these deeper ingroup affinities, bottom-up approaches, such as those that have explored the Ptychagnostidae (Westrop et al., 1996, Laurie, 2008), should be conducted for each agnostine family. Supertree methods, rigorous approaches to phylogenetic reconstruction that use combined topological information instead of the direct analysis of character data, are a promising next step to examine the relationships between agnostine clades. These techniques offer the opportunity to assemble large phylogenies that allow for between-clade affinities to be examined by utilizing multiple lines of evidence (Bininda-Emonds et al., 2002). The results provided in this study provide support for much of the existing rank-based systematic framework of the Agnostina, allowing for continuing research that relies on robust classification at higher taxonomic levels of this important group of arthropods.

CHAPTER TWO:

ASSESSMENT OF THE STRUCTURE OF INTEGRATION IN THE CAMBRIAN AGNOSTINE ARTHROPOD *PENTAGNOSTUS BRIGHAMENSIS* (RESSER, 1939)

ABSTRACT—

Morphological traits within an organism can be functionally or developmentally coupled into integrated units. Such modules are empirically recognized as sets of traits that have stronger interactions within the set and fewer, weaker interactions between sets. Evolutionary change to one trait within a module begets changes to the other traits within that module, leading to a channeling of variation into a few directions. The strength and structure of integration may therefore play a role in constraining morphological evolution. This study investigates the structure of integration in *Pentagnostus brighamensis* (Resser, 1939), a species of middle Cambrian agnostine arthropod recovered from the Spence Shale unit of the Langston Formation. In order to assess the structure of integration, geometric morphometric methods were used to detect patterns of fluctuating asymmetry (FA) that can be used to delimit modules and infer the structure of integration that arises from direct interactions among developmental pathways. The glabella was divided into six partitions that define anatomical regions and analyses were conducted to determine the strength of covariation in FA between these partitions. Results suggest a glabellar integration structure that is driven primarily by direct interactions and shows a characteristic anterior-posterior element coupling. This study serves as a starting point to compare other closely-related species, culminating in an understanding of whether and how the evolution of this clade was constrained by integration.

INTRODUCTION—

Phenotypic integration and modularity are two tightly associated concepts that describe how the traits of organisms are correlated. Integration is the degree to which morphological traits within an organism are functionally or developmentally coupled, resulting in a channeling of variation into a few dimensions. This coupling leads to the creation of modules: sets of traits that have stronger interactions within the set and fewer, weaker interactions between them (Olson and Miller, 1958; Cheverud, 1996; Wagner and Altenberg 1996). An intriguing consideration in terms of identifying drivers of macroevolutionary patterns is the degree to which the structure of integration acts as a constraint on the direction of morphological evolution and how it may impede or enhance the rate of that evolution depending on the nature of the adaptive landscape (Burger, 1986; Schluter, 1996; Wagner and Altenberg, 1996; Marroig and Cheverud, 2005; Renaud et al., 2006; Hunt, 2007; Goswami et al., 2014; Felice et al., 2018). The fossil record provides the opportunity to explore patterns of integration on the long timescales upon which macroevolutionary trends manifest, allowing for direct testing of evolutionary hypotheses. One such line of inquiry is the investigation of how disparification is influenced by integration, if at all; and further explore the timescales over which integration itself evolves. In order to appropriately assess the contribution of integration to large scale patterns of disparity, it is necessary to identify the cause of trait covariations and determine the potential for them to be conserved through deep time.

While some studies have inferred the structure of integration as a constraint by making large cross-clade comparisons of extant taxa (e.g., Goswami, 2006a, 2006b, 2007; Goswami et al., 2009; Goswami and Polly, 2010b), very few have used the fossil record. Given that most

studies that explore this aspect of variation focus on extant taxa, it is difficult to apply these observations to processes on macroevolutionary timescales. The fossil record offers the direct means of studying the evolution of integration over these long timescales. In order to investigate the role that developmental constraints play in macroevolutionary trends, it is of critical importance to identify an organism that is sufficiently well preserved to obtain information on the developmental mechanisms that govern morphological variation. Here I analyze the structure of integration of the extinct agnostine arthropod *Pentagnostus brighamensis* (Resser, 1939), from the mid-Cambrian Spence Shale Member of the Langston Formation, Utah. Agnostines are a taxonomically diverse yet morphologically conserved clade of small, blind arthropods that spanned from Lower Cambrian to the Upper Ordovician. Landmark-based geometric morphometric methods are used to analyze the shape of this agnostine and isolate the components of symmetric variation and fluctuating asymmetry, so as to determine the structure of integration and how it contributed to shape variation in this species. The extent to which this structure of integration is determined by direct interactions among developmental pathways is explored, and the potential for integration having acted as a long-term constraint on the direction of phenotypic evolution is discussed.

METHODS—

Sources of covariation—In studies of integration and how and if it affects patterns on macroevolutionary timescales, it is instructive to distinguish between developmental pathways in which covariance in phenotypic traits results from parallel variation from those in which covariance results from direct interactions (Klingenberg, 2005). Parallel variation arises when two or more developmental pathways respond independently to a common source of variation,

producing covariation of the resultant traits. By contrast, covariation that arises from direct interactions is that which is caused by some source of variation acting upon a common upstream portion of a shared pathway or transmitted between pathways via inductive signaling (Klingenberg and Zaklan, 2000; Klingenberg et al., 2003; Klingenberg, 2005). Klingenberg (2005) suggested that covariation resulting from parallel variation can be more easily restructured over time than that produced by direct interactions, because the former can be the result of pleiotropic patterns whereas the latter requires the restructuring of developmental pathways and thus should be more temporally conservative.

The spatial structure of fluctuating asymmetry (FA) can indicate which traits are coupled through direct interactions among their respective developmental pathways. FA is random, small deviations from perfect symmetry during development of a nominally symmetrical trait within individuals and populations (Van Valen, 1962; Møller and Swaddle, 1997; Palmer and Strobeck, 2003; Graham et al., 2010). Since FA arises from developmental noise, it arises independently on both sides of a symmetrical trait and can be distinguished from the symmetrical variation that results from sources of parallel variation. Therefore, covariation that arises from parallel variation is controlled for and correlated patterns of FA among traits both delimit the spatial extent of modules and indicate direct interactions among morphogenetic pathways (Klingenberg and Zaklan, 2000; Klingenberg et al., 2001, 2003; Klingenberg, 2005). For this reason, fluctuating asymmetry has been used to investigate the developmental underpinnings of phenotypic integration (e.g. Klingenberg and Zaklan, 2000; Klingenberg et al., 2001, 2003, 2012; Hallgrímsson et al., 2004; Breuker et al., 2006; Young and Badyaev, 2006; Zelditch et al., 2008, 2009; Klingenberg, 2009; Laffont et al., 2009; Drake and Klingenberg, 2010; Ivanovic and Kalezic, 2010; Klingenberg et al., 2010; Jamniczky and Hallgrímsson, 2011; Jojic et al., 2011,

2012; Webster and Zelditch, 2011a, 2011b). The contribution of direct interactions to phenotypic variation has been investigated in few studies (e.g. Klingenberg et al. 2003, 2004; Klingenberg 2004, 2011; Zelditch et al. 2008, 2009; Drake and Klingenberg, 2010; Muñoz- Muñoz et al., 2016), and even more rarely in extinct taxa (Webster and Zelditch, 2008, 2011a, 2011b), illustrating the need for studies such as the one presented here that employ this concept to explore the role of integration as a developmental constraint through deep time.

Material collection and preparation—Material was collected from the Spence Shale Member of the Langston Formation, a mid-Cambrian (Miaolingian Series, Wuliuan Stage) Lagerstätte in northeastern Utah and southeastern Idaho that preserves a diverse soft-bodied and skeletonized fauna dominated by arthropods (Robison et al., 2015; Kimmig, 2018). Bulk rock samples containing specimens of *P. brighamensis* were collected from Miners Hollow, a section within the Wellsville Mountains of northeastern Utah that contains exposures of the Spence Shale (Appendix B, Fig. B.1). Collections were made from the top 20 cm of a limestone ledge that caps the second recognized parasequence (PS 2) in the unit (Appendix B, Fig. B.2). Since the analyses of FA in this study are sensitive to the effects of taphonomic distortion, only non-compacted, silicified sclerites were included. The sclerites were extracted via dilute acetic acid dissolution of the carbonate rock and picked from the insoluble residue. They were then cleaned, blackened with dilute India ink, mounted on toothpicks in the standard orientation as defined by Shaw (1957). While this orientation is defined for non-agnostoids, the alternative orientation for eyeless forms I, the horizontal orientation of lateral dorsal furrows, is suitable for agnostines as well. They were then whitened with ammonium chloride to temporarily enhance the contrast of dorsal features, and digitally photographed with image-stacking software. After dismounting of

each specimen, a repeat of the entire process from mounting to photography with at least a day between replicates was performed in order to quantify measurement error. To limit potential allometric shape variation, the smallest specimens were excluded. Specimens with obvious distortion and significant damage to glabellar elements were also excluded. In total, 48 cephala are included in the subsequent analyses.

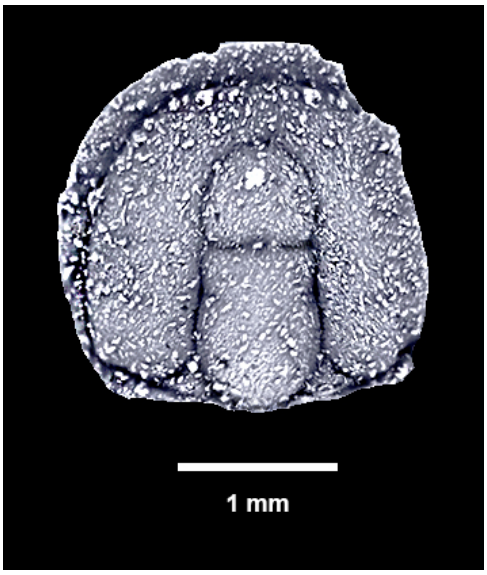

Figure 2.1—Cephalon (partially damaged) of *Pentagnostus brighamensis.* From ICS-10316

Quantifying glabellar shape—Landmark and curve data were acquired from photographed specimens using the tpsDIG2 software (Rohlf, 2017). A total of 11 landmarks and 116 sliding semilandmarks were selected based on the ease of repeated identification and the preservational completeness of specimens (Fig. 2.3). Superimposition and semilandmark sliding was performed in CoordGen8 and SemiLand8, respectively, which are included in the IMP8 suite of morphometrics software (Sheets, 2014). While Procrustes superimposition rescales all

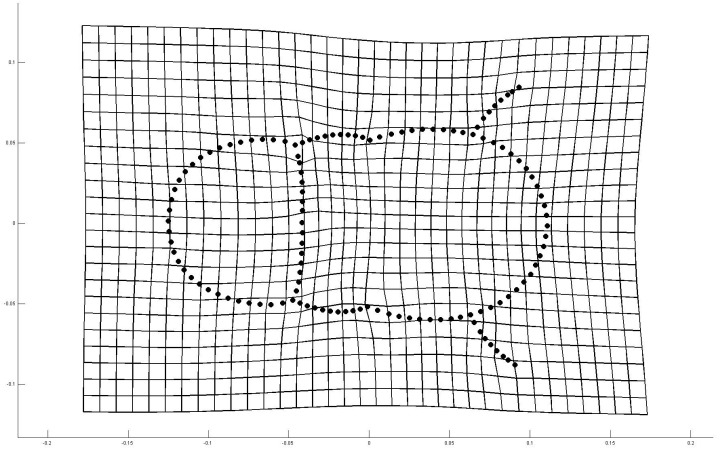

Figure 2.2—Thin plate spline deformation grid showing allometric variation in glabellar shape among specimens during the sampled portion of ontogeny. Reference form is consensus of all 48 landmark/sliding semilandmark configurations. Variation is concentrated primarily in the M3 region of the glabella, resulting from variable positioning of the transglabellar furrow relative to the F2 furrow.

configurations to a common size, it does not remove any allometric signal in shape variation that remains even after the smallest specimens are removed from the specimen pool (Fig. 2.2, multivariate regression of shape variables against log centroid size SS_{total}=0.1565; $SS_{residual}$=0.1433, percent variance explained = 8.445%; p-value<0.0006; significance determined by 1600 bootstraps). Such allometric variation is concentrated within the M3 portion of the glabella, which is the anteriormost region of the posteroglabella. The transglabellar furrow shows slight variation in its position relative to the F2 furrow (See Appendix A, Terminology). This portion of the glabella is related to raised rims that are seen on internal molds and are thought to be sites of muscle attachment (Shergold, 1975), and agnostine specimens with preserved soft tissue indicate that this anatomical location is also related to the position of structures of the digestive tract (Moysiuk and Caron, 2019).

In studies of integration and modularity, allometric covariation might truly be the product of integration, but it might also artificially inflate the perceived degree of integration. In order to further remove any portion of shape variation related to allometric variation, the data were size-standardized using the Standard8 program of the IMP8 suite (Sheets, 2014). Size-standardization is performed with a linear multivariate regression of shape variables against the natural logarithm of centroid size (lnCS), which allows the shape of each specimen to be predicted at any specified size with the assumption that the growth trajectory is linear, a characteristic of the data that was confirmed by visual inspection of the partial Procrustes distance and warp scores plotted against the log centroid size of specimen. The residuals for each specimen describe the amount of shape deviation away from the regression and are retained with each specimen through the size-standardization procedure. This method has often been used to remove the effects of allometry (e.g., Zelditch et al. 2004; Hopkins and Webster 2009; Webster and Zelditch, 2011a, 2011b). The

size of specimens sampled ranged from lnCS 1.06 (approximately 1.5 mm sagittal cephalic length) to lnCS 2.43 (approximately 3.4 mm sagittal cephalic length), and were standardized to a size of lnCS 2.4, equivalent to a sagittal cephalic length of approximately 3.3 mm. This value is close to the maximum of all specimens, but within the sampled range of specimens, and thus involved no extrapolation beyond the sampled range. All analyses were conducted on size-standardized data.

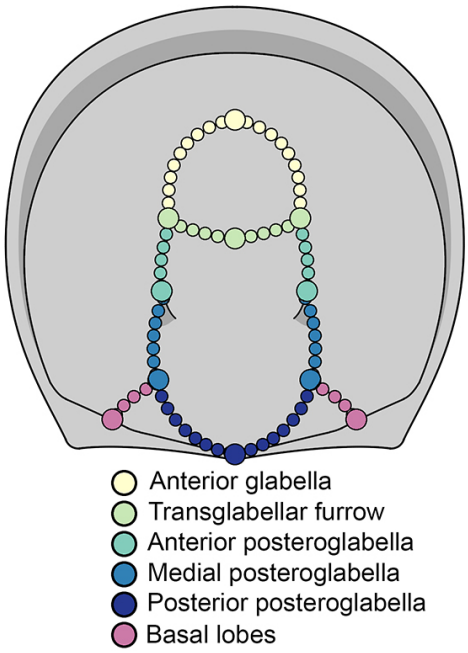

Figure 2.3—Partitions of the landmark configuration that define regions of the agnostine glabella.

Isolating the components of variance— The favored method of isolating the FA component of variation is a two-factor mixed-model ANOVA (Leamy, 1984; Palmer and Strobeck, 2003); this method has been adapted to geometric morphometric data (Auffray et al., 1996; Klingenberg and McIntyre, 1998; Klingenberg et al., 2001). The two effects are "Individuals" which is the symmetrical component of variation among individual genotypes, and "Sides" which is the variation between the two sides that is used to interpret directional asymmetry. The interaction term ("Individuals x Sides") represents the failure of the individuals to achieve perfect bilateral symmetry: the FA term. The significance of FA is determined by the F-ratio between the mean square of the interaction and the mean square of the measurement error (Leamy, 1984; Palmer & Strobeck, 2003). Decomposition of the symmetrical and asymmetrical components of variation was performed with SAGE (Márquez 2007a).

The among-partition correlation matrix—Subsets of landmarks and semilandmarks were defined to serve as the potential components of modules. Six of these partitions were defined (Fig. 2.3), representing different parts of the glabella: the anterior glabella, the transglabellar furrow (also termed F3) that separates the anteroglabella from the posteroglabella; the anterior portion of the posteroglabella, the medial portion of the posteroglabella which is distinguished from the anterior part by the F2 furrow; the posterior end of the posteroglabella which is the portion of behind the point at which the lateral glabellar furrow meets the basal lobes and culminates at the occipital termination of the glabella; and the basal lobes. In order to avoid the potential of artificially inflating the degree of covariation, no landmarks or semilandmarks are shared between partitions. The full configuration was partitioned using the VisProto8 software (Sheets, 2014).

For each partition, pairwise Procrustes distances between all specimens were calculated for both the Individuals (symmetrical) and the FA components of variation. Matrix correlations were calculated between those distance matrices, resulting in matrices for each component of variation that show the degree of covariation between the partitions in terms of shape variation among all specimens. This "among-partition correlation matrix" (Webster and Zelditch, 2011a, 2011b) was calculated in CORIANDIS (Marquez, 2007b) and used in subsequent analyses to explore the structure of integration.

Determining the contribution of direct interactions—The correlation between the Individual component and FA component represents the extent to which phenotypic variation is controlled by direct interactions among developmental pathways: a high value indicates a strong influence

of direct interactions on phenotypic variation whereas a low value indicates that the dominant signal is parallel variation. The matrix correlation was performed on the among-partition correlation matrices for each component of variation, testing the significance of that correlation with a Mantel test (1000 permutations). The null hypothesis of a conventional Mantel test is that the matrices are no more similar than expected by chance (R_M=0). A statistically significant correlation means that the structure of the Individuals component (phenotypic integration) is more similar to that of FA component (direct interactions) than expected by chance. This would indicate that direct interactions contribute to morphological integration and therefore may influence the direction of phenotypic evolution. The Mantel test was performed in R using the "vegan" package (Oksanen et al., 2019). A complementary procedure uses a parametric bootstrap to test the null hypothesis that there is no more divergence between the matrices than expected by chance, and therefore the matrices are statistically indistinguishable (R_M=1). This method generates simulated matrices with the same structure as the two observed matrices (Individuals component and FA component) that consist of random numbers drawn from a multivariate normal distribution. This procedure is repeated 1000 times, generating a distribution of simulated matrix correlations that can be compared to the observed matrix correlation. The probability of obtaining a matrix correlation between the observed correlation matrices if those matrices were drawn from the same population is given by the proportion of the simulated distribution having a lower correlation value. This alternative method has been described and employed in a prior study on phenotypic integration in trilobites (Webster and Zelditch, 2011b) and is comparable to methods used by Hunt (2006) and Hallgrímsson et al. (2007). The R code for this procedure was created by Annat Haber (unpublished).

Hierarchical cluster analyses—Cluster analyses are routinely used in studies that explore patterns of integration and modularity (e.g. Cheverud, 1982; Atchley, 1993; Monteiro et al., 2005; Goswami, 2006; Zelditch et al., 2008; Webster and Zelditch, 2011a). These exploratory analyses propose a structure of integration based on cluster distances, and therefore potentially delimit modules. Clustering methods require the definition of a distance metric and a linkage algorithm. Euclidean distance, which describes the shortest distance between two objects, was the metric used here as it is most commonly used in morphometric studies. The among-partition correlation matrices for Individuals and FA components were used in hierarchical cluster analyses. The linkage algorithms employed here are those that are often used in integration studies (Webster and Zelditch, 2011a): unweighted pair-group average (UPGMA, Farris, 1969) and Ward's method (Ward, 1963) of hierarchical clustering. The extent to which the resulting dendrogram adequately describes the structure of the underlying data is assessed by the cophenetic correlation (CC; Sneath and Sokal, 1973). Values that are less than 0.85 indicate that the clustering method is a poor fit. To test the assumption that the clusters are structured hierarchically, the agglomerative coefficient (AC; Kaufman and Rosseeuw, 1990; Zelditch et al., 2008) was calculated. Values of the AC range from 0 to 1, with higher values indicating a strong hierarchical structure that is measured by greater similarity among first-merged observations than among those that were merged last. Hierarchical clustering and the associated metrics were calculated using the "cluster" package in R (Maechler et al., 2018).

Reticulate network analysis—Cluster analyses inherently impose a hierarchical structure even though it might not be present in the data. Other methods are therefore necessary to explore patterns in the data. As a complement to cluster analyses, reticulate network analysis is an

additive approach that relaxes some of the constraints on distances between and within clusters that are seen in strict ultrametric, hierarchical clustering methods. Reticulate network analysis relaxes the assumption that traits cannot be shared between clusters by adding reticulations among clusters that indicate shared traits. This concept originates in studies of horizontal gene transfer and hybridization (Makarenkov and Legendre, 2004; Makarenkov et al., 2004) and utilizes a least-squares approach that minimizes the squared deviations between the original dissimilarities and the reticulation distances. Reticulations are only added to tree if it minimizes the conservative Q1 optimization criterion (Zelditch et al., 2008, 2009). Reticulate network analysis was conducted in T-REX v.4.0a1 (Makarenkov, 2000) on the among-partition correlation matrices for the Individuals and FA components.

Graphical modeling—The final exploratory method used here is graphical modeling, as described by Magwene (2001, 2008, 2009) and implemented in many subsequent studies of integration and modularity (e.g., Zelditch et al. 2009, Webster and Zelditch 2011a, 2011b). This method discovers modules by calculating conditional independence between traits. Vertices representing the objects of interest (in this case, partitions) are connected by edges, the strength of which are based on high partial correlations. The practical application of this method uses the inverse of the among-partition correlation matrix, in which each diagonal element is related to the multiple correlation coefficient between one trait and all others (Whittaker, 1990). The

inverted matrix is then rescaled so that the diagonals equal 1 in the same manner that a correlation matrix is derived from a covariance matrix. This results in the off-diagonals being the negative partial correlation coefficients given all other traits (Appendix B, Table B.2) (Magwene, 2001). Graphical modeling analyses were performed using MIM v.3.2.0.7 (Edwards, 2008). Heuristic searches were conducted in order to find the model with the fewest edges and as it is not uncommon for this sort of search to result in different models being preferred, the search was conducted three times for each component to check for consistency. The search method was stepwise with parameters defined as headlong (edges considered in random order), bidirectional (edges able to be added and deleted), and unrestricted (allowing edges that were previously removed to be reconsidered). Edge strengths were calculated with the partial correlation coefficients derived from the among partition correlation matrix (Appendix B, Table B.4) and following the procedure described by Lawler (2008) in which values greater than 0.025 are considered strong.

RESULTS—

Components of variance—Results from the ANOVA are shown in Table 2.1. The majority of variation (> 92%) in the sample is attributed to symmetric variation as described by the Individuals component. As expected for a bilaterally-symmetrical organism, the Sides

Table 2.1—Results of the two-factor mixed model ANOVA. SS = sum of squares; d.f. = degrees of freedom; MS = mean square. See text for interpretation.

Effect	SS	d.f.	MS	F-value	P-value	% Variance
Individuals	0.269	5875	4.58E-05	17.9303	<0.0001	92.7%
Sides	0.003	125	2.12E-07	11.6283	<0.0001	0.9%
Individuals x Sides	0.015	5875	2.55E-06	12.0193	<0.0001	5.2%
Measurement Error	0.004	12000	2.97E-05	—	—	1.3%
Total	0.290					100.0%

component accounts for a negligible proportion of the variance. The interaction term, which describes the proportion of variation that is contributed by FA, explains the remaining variance (> 5%) and is highly significant. The proportion of variance attributable to measurement error associated with replicate measures is smaller than the FA term.

The among-partition correlation matrix for both components of variation is shown in Table 2.2. The lower triangle is the correlation matrix for symmetric variation among individuals. Notably, the correlations between partitions are stronger toward the anterior glabella and become weaker rearward, with the exception of the transglabellar furrow. The anterior glabella correlates strongly with the anterior portion of the posteroglabella, and is significant at 95%. It is also moderately correlated with the medial posteroglabella, and only weakly with the posterior posteroglabella and basal lobes. The anterior portion of the posteroglabella is somewhat strongly correlated with the medial posteroglabella, and weakly (but significantly) correlated with the posterior posteroglabella and basal lobes. The medial posteroglabella is moderately correlated with the posterior posteroglabella and somewhat weakly (but significantly) with the basal lobes. The posterior portion of the posteroglabella is also only weakly correlated with the

Table 2.2—Among-partition correlation matrix for the Individuals (lower triangle) and FA (upper triangle) components of variation. Bolded values are significant at 95%. Results of significance testing can be found in Appendix B (Table B.1)

	Anterior glabella	Transglabellar furrow	Anterior posteroglabella	Medial posteroglabella	Posterior posteroglabella	Basal lobes
Anterior glabella		0.081	**0.473**	**0.606**	**0.356**	0.226
Transglabellar furrow	**0.240**		-0.075	-0.098	**-0.097**	-0.056
Anterior posteroglabella	**0.714**	0.150		**0.463**	0.188	**0.508**
Medial posteroglabella	**0.406**	0.045	**0.680**		**0.542**	**0.453**
Posterior posteroglabella	**0.180**	0.022	**0.211**	**0.481**		**0.272**
Basal lobes	0.122	0.160	**0.221**	**0.297**	**0.298**	

basal lobes. The transglabellar furrow does not correlate strongly with any other glabellar region, but its correlation with the anterior glabella is significant.

The among partition correlation matrix for the FA component of variation (Table 2.2, upper triangle) is similar to that of the Individuals component, with a couple of notable differences. The anterior glabella correlates more strongly with the medial portion of the posteroglabella than it does with the neighboring anterior portion, which is the exception in an otherwise similar posterior-ward decrease in the correlation structure that is exhibited in the Individuals component. The transglabellar furrow, again, is not associated with any other partition and, in fact, is very weakly negatively correlated with most partitions. Its correlation with the posterior posteroglabella is significant, but very weak.

Table 2.3—Results from the Mantel tests on the correlation between the Individuals and FA components of variation. Both hypotheses $R_M = 0$ and $R_M = 1$ were tested. The high values indicate the strong contribution of direct interactions.

Observed matrix correlation	Adjusted matrix correlation	Repeatability		Probability of matrices being indistinguishable	
		Individuals component	FA component	Individuals component	FA component
0.717	0.722	0.993	0.996	0	0

Contribution of direct interactions—The among-partition correlation matrices for the Individuals and FA components of variation are highly correlated (Table 2.3), with an observed correlation of 0.717 that is more similar than expected by chance ($p = 0.004$). This correlation value can be adjusted given the repeatability for each matrix (0.993 and 0.996, respectively) to a value of 0.722. This high value suggests that direct interactions have strongly influenced phenotypic variation in this species. The alternative null model approach ($R_M = 1$) shows that the probability that the matrices for each component are identical is 0, indicating that the matrices are not statistically indistinguishable.

Hierarchical cluster analyses—Dendrograms for both components show AC values that are less than 0.55 across methods, which indicates that the hierarchical structure is weak in all cases. The highest CC value (0.53) is shown in the Individuals dendrogram that was calculated with the UPGMA method (Fig. 2.4a), which is well below the threshold (0.85) at which the dendrograms would be considered as adequately reflective of the data.

The dendrograms for the Individuals component of variation show a similar structure regardless of the linkage algorithm used (Fig 2.4a, b). Both methods recover clusters of [Anterior glabella + Anterior posteroglabella] Medial posteroglabella]] and [Posterior posteroglabella + Basal lobes]. The transglabellar furrow is depicted as more similar to the [Posterior posteroglabella + basal lobes] cluster in Ward's method than in the UPGMA dendrogram, but it

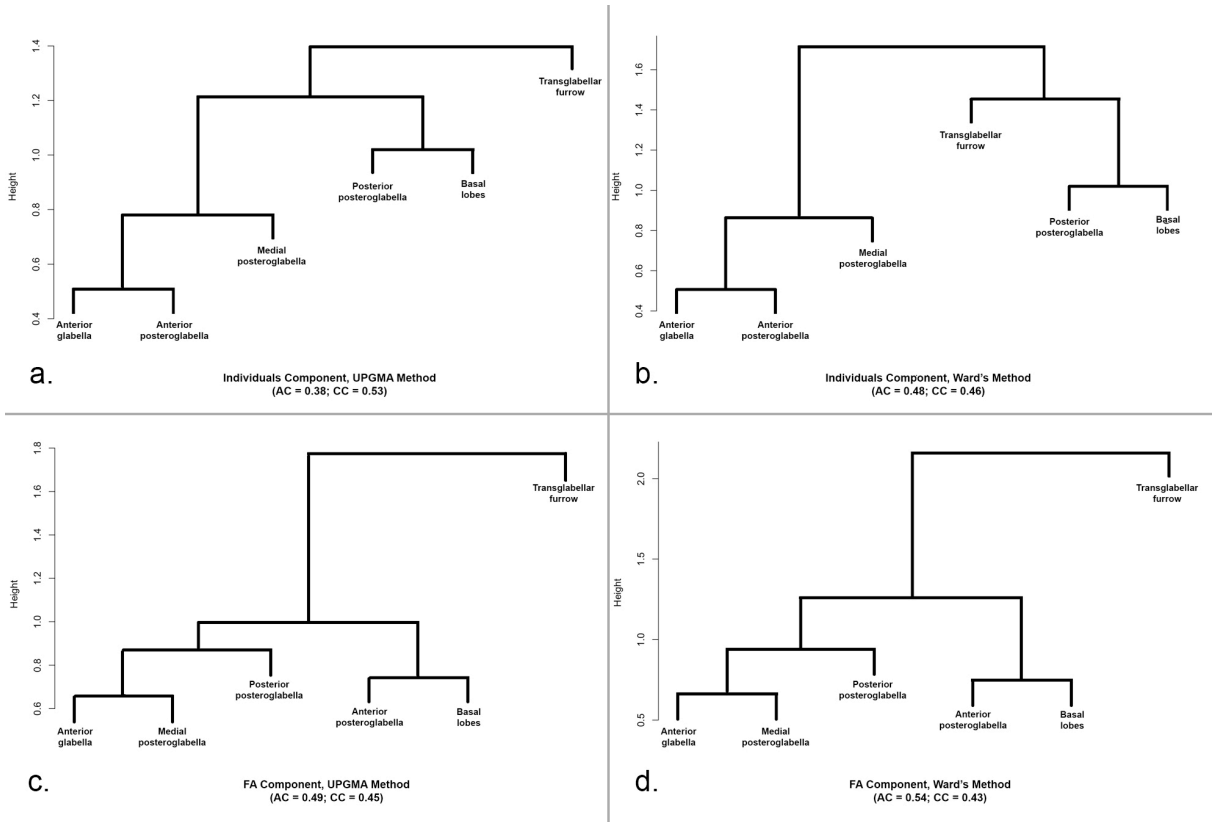

Figure 2.4—Results from hierarchical cluster analyses for the Individuals component using a) UPGMA and b) Ward's method; and the FA component using c) UPGMA and d) Ward's method.

should be noted that the UPGMA dendrogram has a slightly higher CC. The dendrograms for the FA component are nearly identical to each other across methods (Fig. 2.4c,d). The transglabellar furrow is again far removed from the main clusters, which consist of [Anterior glabella + Medial posteroglabella] Posterior posteroglabella]] and [Anterior posteroglabella + Basal lobes].

Reticulate network analysis—The reticulograms (Fig.2.5 a,b) for both components recover a structure similar to that of the hierarchical cluster analyses. The reticulogram for the Individuals component (Fig. 2.5a) again recovers a cohesive grouping of [Anterior glabella + Anterior posteroglabella] Medial posteroglabella]]. A reticulation has been added to indicate that the transglabellar furrow belongs to both the [Anterior glabella + Anterior posteroglabella] Medial posteroglabella]] set and a neighboring group that also contains the basal lobes. The Posterior posteroglabella shows the weakest relationship with the other regions. The reticulogram for the

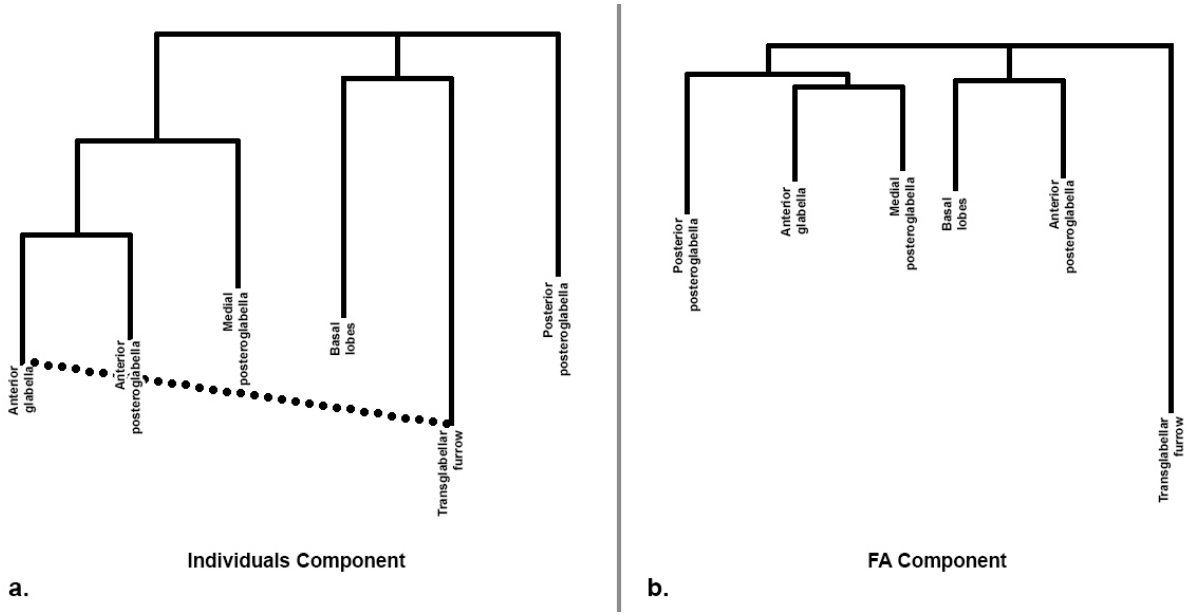

Figure 2.5—Reticulograms for a) the Individuals component and b) the FA component. Dotted line indicates a reticulation that has been added.

FA component (Fig. 2.5b) shows an identical structure to the dendrograms produced with the clustering methods. The groups of [Anterior glabella + Medial posteroglabella] Posterior posteroglabella]] and [Anterior posteroglabella + Basal lobes] have again been recovered with the transglabellar furrow being the farthest removed. No reticulations were added to the grouping structure of the FA component.

Graphical modeling—The heuristic searches recovered a single supported graphical model for each of the components of variation. The graphical model for the Individuals component (Fig 2.6a) is described as [Anterior glabella + Anterior posteroglabella + Medial posteroglabella][Transglabellar furrow][Medial posteroglabella + Posterior posteroglabella][Basal lobes], suggesting a nested modular structure. Similar to the relationship structure in previous analyses, the strength of associations between partitions becomes generally weaker posterior-ward with the exception of the transglabellar furrow, which is not linked to any other partition. It is also worth noting that the relationship between the anterior glabella and medial posteroglabella is shown as weaker than in previous analyses, but it is strong enough to be retained as an edge. As with the transglabellar furrow, edges that link the basal lobes to any other glabellar region have been excluded in this model.

The graphical model recovered for the FA component (Fig. 2.6b) is described as [Anterior glabella + Anterior posteroglabella + Medial posteroglabella][Anterior glabella + Medial posteroglabella + Posterior posteroglabella][Transglabellar furrow][Anterior posteroglabella + Medial posteroglabella + Basal lobes], which recovers a similar structure to previous analyses. The sets of [Anterior glabella + Medial posteroglabella + Posterior

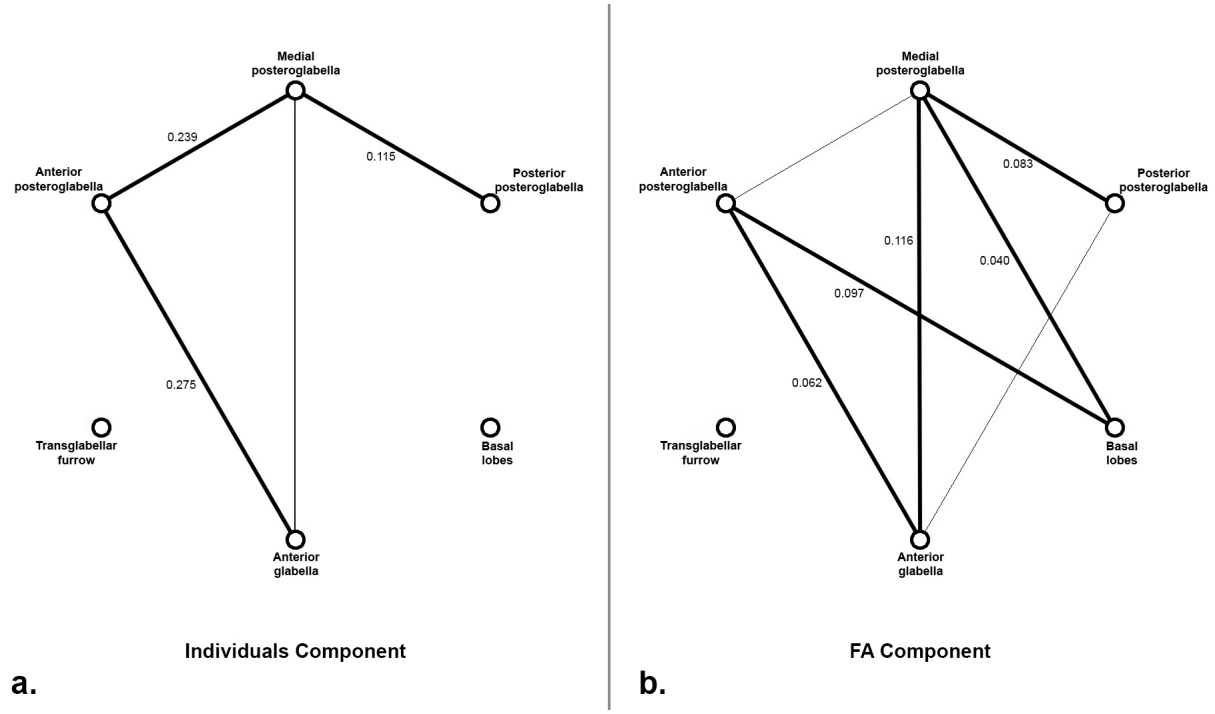

Figure 2.6—Graphical models generated for a) the Individuals component; and b) the FA component of variation. Labeled vertices represent partitions of interest, bolded lines indicate edge strengths > 0.025. Partial correlation values are labeled next to corresponding edges.

posteroglabella] and [Anterior posteroglabella + Basal lobes] are consistently recovered through all analyses and illustrate an interesting and somewhat unexpected link between anterior elements and posterior elements of this agnostine glabella. The transglabellar furrow is consistently not linked to any other region. Test statistics for all of the edges included for each model (Appendix B, tables B.5 a,b), in addition to the matrices used in this analysis (Appendix B, table B.3) can be found in the appendix.

Inferred structure of integration—Figure 2.7a depicts the *a posteriori* hypothesis for the structure of integration for the symmetric component of variation among individuals. Strong associations between the anterior glabella and the anterior posteroglabella are supported by all analyses; those partitions are considered to be conditionally dependent. A weaker association between the

medial glabella and [Anterior glabella + Anterior posteroglabella] is consistently detected and is also conditionally dependent, with a link to the posterior posteroglabella that is recovered with in the graphical modeling analysis. The basal lobes are only weakly associated with other partitions, as is the transglabellar furrow. The latter is depicted as part of the outermost nested module as there is some evidence of its association with the basal lobes in the reticulate network analysis.

The inferred structure of FA is summarized in Figure 2.7b and shows a similarly nested structure to that of the Individuals component. The [Anterior glabella + Medial posteroglabella] set is consistently recovered in all analyses, with a slightly weaker association with the posterior posteroglabella. Additionally, the [Anterior posteroglabella + Basal lobes] module is recovered in all analyses, suggesting conditional dependence. The transglabellar

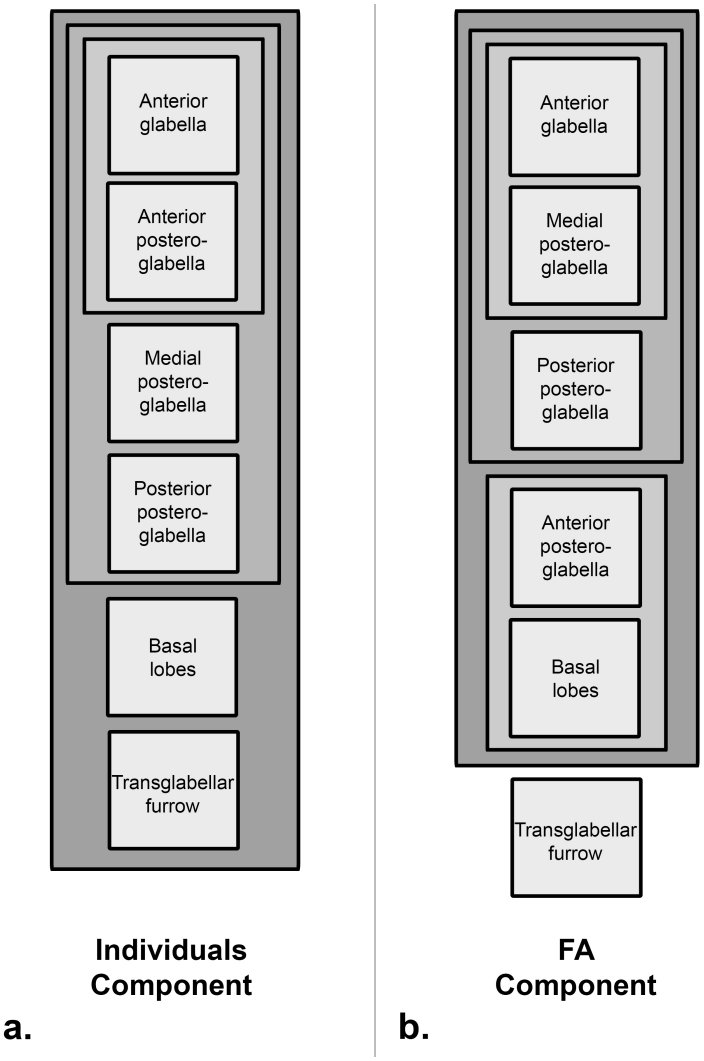

Figure 2.7—Inferred models of the structure of integration for the a) Individuals component and b) FA component. Labeled interiormost boxes designate partitions whereas enclosing boxes represent the modular structure.

furrow is depicted outside of the nested module structure as it does not show an association with any partition in any analysis.

DISCUSSION—

Contribution of direct interactions—Comparison of the correlation structures between the symmetric component of variation among individuals and that which describes FA suggest that direct interactions among developmental pathways did direct phenotypic variation in *P. brighamensis*. Similar high degrees of correspondence between FA and symmetric components of variation, implying the influence of direct interactions, has only been found previously in studies on extant organisms, such as species of *Drosophila* (Klingenberg and Zaklan, 2000; Breuker et al., 2006, Rego et al., 2006), tsetse flies (Klingenberg and McIntyre, 1998), and bumble bees (Klingenberg et al., 2001).

These results stand in contrast to the findings of Webster and Zelditch (2011a, 2011b) for ptychoparioid trilobites, in which the structure of phenotypic variation was shown be controlled primarily through parallel variation. Variation arising from parallel variation is thought to be more labile over deep time as it is not driven by hardwired developmental mechanisms that would need to be restructured and therefore, not expected to serve as a long-term constraint on evolution. Given that ptychoparioid trilobites are at the base of an early major diversification, it is reasonable to suggest that the lack of such constraints contributed to the potential for greater morphological diversification than what is observed in the agnostines (Webster and Zelditch 2011a, 2011b).

The results from this study are unsurprising in the sense that agnostines form a morphologically conservative clade showing little phenotypic variation throughout its history,

thus it is expected that developmental constraints may have played a role in maintaining aspects of its phenotype. This study confirms that phenotypic conservation of the glabella of this species may result from an integration structure that is driven by direct interactions; however, this cannot necessarily be extended to the entire cephalic sclerite. Furthermore, the pygidium shows more variation across agnostine taxa, a fact that is illustrated by the use of pygidial trait complexes to delineate morphogroups that aid in the most current species diagnoses in the absence of reliable cephalic characters (Naimark, 2012, 2014; Naimark and Pegel, 2017). Since it has been shown herein that the glabella in one species of agnostine arthropod is an integrated part of the anatomy, a logical next step would be to investigate if the pygdial sclerite of the same species is similarly influenced by direct interactions.

Structure of integration—While the matrices for the phenotypic integration and direct interactions are strongly correlated, there are a couple of notable differences in the inferred structure of integration between the two components of variation. The Individuals component (Fig. 2.7a) shows a clear anterior-to-posterior sequential weakening of the among-partition correlations. This may be indicative of "neighborhood effects": neighboring regions of the glabella showing shared patterns of variation due to localized morphogenetic controls. However, it has been shown that the structure of phenotypic integration in this species is similar to that of the direct interactions. The structure of this component (Fig. 2.7b) does not strictly follow the anterior-to-posterior pattern that is seen in the Individuals component. Instead, there is an unexpected linkage of anterior and posterior elements: the module consisting of the anterior glabella plus the medial posteroglabella associated with the posterior posteroglabella, and the anterior region of the posteroglabella consistently linked to the basal lobes. It is unclear what this

pattern suggests about the biology of this organism as any functional association is not readily evident, but it is not a wholly new pattern seen in ancient arthropods. Webster and Zelditch (2011a, 2011b) recovered a similar association of anterior and posterior regions of the cranidium in all three ptychoparioid trilobites studied. In those studies, it was suggested that *Hox* gene expression could be responsible for the pattern of anterior regions tightly associated with posterior regions, but while such models have been suggested for trilobites (Sundberg, 2000; Hughes, 2003), a more complete model for *Hox* expression domains is needed in order to test this hypothesis. The recovery of this pattern in agnostine arthropods suggests that this could be a common pattern within Artiopoda.

The results of both analyses conducted herein show that the region defined by the transglabellar furrow is strikingly disconnected from the rest of the integration structure. This feature is also the site of a large amount of the observed variation in the sample (see Methods-Quantifying glabellar shape). Its association to sites of muscle attachment and adjacency to digestive structures suggests that the transglabellar furrow may be more closely associated with regions of the anterior portion of the agnostine body that are not included in this study, such as the hypostome or other ventral features.

Caveats—It should be noted that there are a few weaknesses in this study. First is the *a priori* definition of partitions. The boundaries of the partitions were based on common anatomical features of the agnostine glabella, but they are treated as hard boundaries with no possibility of overlap. It is possible that correlation of neighboring partitions could be artificially inflated if there was not adequate subdivision of the region. Klingenberg (2011) offers a method in the MorphoJ software that iteratively searches for covarying structures without *a priori* partitioning;

however, it can only be used on models of two modules. The second caveat is that the FA signal in the data is rather weak, and the structure of integration for this component should therefore be considered with caution. Finally, this study does not explicitly test any *a priori* models of modularity because not enough is known about agnostine arthropods to propose a reasonable model of integration; this study is therefore entirely based on exploratory methods. In a review on approaches to studying integration and modularity, it was shown and noted that exploratory methods were generally less informative and less consistent with each other than were model-testing approaches (Goswami and Polly, 2010a). Despite this realization, the results of the study presented herein are consistent for all approaches used.

Future work—Agnostines are the second fossil taxon to be the subject of a study on integration and modularity using the methods employed here. The first set of studies explored patterns of integration in trilobites (Webster and Zelditch, 2011a, b) and were the first step to investigating the structure of integration as a potential constraint acting on evolutionary timescales. As the present study has focused on a taxon close to the base of the agnostine clade, a generalized statement of the effect of intrinsic constraints within Agnostina cannot be made. The question of how conserved is the structure of integration through time and how it influenced macroevolutionary patterns of disparity will be investigated by comparative studies on other agnostines: both within the same clade as *P. brighamensis* and in agnostines that are more derived.

CONCLUSION—

The results in this study support the conclusion that the structure of integration in *P. brighamensis* may have served as a long-term developmental constraint. This is potentially reflective of a tendency within the Agnostina to be morphologically conserved; however future studies on the degree and structure of integration in other agnostine taxa are required in order to explore the possibility that this represents a pattern manifested throughout the clade. Additionally, the pattern of covarying anterior and posterior elements in the cephalon in *P. brighamensis* is consistent with previous findings in trilobites (Webster and Zelditch, 2011a,b), suggesting that this characteristic structure may be present throughout Artiopoda. This consistently-recovered structure of integration may be evidence of axial patterning related to early *Hox* gene expression.

CHAPTER THREE:

A COMPARATIVE STUDY OF INTEGRATION PATTERNS IN THE AGNOSTINE FAMILY PERONOPSIDAE WESTERGÅRD, 1936

ABSTRACT—

While studies of integration and their evolutionary significance have grown increasingly complex over the years, the extent to which phenotypic integration serves as a constraint over macroevolutionary timescales remains a relatively unexplored topic. Here I seek to comprehensively explore that topic in several steps, utilizing the middle Cambrian agnostine clade, Peronopsidae Westergård, 1936. First, a phylomorphospace of Agnostina was generated showing that the group of interest is relatively morphologically conserved. Geometric morphometric methods were used to acquire data necessary to assess the level of integration in the peronopsid sister taxa, *Pentagnostus brighamensis* (Resser, 1939) and *Pentagnostus segmenta* (Robison, 1964). The landmark configuration for the glabella of *P. segmenta* was divided into six partitions that define anatomical regions and analyses were conducted to determine the strength of covariation in fluctuating asymmetries (FA) between these partitions. The structure of integration that arises from direct interactions among developmental pathways was determined for *P. segmenta*, the results of which were compared to those previously obtained for *P. brighamensis*. The outcomes of this study demonstrate that the level of integration in Peronopsidae was weak, and thus did not play a role in the phenotypic conservatism shown in this clade. Moreover, the structure of integration in *P. segmenta* was not driven by direct interactions, standing in contrast to the integration structure of *P. brighamensis*. However, the consistent recovery of an anterior-posterior region covariation was discovered, which may suggest a common module throughout Artiopoda.

INTRODUCTION—

Integration and modularity are closely related concepts relevant to the evolvability of clades and their constituent species. Phenotypic integration is the degree to which morphological traits within an organism are functionally or developmentally coupled; and modularity is the partitioning of that structure into sets of distinct traits, or modules, that have more and stronger interactions within them relative to the interactions between them. The result of phenotypic integration is a channeling of variation into a few dimensions, constraining the ability of an organism to generate novel phenotypes. Evolutionary change is expected to preferentially occur in the direction of covariance among integrated traits, which forms an axis of evolutionary "least resistance"; combinations of trait values that do not align with this axis are expected to be difficult to achieve. If selection pressures align with the line of least resistance, evolutionary rate may be enhanced in that direction. A key question regarding the shaping of macroevolutionary patterns of disparity is the extent to which the structure and degree of integration acts as a long-term constraint on morphological evolution and how it may affect the rate of that evolution, either impeding or enhancing depending on the nature of the adaptive landscape (Burger, 1986; Schluter, 1996; Wagner and Altenberg, 1996; Marroig and Cheverud, 2005; Renaud et al., 2006; Hunt, 2007; Goswami et al., 2014; Felice et al., 2018). Investigating that first aspect relies on the expectation that if the degree and structure of integration are strong and consistent through time, the potential for expansion into different areas of morphospace will be low regardless of evolutionary rate. Conversely, high disparity would be permitted if the degree and structure of integration is low and labile.

Here I investigate several aspects regarding the influence of integration on the disparification of the agnostine clade Peronopsidae Westergård, 1936. Agnostine arthropods

serve as a good system for investigating shape change throughout the clade as the morphological diversity of cephalic elements is minimal, allowing for homologous loci to be identified across species that do not exhibit effacement. For the initial part of this study, I generate a phylomorphospace of Agnostina Salter, 1864 in order to test the hypothesis that Peronopsidae is morphologically conserved, thus serving as a foundation for the remaining lines of inquiry. Using landmark-based geometric morphometric methods, I analyze the shape of the mid-Cambrian (Miaolingian Series, Drumian Stage) agnostine *Pentagnostus segmenta* (Robison, 1964) to determine the degree of integration in this species, and compare it to that of *Pentagnostus brighamensis* (Resser, 1939*)*, the sister taxon (Chapter 1) to *P. segmenta* collected from a slightly older (Miaolingian Series, Wuliuan Stage) assemblage in the Spence Shale (Langston Formation) (Chapter 2). I then isolate the symmetric component of variation from that which is comprised of fluctuating asymmetry for *P. segmenta* with the aims of determining the structure of integration and how it has contributed to shape variation in this species, comparing it to that of *P. brighamensis*. These steps aid in determining the extent to which the level and structure of integration are conserved within sister taxa. Finally, I explore the extent to which this structure of integration in *P. segmenta* is determined by direct interactions among developmental pathways (See Methods: Isolating the components of variance). Those results are then compared to those from the study of *P. brighamensis*, allowing for the investigation of whether and how integration acts as a long-term constraint on the morphological diversity of this clade. I further test the expectation that integration arising through direct interactions among developmental pathways is more phylogenetically stable than is integration arising through parallel variation among traits by comparing the components of variation for each species. The expectation is that if Peronopsidae occupies a small area of morphospace relative to other

agnostines, it may exhibit a high degree of integration acting as a long-term constraint on the morphological evolution in this clade relative to other, more disparate, agnostine arthropod clades.

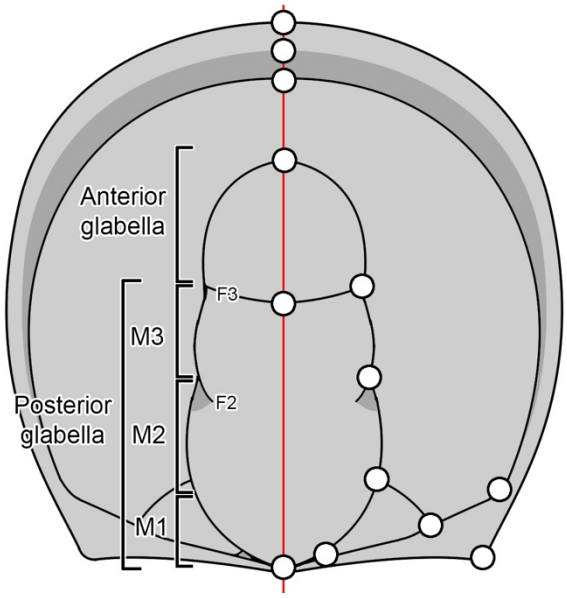

Figure 3.1—Landmarks selected to describe shape variation in the agnostine cephalon. Key anatomical features are indicated. F2 and F3 refer to the lateral notch and transglabellar furrow, respectively.

METHODS—

Phylomorphospace—In order to determine the relative disparity of agnostine clades, a phylomorphospace of Agnostina Salter, 1864 was constructed. A total of 51 agnostine species were included in this analysis, including representatives from all but one of the families within Agnostoidea M'Coy, 1849, the superfamily Condylopygoidea Raymond, 1913, and species of uncertain familial affiliation. Images of the cephala from each species were collected from the literature to be included in geometric morphometric analyses (see Chapter 1, Table 1.1). A set of 13 landmarks were selected based on homology throughout Agnostina (Fig. 3.1) and digitized with the tpsDIG2 software (Rohlf, 2017). Landmark data were subjected to partial Procrustes superimposition using CoordGen8 (Sheets, 2014). A PCA-generated morphospace was overlain with the maximum clade credibility tree for Agnostina (Chapter 1) to generate a phylomorphospace using the package 'phytools v. 0.6-99' in R (Revell, 2019). Disparity of each taxonomic group was calculated by determining the Procrustes variances (PV), which involve taking the sum of the diagonal elements of the group covariance matrix and dividing it by the number of observations in the group. Additionally, partial disparity (PD, Foote, 1993) was

calculated to quantify the contribution that a particular subgroup makes to the overall disparity of the larger group. Disparity metrics were calculated using the 'geomorph' package in R (Adams et al., 2019).

Material collection and preparation for integration analyses—Samples containing silicified material were collected from the Marjum Formation in the Wheeler Amphitheater, a well-known outcropping of middle Cambrian (Miaolingian Series, Drumian Stage) rocks in the House Range west of Delta, Utah (Appendix C, Fig. C.1). This site is characterized by limestone and shale facies containing a diverse fauna including trilobites, agnostoids, and brachiopods (Smith, 2007). Bulk rock samples containing specimens of *P. segmenta* were collected from a 36 cm limestone bed near the base of the formation. Only non-compacted, silicified sclerites were included in subsequent analyses in order to minimize the potential for taphonomic distortion. The sclerites were extracted via dilute acetic acid dissolution of the carbonate rock and picked from the insoluble residue. They were then cleaned, blackened with dilute India ink, mounted on toothpicks in the standard orientation as defined by Shaw (1957, p. 194) for eyeless non-agnostines, which is

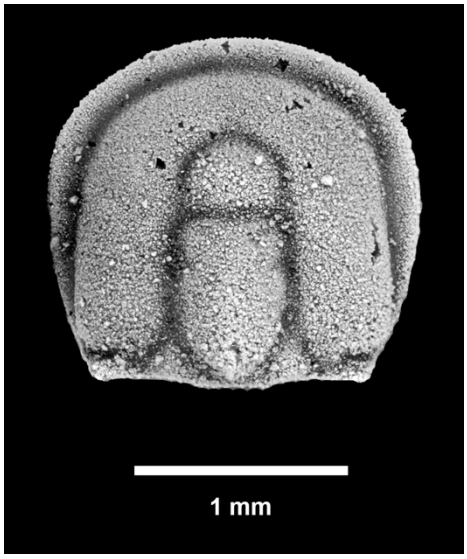

Figure 3.2—Silicified cephalon of *P.*

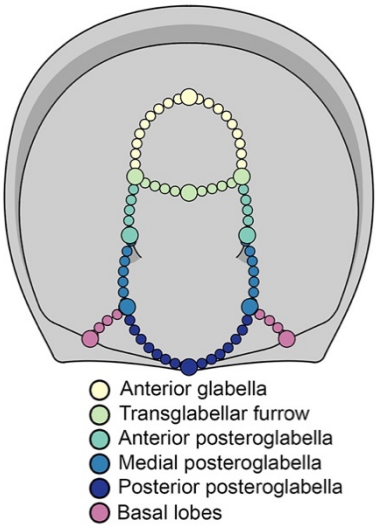

Figure 3.3—Partitions of the landmark configuration that define regions of the agnostine glabella.

suitable for consistent orientation in agnostines as well. Sclerites were whitened with ammonium chloride to temporarily enhance the contrast of dorsal features, and digitally photographed (Fig. 3.2). To quantify measurement error, the entire procedure from mounting to photography was repeated with at least a day between replicates. To reduce the magnitude of any allometric shape variation, the smallest specimens were excluded. Specimens with obvious distortion and significant damage to glabellar elements were also excluded. The analyses herein are based upon a sample size of 42 cephala of *P. segmenta* and are compared to previous results that were based on a sample size of 48 cephalic sclerites of *P. brighamensis* (Chapter 2).

Quantifying glabellar shape—The x-, y-coordinates of 11 landmarks and 116 sliding semilandmarks were digitized from all photographed specimens using the tpsDIG2 software (Rohlf, 2017). These landmarks were selected based on ease of identification and the preservational completeness of specimens (Fig. 3.3). Superimposition and semilandmark sliding were performed in CoordGen8 and SemiLand8, respectively, which are included in the IMP8 suite of morphometrics software (Sheets, 2014). While the size component of variation is removed through Procrustes superimposition, there is a small amount of allometric signal in shape variation that remains even after the smallest specimens are removed from the sample (Fig.

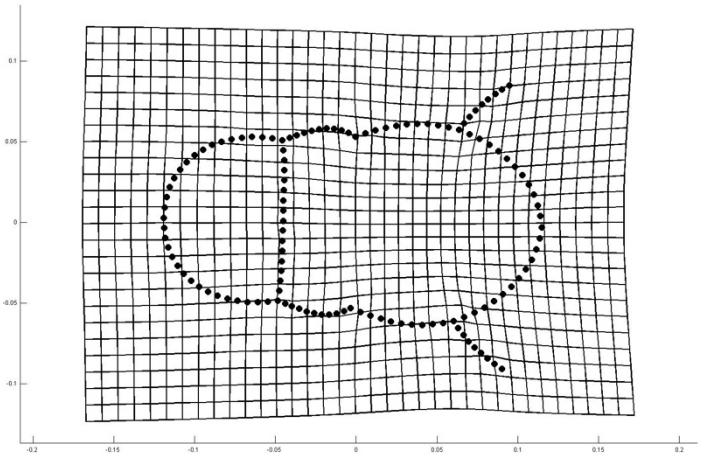

Figure 3.4— Thin plate spline deformation grid showing allometric variation in glabellar shape among specimens during the sampled portion of ontogeny. Reference form is consensus of all 42 landmark/sliding semilandmark configurations. Variation is concentrated primarily in the M2 region of the glabella.

3.4, multivariate regression of shape variables on log centroid size SS_{total}=0.0849; $SS_{residual}$=0.0787, percent variance explained = 7.327%, based on summed squared Procrustes distances; p-value<0.001; significance determined by 1600 bootstraps). This variation is concentrated in the M2 portion of the glabella, the median lateral notch (F2) shifting posteriorward (see Fig. 3.1 for anatomical terminology). It has been suggested that this feature corresponds to internal segmentation (Robison, 1982), and agnostine specimens with preserved soft tissue indicate that this anatomical location is related to the position of structures of the digestive tract (Moysiuk and Caron, 2019). To remove any shape variation related to allometry, data were size-standardized. This procedure involves a linear multivariate regression of shape variables against the natural logarithm of centroid size (lnCS), which allows the shape of each specimen to be predicted at any specified size with the assumption that the growth trajectory is linear, a characteristic of the data that was confirmed by visual inspection of the partial Procrustes distances, warp scores, and first five principal components (>81% of the total variance) plotted against the log centroid size associated with each specimen. The residuals for each specimen describe shape deviation away from the regression and are retained with each specimen through size-standardization. The size of specimens sampled ranged from lnCS 1.03 (corresponding to a sagittal cephalic length of approximately 1.0 mm) to lnCS 1.83 (corresponding to a sagittal cephalic length of approximately 2.1 mm), and were size-standardized to lnCS = 1.8 (equivalent to a sagittal cephalic length of approximately 2.0 mm). This value lies within the sampled size range of specimens and close to the maximum size of all specimens, so there was no extrapolation of predicted shape beyond the sampled range. All

analyses presented herein were conducted on size-standardized data. Size-standardization was performed using the Standard8 program of the IMP8 suite (Sheets, 2014).

Determining the degree of integration—Investigation of the degree of integration using morphological data utilizes an array of common methods. To employ these methods, six subsets of landmarks and semilandmarks were defined as the partitions, representing various anatomical regions of the glabella (Fig. 3.3): the anterior glabella, the transglabellar furrow that separates the anteroglabella from the posteroglabella; the anterior portion of the posteroglabella, the medial portion of the posteroglabella which is separated from the anterior part by the F2 furrow; the posterior end of the posteroglabella which is the portion of behind the point at which the lateral glabellar furrow meets the basal lobes and culminates at the occipital termination of the glabella; and the basal lobes. To avoid artificially inflating the degree of covariation, no landmarks or semilandmarks are shared between partitions.

The first method used to determine the degree of integration is based on two-block partial least squares (PLS), where a singular value decomposition of the covariance matrix between two sets of variables is used to describe the maximum degree of covariation between them (Bookstein et al. 2003; Mitteroecker and Bookstein, 2007). When this method is applied to geometric morphometric data, it is termed "Singular Warps Analysis". This general method has been extended so that more than two subsets of variables can be defined (Streissguth et al. 1993), in which case the average pairwise PLS correlation is used. The observed test value (r_{PLS}) is compared to that of a distribution generated by random permutation of the rows in one partition relative to those in another partition. A statistically significant result is found when the r_{PLS} value is greater than 95% of the generated distribution. High correlation values (close to 1) indicate

stronger integration whereas low correlation values (closer to 0) indicate a more modular structure. An alternative approach is the use of Escoufier's (1973) RV coefficient (Klingenberg, 2009), a ratio that describes the degree of covariation within sets of variables relative to the covariation between sets of variables. Several studies have utilized the RV coefficient as it is an intuitive metric (e.g. Drake and Klingenberg, 2010; Jojic et al., 2012; Goswami et al., 2014; Sorenson et al., 2014); however, it has been shown that both Singular Warps Analysis (Adams and Collyer, 2016) and the RV coefficient (Adams, 2016) are highly sensitive to both sample size and number of variables. An alternative approach, the covariance ratio (CR) has been proposed (Adams, 2016). The structure of the CR is similar to that of the RV coefficient, but unlike the RV coefficient, the CR uses the pairwise covariances between variables to determine the degree of integration:

$$\mathrm{CR} = \sqrt{\frac{trace(\mathbf{S}_{12}\mathbf{S}_{21})}{\sqrt{trace(\mathbf{S}_{11}^{*}\mathbf{S}_{11}^{*})\,trace(\mathbf{S}_{22}^{*}\mathbf{S}_{22}^{*})}}} \tag{3.1}$$

…where S_{11} and S_{22} are the covariance matrices within each partition and S_{12} and S_{21} are the covariances between partitions. S_{11}* and S_{22}* are the covariance matrices within partitions with zeroes replacing the diagonal elements (Adams, 2016, p. 568).

The notable difference between the RV coefficient and the CR is the exclusion of the variance in the latter, which allows for the CR to be insensitive to sample size and number of variables. The CR is the ratio of the covariation between modules relative to the covariation within them, with values ranging from 0 to positive values and an expected value of 1. Values less than one describe a situation in which the covariance between modules is less than that within modules and can interpreted as a more modular structure. Conversely, values greater than

1 describe a higher degree of integration with the covariance between modules greater than that found within them.

The landmark configurations for both *P. brighamensis* and *P. segmenta* were subjected to CR analysis using 1000 iterations of the permutation procedure to evaluate significance. For comparison, Singular Warps Analyses was also performed with 1000 permutations. Both CR analyses and Singular Warps Analyses were performed using the 'geomorph' package in R (Adams et al., 2019).

A complementary approach to determine the overall degree of integration by utilizing a novel "deflation" technique to analyze mean shape has been suggested by Bookstein (2015). By estimating the set of bending energies of aligned specimens and plotting the log of the variance of the partial warps versus the log of their bending energies, a metric of global integration can be generated that considers shape variation across spatial scales. The null hypothesis is that the slope is equal to -1, which indicates self-similarity. Isotropic data would be expressed as a slope of 0 and slopes steeper than -1 indicate more integrated forms. Landmark configurations for *P. brighamensis* and *P. segmenta* were used in this global integration analysis using the 'geomorph' package in R (Adams et al., 2019).

Isolating the components of variance—In order to determine the potential for integration to act as a long-term constraint, it is necessary to distinguish between two potential developmental causes of covariation among traits: that which is caused by parallel variation and that which is caused by direct interactions among their developmental pathways. Parallel variation is the result of some source of variation that acts independently on two or more developmental pathways, producing covariation of the resultant traits. By contrast, covariation that arises from direct interactions

among developmental pathways is that which is caused by some source of variation acting upon a common upstream portion of a shared developmental pathway or transmitted between developmental pathways via inductive signaling (Klingenberg and Zaklan, 2000; Klingenberg et al., 2003; Klingenberg, 2005). The latter is expected to be more temporally conservative than the former as it requires the restructuring of developmental pathways whereas the former can result from either favorable patterns of pleiotropy or environmental factors acting upon more than one developmental pathway simultaneously (Klingenberg, 2005). The spatial structure of fluctuating asymmetry (FA) reveals which traits are coupled through direct interactions among their respective developmental pathways, lending insight into the structure of integration. Since the two sides of a bilateral organism share the same genome and the same environment, focusing on the fluctuating asymmetries provides a means to filter out the variation that may be caused by external mechanisms. Using a novel approach suggested by Klingenberg and Zaklan (2000), correlated patterns of FA can be compared to those exhibited by the symmetric component of variation to determine the degree to which the symmetric variation is influenced by direct interactions. If the FA component of variation is highly correlated with the symmetric component of variation in an organism, it implies that direct interactions are driving the integration of the phenotype. A two-factor mixed-model ANOVA is the favored method of isolating the FA component of variation (Leamy, 1984; Palmer and Strobeck, 2003) adapted for use with geometric morphometric data (Auffray et al., 1996; Klingenberg and McIntyre, 1998; Klingenberg et al., 2001). The two effects are "Individuals" which is the symmetrical component of variation, and "Sides" which is the variation between the two sides that is used to interpret directional asymmetry. The interaction term ("Individuals x Sides") represents FA. Replicate measurements allow for an estimate of measurement error, which can be of substantial

importance in studies that incorporate the small signal of FA (Palmer, 1994). The significance is determined by the F-ratio between the mean square of the interaction and the mean square of the measurement error (Leamy, 1984; Palmer & Strobeck, 2003). Decomposition of the symmetrical and asymmetrical components of variation was performed with SAGE (Márquez 2007a).

The among-partition correlation matrix—The six partitions of landmarks and semilandmarks defined above (Fig. 3.3) were also used in analyses to explore the structure of integration. The full landmark configuration for *P. segmenta* was subsetted into these partitions using the VisProto8 software (Sheets, 2014). For each partition, pairwise Procrustes distances between all specimens were calculated for both the Individuals (symmetrical) components and the FA components of variation. Matrix correlations were calculated between those distance matrices, resulting in correlation matrices for each component of variation that show the degree of covariation between the partitions in terms of shape variation among all specimens. This "among-partition correlation matrix" (Webster and Zelditch, 2011a, 2011b) was calculated in CORIANDIS (Marquez, 2007b) and used in subsequent analyses to assess the structure of integration in *P. segmenta*.

Determining the contribution of direct interactions among developmental pathways to phenotypic integration—The extent to which phenotypic variation is controlled by direct interactions among developmental pathways is shown by the correlation between the Individual component and FA component of variation. A high correlation indicates a strong influence of direct interactions on phenotypic variation whereas a low value indicates that integration among traits arises primarily through parallel variation. Matrix correlation was performed on the among-

partition correlation matrices for each component of variation, testing the significance of the observed correlation with a Mantel test with 1000 permutations in R using the "vegan" package (Oksanen et al., 2019). This tests the null hypothesis that the two matrices are no more similar than expected by chance (R_M=0). In addition to the conventional Mantel test, a complementary procedure that uses a parametric bootstrap to test an alternative null hypothesis that the matrices are no more different than expected by chance, and therefore the matrices are statistically indistinguishable (R_M=1), was performed in R (Annat Haber, unpublished code).

The same methods were employed when determining if covariation arising from direct interactions among developmental pathways is more phylogenetically conserved than that arising from parallel variation. First the among partition correlation matrices for the FA components of variation (that which is controlled by direct interactions), and then the components for symmetric variation, were compared between each species. A higher correlation value between the FA components of each species relative to that of the Individuals components of each species would indicate that the former is less variable through time, supporting the conclusion that trait covariations controlled by direct interactions are, indeed, more temporally conservative and may serve as a long-term constraint on morphological variation.

Hierarchical cluster analyses—Cluster analyses are often used in studies to explore patterns of integration and modularity (e.g., Cheverud, 1982; Atchley, 1993; Monteiro et al., 2005; Goswami, 2006; Zelditch et al., 2008; Goswami and Polly, 2010; Webster and Zelditch, 2011a). These methods propose a structure of integration based on cluster distances, requiring the definition of a distance metric and a linkage algorithm in order to generate those clusters. Euclidean distance was the metric used here as it describes the shortest distance between two

objects. The among-partition correlation matrices for the Individuals and FA components were used in hierarchical cluster analyses and the linkage algorithms employed are those that are most often used in integration studies (Goswami and Polly, 2010): unweighted pair-group average (UPGMA, Farris, 1969) and Ward's method (Ward, 1963) of hierarchical clustering. Hierarchical clustering and the associated metrics were calculated using the 'cluster' package in R (Maechler et al., 2018).

Reticulate network analysis—Reticulate network analysis is a complement to cluster analyses, as it is an additive approach that relaxes some of the constraints on distances between and within clusters that are seen in hierarchical clustering methods, allowing an object (here, a partition of the landmark configuration) to belong to more than one cluster. This method utilizes a least-squares approach that minimizes the squared deviations between the original dissimilarities and the reticulation distances. Reticulations are only added to tree if it minimizes the conservative Q1 optimization criterion (Zelditch et al., 2008, 2009). This analysis was conducted in T-REX v.4.0a1 (Makarenkov, 2000).

Graphical modeling—Graphical modeling, as described by Magwene (2001, 2008, 2009) and implemented in many subsequent studies of integration and modularity (e.g., Zelditch et al. 2009, Webster and Zelditch 2011a, 2011b), is the final method used to explore the structure of integration in this species. This method discovers modules by calculating conditional independence between traits which is then expressed in a graphical representation of modularity with vertices representing traits (in this case, partitions) that are connected by edges, the strength of which are based on high partial correlations. The practical application of this method uses the

inverse of the among-partition correlation matrix, in which each diagonal element is related to the multiple correlation coefficient between one trait and all others (Whittaker, 1990). The details of this method can be found in Chapter 2. Stepwise heuristic searches were conducted to find the model with the fewest edges. As it is common for this sort of search to result in different models being preferred, the search was conducted three times for each component to confirm a consistent result. The search parameters were defined as headlong (edges considered in random order), bidirectional (edges able to be added and deleted), and unrestricted (allowing edges that were previously removed to be reconsidered). Edge strengths were calculated with the partial correlation coefficients derived from the among partition correlation matrix (Appendix C, Table C.4) and following the procedure described by Lawler (2008) in which values greater than 0.025 are considered strong. Graphical modeling analyses were performed using MIM v.3.2.0.7 (Edwards, 2008).

RESULTS—

Phylomorphospace—The phylomorphospace shows considerable overlap in morphospace between all of the agnostine groups included with the exception of the Condylopygidae, which separates out into its own area of morphospace on PC 1 (Fig. 3.5). Nearly half (44.1%) of the total morphological variation is summarized by the first two PC axes: PC 1(26.3%) describes the inflation of the anterior glabella and PC 2 (17.8%) captures the variation in the position of the transglabellar furrow and the size of the preglabellar field. PC 3 (11.1%) and PC 4 (8.6%) describe less than 20% of the remaining variation and primarily describe shifts in the position of the basal lobes. A scree plot can be found in Appendix C (Fig. C.2). The group of interest for this study, the Peronopsidae, covers a small region of morphospace that varies primarily along PC 1.

Moreover, Table C.6 (Apprendix C) shows that Peronopsidae accounts for 6.5% of the total morphological diversity in Agnostina (PV=0.0036, PD=0.0005), supporting the hypothesis that it is an example of a morphologically conserved group relative to other agnostine groups.

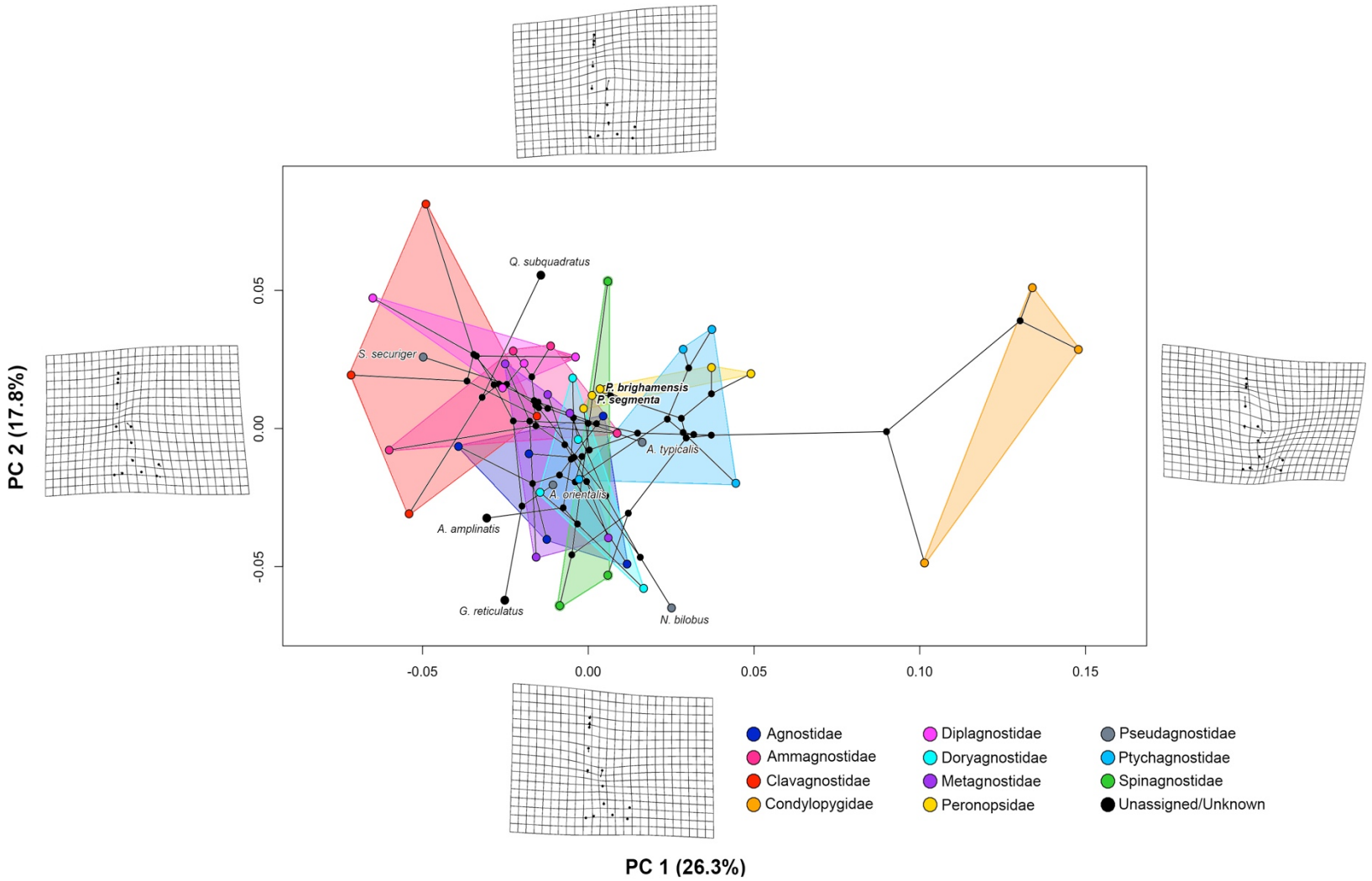

Figure 3.5—Phylomorphopace for the Agnostina. Colors denote designation in traditional agnostine families. Axes with deformation grids for variation along PC 1 and PC 2 axes are shown. P. brighamensis and P. segmenta are labeled and bolded.

Degree of integration—When analyzed with the CR, *P. brighamensis* and *P. segmenta* show similar degrees of integration in the sense that they are both less than 1(0.697 for *P. brighamensis* and 0.548 for *P. segmenta*), indicating that the covariance between modules is less than that within modules (Fig. 3.6; Appendix C, Fig. C.3). For both species, this value is significantly different from the null expectation of a CR of 1 at 95% confidence. This supports the somewhat unexpected conclusion that the degree of integration for both of these species is relatively low and more modular. *Pentagnostus segmenta* exhibits a slightly stronger degree of integration than *P. brighamensis* (Fig. 3.6), but significantly so.

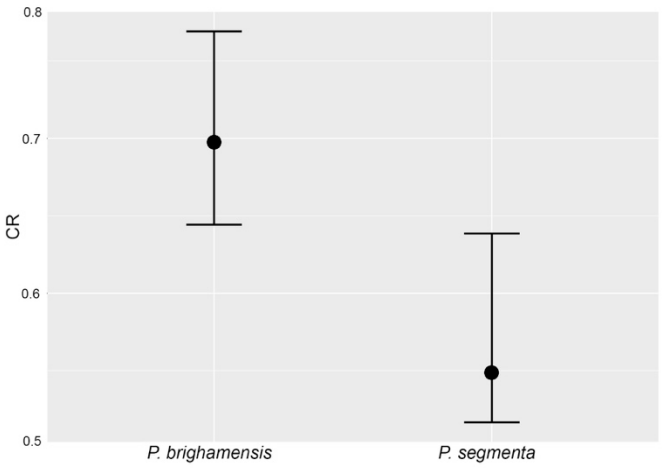

Figure 3.6—CR values for *P. brighamensis* and *P. segmenta*. 95% CI values are shown.

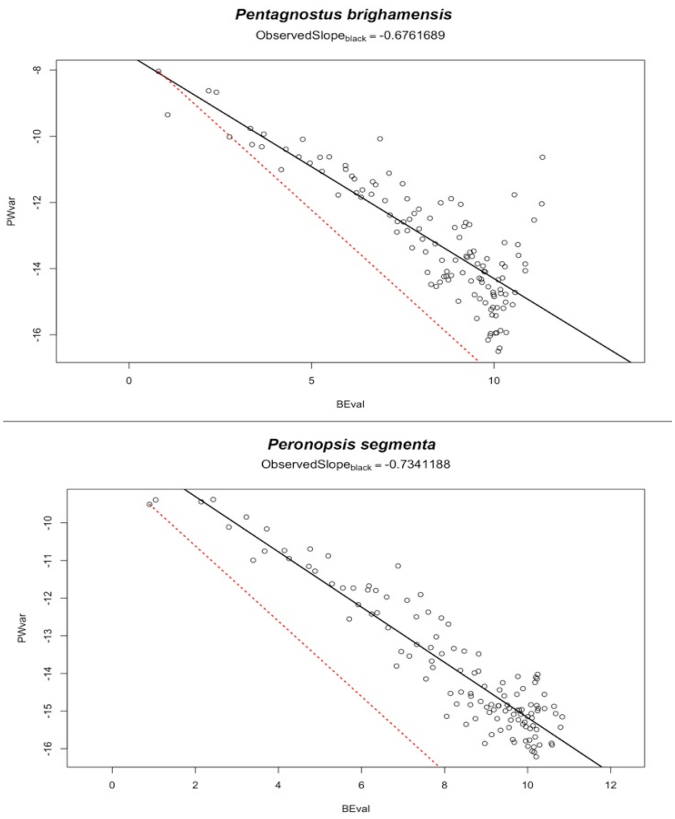

Figure 3.7—Graphs showing a metric of global integration based on Bookstein's (2015) method. PWvar = variance of the partial warps (log) and BEval = bending energy values (log). Slope of -1 (red) indicates the null of self-similarity. Slopes steeper than -1 indicate stronger integration.

The results from the Singular Warps Analysis contrast to those of the CR analysis. The r_{PLS} values for *P.*

brighamensis and *P. segmenta* are 0.767 (p=0.001) and 0.660 (p=0.001), indicating a relatively high degree of integration given this metric. *Pentagnostus brighamensis* shows a slightly higher degree of integration than *P. segmenta*, which agrees with the results from the CR analyses. However, these results should be taken with caution given the small sample sizes and large number of landmarks used.

Similar to the results of the CR analysis, the analyses that measured shape variance across spatial scales resulted in shallow slopes (Fig. 3.7). Slopes for *P. brighamensis* (-0.676) and *P. segmenta* (-0.734) are both more shallow than the null of -1, indicating that neither species exhibits a strong signal of integration.

Table 3.1—Results of the two-factor mixed model ANOVA. SS = sum of squares; d.f. = degrees of freedom; MS = mean square. See text for interpretation.

Effect	SS	d.f.	MS	F-value	P-value	% Variance
Individuals	0.153	5125	2.98E-05	44.4551	<0.0001	96.8%
Sides	0.001	125	4.28E-06	6.3802	<0.0001	0.3%
Individuals x Sides	0.003	5125	6.70E-07	6.6714	<0.0001	2.2%
Measurement Error	0.001	10500	1.00E-07	—	—	0.7%
Total	0.158					100.0%

Components of variance for *Pentagnostus segmenta*—A vast majority of variation (> 96%) in the sample of *P. segmenta* is attributed to symmetric variation as described by the Individuals

Table 3.2—Among-partition correlation matrix for the Individuals (lower triangle) and FA (upper triangle) components of variation. Bolded values are significant at 95%. Results of significance testing can be found in Appendix C (Table C.2).

	Anterior glabella	Transglabellar furrow	Anterior posteroglabella	Medial posteroglabella	Posterior posteroglabella	Basal lobes
Anterior glabella		**0.584**	**0.405**	0.278	**0.596**	**0.340**
Transglabellar furrow	**0.463**		**0.351**	0.112	**0.514**	0.219
Anterior posteroglabella	**0.301**	**0.320**		**0.475**	0.220	**0.281**
Medial posteroglabella	**0.317**	**0.279**	**0.500**		0.240	**0.471**
Posterior posteroglabella	**0.281**	0.184	0.199	**0.442**		0.100
Basal lobes	0.183	0.159	**0.255**	0.194	**0.361**	

component, shown in Table 3.1. The Sides component accounts for a negligible proportion of the variance explained, which is expected in a bilaterally-symmetrical organism. The interaction term, Individuals x Sides, which describes the proportion of variation that is contributed by FA, explains 2.2% of the variance and is highly significant. The proportion of variance attributable to measurement error associated with replicate measures is smaller than the FA term.

The among-partition correlation matrix for both components of variation is shown in Table 3.2. The correlation values for the symmetric component of variation are given in the lower triangle of that table. The correlations between partitions of this component show a general pattern of significant correlations with neighboring partitions. The anterior glabella correlates moderately strongly and significantly with the transglabellar furrow and anterior portion of the posterior glabella. Its correlations with the medial and posterior posteroglabella regions are slightly weaker but still significant. The transglabellar furrow shows similar pattern of correlation to that shown by the anterior glabella, with significant correlations with the anterior and medial portions of the posteroglabella. The anterior portion of the posteroglabella is moderately correlated with the medial posteroglabella, and weakly (but significantly) correlated with the basal lobes. The medial posteroglabella is somewhat strongly and significantly correlated with the posterior posteroglabella. The posterior posteroglabella is significantly correlated with the basal lobes.

The among partition correlation matrix for the FA component of variation (Table 3, upper triangle) is shows a markedly different pattern of correlation. The anterior glabella correlates most strongly with the transglabellar furrow and posterior portion of the posteroglabella, and has a slightly weaker but still significant correlation with the anterior posteroglabella and basal lobes. The transglabellar furrow correlates strongly with the posterior posteroglabella. The anterior

posteroglabella correlates strongly with the neighboring medial posteroglabella and more weakly with the basal lobes. The medial posteroglabella also correlates strongly and significantly with the basal lobes.

Table 3.3—Results from the Mantel tests on the correlation between the Individuals and FA components of variation for *P. segmenta*. Both hypotheses $R_M = 0$ and $R_M = 1$ were tested. The high values indicate the strong contribution of direct interactions.

Observed matrix correlation	Adjusted matrix correlation	Repeatability		Probability of matrices being indistinguishable	
		Individuals component	FA component	Individuals component	FA component
0.147	0.189	0.714	0.855	0	0.04

Contribution of direct interactions—Table 3.3 shows that the among-partition correlation matrices for the Individuals and FA components of variation for *P. segmenta* are very weakly correlated, with an observed non-significant correlation of 0.147 (p=0.313). The observed correlation value can be adjusted given the repeatability for each matrix (0.714 and 0.855, respectively) to a value of 0.189. The alternative null model shows that the probability that the matrices for each component differ no more than expected by chance is 0 (Individuals component) and 0.04 (FA component). These results suggest that direct interactions among developmental pathways make only a weak contribution to the structure of (symmetric) phenotypic variation in this species.

When comparing the respective components of variation between species in order to determine the relative phylogenetic conservatism of patterns of covariation controlled by direct interactions, the correlation values for each component do not support the hypothesis (Table 3.4). The observed correlation value for the FA components of *P. brighamensis* and *P. segmenta* is low (0.077) and non-significant (p=0.413), even when adjusted for repeatability (0.090).

Table 3.4— Results from the Mantel tests on the correlation between the FA components of variation for P. brighamensis and P. segmenta (upper) and for the correlation between the Individuals components (lower). Both hypotheses $R_M = 0$ and $R_M = 1$ were tested. Significance testing for $R_M = 0$ generated a p-value of 0.413 (FA) and 0.014 (Individuals)

FA Components					
Observed matrix correlation	Adjusted matrix correlation	Repeatability		Probability of matrices being indistinguishable	
		P. brighamensis	*P. segmenta*	*P. brighamensis*	*P. segmenta*
0.077	0.090	0.910	0.804	0.000	0.002
Individuals Components					
Observed matrix correlation	Adjusted matrix correlation	Repeatability		Probability of matrices being indistinguishable	
		P. brighamensis	*P. segmenta*	*P. brighamensis*	*P. segmenta*
0.585	0.780	0.874	0.645	0.077	0.775

Conversely, the observed correlation value of the Individuals component is moderately high (0.585), and even higher in light of repeatability (0.78) and is significant (p=0.014). This is contrary to the expectation that covariation patterns that arise from direct interactions should be more stable over time relative to those that arise from parallel variation.

Hierarchical cluster and reticulate network analyses—Results from hierarchical cluster analyses for both components of variation are shown in Appendix C (Figure C.4). The dendrograms for both components show AC values that are less than 0.55 across methods, which indicates that the hierarchical structure is weak in all cases. The highest CC value (0.83) is shown in the FA

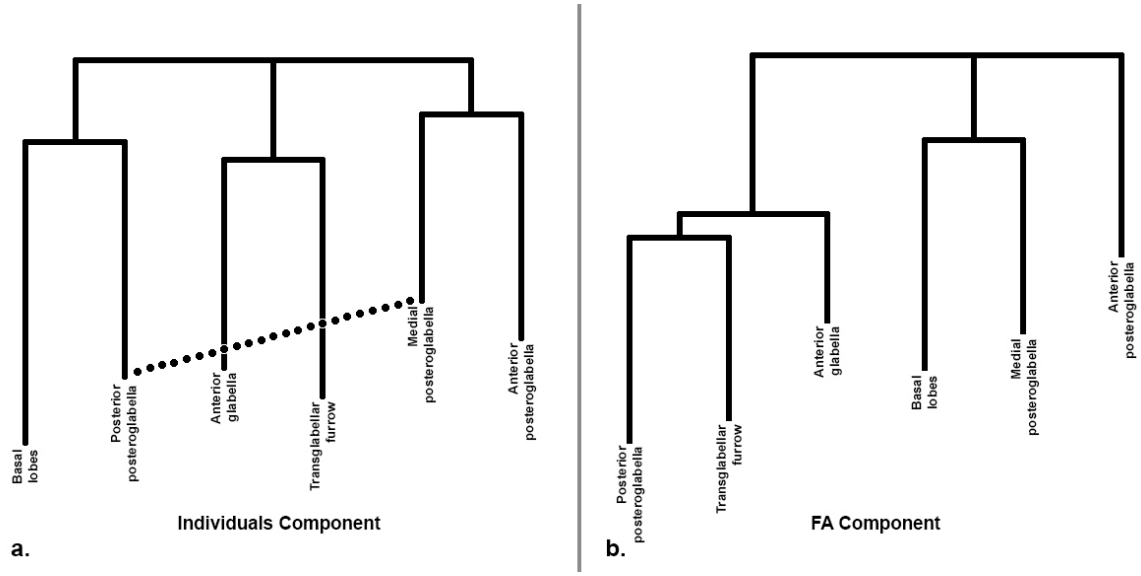

Figure 3.8—Reticulograms for a) the Individuals component and b) the FA component. Dotted line indicates a reticulation that has been added

dendrograms calculated using both method, which is below the threshold (0.85) at which the dendrograms would be considered as adequately reflective of the data.

The reticulograms (Fig. 3.8) for both components recover a very similar structure to that of the hierarchical cluster analyses. The reticulogram for the Individuals component (Fig. 3.8a) recovers a cohesive grouping of [Anterior glabella + Transglabellar furrow], [Anterior posteroglabella + Medial posteroglabella], and [Posterior posteroglabella + Basal lobes]. A reticulation has been added which indicates that the Posterior posteroglabella and Medial posteroglabella also covary strongly. The reticulogram for the FA component (Fig. 3.8b) also shows a similar structure to the dendrograms produced with the clustering methods. The cluster of [Medial posteroglabella + Basal lobes] is recovered. A group of [Anterior glabella [Transglabellar furrow + Posterior posteroglabella]] is shown, which is only slightly different than the topology recovered with the cluster analyses. The Anterior posteroglabella is shown as being the farthest removed and no reticulations were added to the grouping structure of the FA component.

Graphical modeling—The heuristic searches recovered a single supported graphical model for each of the components of variation. The Individuals component (Fig 3.9a) is depicted as being comprising modules that succinctly describe the anterior glabella and posterior glabella: [Anterior glabella + Transglabellar furrow] and [Anterior posteroglabella + Medial posteroglabella + Posterior posteroglabella + Basal lobes]. This structure is in agreement with the other analyses presented in this study.

The graphical model recovered for the FA component (Fig. 3.9b) is shows a different structure composed of two main modules: [Anterior glabella + Transglabellar furrow + Posterior

posteroglabella] and [Anterior posteroglabella + Medial posteroglabella + Basal lobes]. The recovered structure is in agreement with previous analyses. The sets recover an interesting and recurring link between anterior elements and posterior elements of this agnostine glabella. Test statistics for all of the edges included for each model (Appendix C, Tables C.5), in addition to the matrices used in this analysis (Appendix C, Table C.3) can be found in the appendix.

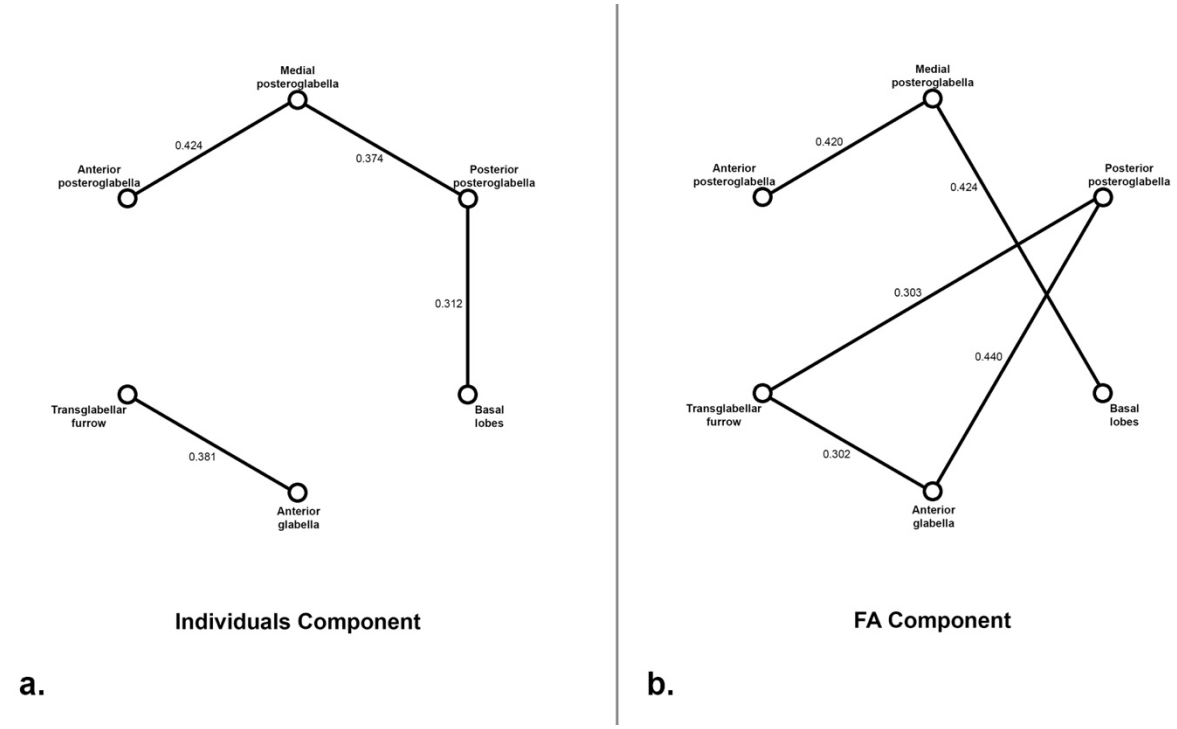

Figure 3.9—Graphical models generated for a) the Individuals component; and b) the FA component of variation. Labeled vertices represent partitions of interest, bolded lines indicate edge strengths > 0.025. Partial correlation values are labeled next to corresponding edges.

Inferred structure of integration—The *a posteriori* hypothesis of the structure of integration for the symmetric component of variation among individuals that is based on all analyses is shown in Figure 3.10a. Strong associations between the anterior glabella and transglabellar furrow are supported by all analyses, and are therefore depicted as a single module. An association between the anterior posteroglabella and medial posteroglabella is often detected, but there are variable

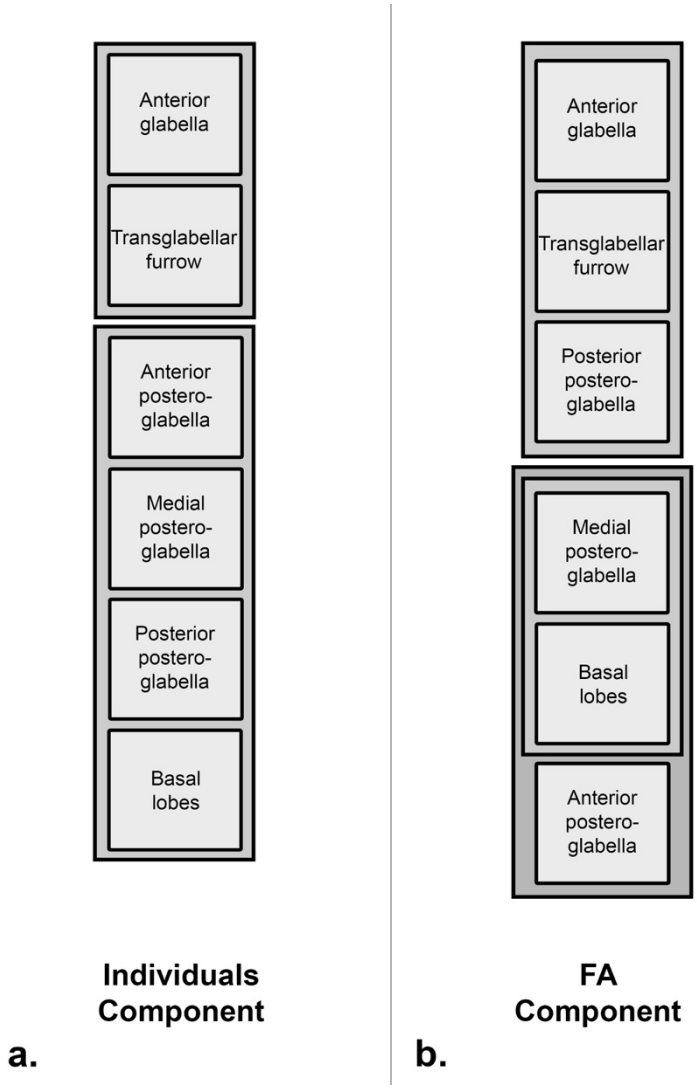

Figure 3.10—Inferred models of the structure of integration for the a) Individuals component and b) FA component. Labeled interiormost boxes designate partitions whereas enclosing boxes represent the modular structure.

associations with the other regions of the posteroglabella as well, leading to the conclusion that the two-module model as recovered in the graphical modeling analysis most accurately reflects the data.

The inferred structure of FA is summarized in Figure 3.10b. This model is also composed of two main modules, but differs markedly in its structure compared to that of the Individuals component. The [Anterior glabella + Transglabellar furrow + Posterior posteroglabella] set is

consistently recovered in all analyses, suggesting conditional dependence. Similarly, the association between the medial posteroglabella and basal lobes is consistently recovered with a slightly weaker, but consistent, link to the anterior portion of the posteroglabella. Thus the modular structure is inferred to comprise two modules: one composed of the elements associated with the anterior glabellar region plus the posterior portion of the posteroglabella, and the second composed of a nested structure of [Medial posteroglabella + Basal lobes] linked with the anterior portion of the posteroglabella.

DISCUSSION—

Degree of overall integration—The level of integration in the two peronopsid species analyzed is relatively low in two of the three analyses performed. Both the CR and the shallow slope of the global integration analysis provide evidence for weak integration in the glabella of *P. brighamensis* and *P. segmenta*. This result is contrary to expectations as it suggests that developmental constraints did not play a role in the morphological conservatism that is seen in this clade. Conversely, the results of the Singular Warps Analysis suggest a strong signal of integration in this species; however, the small sample sizes and large number of landmarks used may have greatly-inflated correlation values (Adams and Collyer, 2016).

Contribution of direct interactions—Another surprising outcome from this study is the markedly different sources of trait covariation for the two peronopsid species. The older species, *P. brighamensis*, has been shown to exhibit an integration structure that was strongly influenced by direct interactions (R_M=0.72). This result seemed reasonable as peronopsids show little phenotypic variation throughout their history, as is shown in the phylomorphospace. Therefore

developmental constraints might be expected to play a role in maintaining that phenotype. In *P. segmenta*, comparison of the correlation structures between the symmetric component of variation among individuals and that which describes FA suggest that parallel variation was the primary influence on the structure of phenotypic variation (R_{Madj}=0.19). While this result is unexpected in terms of agnostine disparification, they are similar to the findings of Webster and Zelditch (2011a, 2011b) in which the structure of phenotypic variation in the cranidium of ptychoparioid trilobites was also shown to be driven by parallel variation.

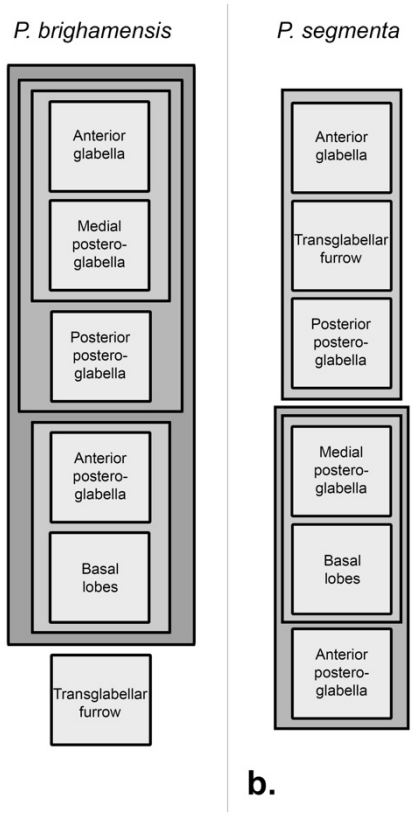

Figure 3.11—Inferred models of the structure of integration for the FA component of a) *P. brighamensis*; and b) *P. segmenta.*

These results should be interpreted with caution given the outcome of the comparison of the components of variation between species, which show that the covariations that are due to direct interactions among developmental pathways may not be as stable over long periods of time as was previously expected. The seeming lack of phylogenetic conservatism in the structure of FA within a relatively short-lived clade is likely due to a very weak FA signal relative to that of the symmetric component of variation.

Comparison of Integration Structures—The low correlation value between the FA component and Individuals component for *P. segmenta* indicates that the spatial structures of covariation between those components are markedly different. The structure of integration within each

component is consistent across all methods, coalescing into two inferred structures that are well-supported (Fig. 3.10). The Individuals component of variation exhibits clear covariation of adjacent partitions, indicative of "neighborhood effects": neighboring regions of anatomy showing shared patterns of variation due to localized morphogenetic controls. This structure stands in stark contrast to the expression of the FA component, which shows a nested module of posteroglabellar elements and a module consisting of regions associated with the anterior glabella linked with the posterior posteroglabella. While statistically different, the inferred structure of integration resulting from direct interactions among developmental pathways for P. *brighamensis* and *P. segmenta* do show a consistency that is notable (see Fig. 3.11). A module composed of anterior and posterior regions of the glabella is recovered, which is a pattern that is consistently seen in both in the agnostoids studied and in ptychoparioid trilobites (Webster and Zelditch (2011a, 2011b). It has been suggested this anterior-posterior link could be related to *Hox* gene expression. However, while such models have been suggested for trilobites (Sundberg, 2000; Hughes, 2003), a more complete model for *Hox* expression domains would be necessary in order to test this hypothesis in any detail. The recovery of this pattern in both agnostine taxa and trilobites suggests that this may be deep common trait of Artiopoda, or at least of the clade that unites Trilobita and Agnostina (see Moysiuk and Caron, 2019).

Caveats and Future Work—Several weaknesses of this study should be noted. As in the previous study of *P. brighamensis*, the results herein rely on the *a priori* definition of partitions. The boundaries of the partitions were based on common anatomical features of the agnostine glabella, but the boundaries between partitions do not allow for overlap. It is possible that correlation of neighboring partitions could be artificially inflated if there was not adequate

subdivision of the region. The second caveat is that the FA signal in the data for both species is very weak compared to that of the symmetric variation, therefore the structure of integration for this component should therefore be considered with caution. In addition to a weak signal in the data, this study has called into question the idea that direct interactions act as long-term constraints at all; however as noted, the recovered pattern may be more due to specimen distortion. The final weakness of this study is the fact each taxon represents a point sample within that species range. Given the markedly contrasting degrees and structures of integration in each of the taxa included in this study, it is possible that patterns of integration vary throughout a species range. Furthermore, it is reasonable to expect that these patterns may be predictable: populations of a species sampled closer to the origin of that species might show more lability than those sampled later. It might also be expected that species exhibit greater lability at points of branching speciation or anagenesis. These hypotheses have not been explicitly tested and in order to do so, it would be necessary to sample a taxon at multiple time slices and compare the patterns of integration between the populations.

CONCLUSION—

While Peronopsidae represents a morphologically conserved clade relative to all other non-effaced groups of agnostines, its phenotypic conservatism is not a result of constraints imposed by a high degree of integration. The opposite has been shown: the peronopsid species studied exhibited low overall levels of integration. Moreover, direct interactions among developmental pathways, as opposed to external drivers of trait covariations, are not shown to generate the structure of phenotypic integration seen in *P. segmenta*. This result was surprising given that direct interactions were found to be the dominant source of integration in *P.*

brighamensis. While phylogenetic stability of integration structures that are driven by direct interactions is not observed in this study, this may be a result of a weak FA signal that is difficult to reliably interpret. This study also highlights the importance of sampling throughout a taxon range in order to gain an understanding of how these patterns evolve within a species; which is a line of inquiry that can only be pursued by utilizing the fossil record. Despite these caveats, a robust general pattern in the structure of integration has been recovered, manifesting in covariation of anterior and posterior elements of the agnostine glabella. This is an encouraging result that further supports this as a characteristic common throughout Artiopoda.

CONCLUSIONS

Agnostina is a notoriously problematic clade in terms of systematic classification given their conserved morphologies and their lack of reliable diagnostic characters; however, its tractable temporal range and abundance of well-preserved fossil material make it a good study system to pursue questions relating to disparification. Here I presented a three-part investigation of Agnostina and explored the role of phenotypic integration acting as a constraint on morphological diversification. Chapter 1 presented a large-scale exploration of the Agnostina through Bayesian and parsimony-based methods to determine the phylogenetic support for the existing taxonomic framework of the group. It was determined that several agnostine rank-based groups are supported, including the Ammagnostidae, Clavagnostidae, Metagnostidae, Spinagnostidae, and Condylopygidae. Despite some topological inconsistencies, Diplagnostidae, Doryagnostidae, Peronopsidae, and Ptychagnostidae were moderately supported while Agnostidae and Pseudagnostidae failed to consistently coalesce into corresponding clades. Future phylogenetic analyses that include thoracic, ventral, and soft tissue characters are suggested to resolve ingroup agnostine relationships and aid in the polarization of characters when resolving affinities to other arthropod groups. Since there was weak support for deep branching patterns among agnostine clades, bottom-up approaches followed by supertree methods may be necessary to examine the relationships between agnostine clades.

The following two chapters investigated the structure and degree of phenotypic integration in two taxa representative of Peronopsidae: *Pentagnostus brighamensis* and *Pentagnostus segmenta*. Chapter 2 presented an investigation into the structure of integration in *P. brighamensis*, with results indicating that direct interactions among developmental pathways influenced the structure of integration in this species. The final chapter presented a

phylomorphospace and associated disparity metrics that supported the hypothesis that Peronopsidae represents a morphologically conserved clade relative to other non-effaced agnostine groups. It was shown that despite being a morphologically conserved group, the two peronopsid taxa studied show a relatively high degree of modularity and as such, their phenotypic conservatism is not a result of constraints imposed by a high degree of integration. The structure of phenotypic integration was evidenced to be conserved between these sister taxa; however they were not characterized by phenotypic integration acting as long-term constraint on patterns of disparity in that clade, suggesting that the structure of integration driven by direct interactions may be labile. Notably, both peronopsid taxa show a coupling of anterior and posterior regions of the glabella, which is similar to a pattern that has been recovered in trilobites, suggesting that this characteristic structure may be present throughout Artiopoda and perhaps indicative of axial patterning related to early *Hox* gene expression.

Future directions of this research may involve the comparison of these results to those that examine a more disparate agnostine clade such as Clavagnostidae, or expanding the scope of investigations to include other groups of artiopodan affinity. As the results of this study have suggested that the structure of direct interactions may be labile on relatively short timescales, it would be worthwhile to explore these patterns within a single species through time. This endeavor would determine if the degree and structure of integration different at the genesis of a species versus its optimum or near the end of its temporal range. The results presented here and subsequent related studies are examples of how the fossil record can provide a means to directly test evolutionary hypotheses, an opportunity that is not afforded by the study of solely extant taxa.

APPENDIX A:

SUPPLEMENTAL INFORMATION FOR CHAPTER ONE

This appendix contains a list of the characters and character states used in phylogenetic analyses of the Agnostina, a brief discussion of terminology (Figure A.1), characters excluded, a table of values for continuous characters and the discretized equivalents (Table A.1), tables that contain the historic cephalic (Table A.2) and pygidial (Table A.3) diagnostic traits for Agnostina, a table of stage and specimen references (Table A.4), the fully discretized character-taxon matrix (Table A.5), the MCC tree with posterior values (Figure A.4), and alternative topologies as described in the main text (Figures A.5-A.8).

List of characters and character states—

All applicable characters from Westrop et al., 1996, Cotton and Fortey, 2005, and Laurie, 2008 have been included with the exception of those that require lateral specimen views. Continuous characters are listed with their discretized equivalents in Table A.1. Terminology is based on Shergold et al., 1990 (Figure A.1).

* Indicates characters used in Westrop et al., 1996; † indicates characters used in Cotton and Fortey, 2005; ‡ indicates characters used in Laurie, 2008.

1. †Spines on the posterior cephalic border. 0: Absent, 1: Present.
2. †Length of posterior border spine. 0: Short (approximately half or less the distance from axial furrows to genal angles), 1: Long (equal to or greater than distance from axial furrows to genal angles).

3. †Shape of cephalic outline in dorsal view. 0: Semicircular (maximum width in posterior 0.25 of length), 1: Rounded (maximum width approximately at cephalic mid-length), 2. Quadrate (maximum width anterior to mid-length)
4. †Shape of cephalon. Sagittal length, excluding glabellar or occipital spines, as a proportion of maximum width in dorsal view. 0: <0.82; 1: 0.82-0.92; 2: >0.92
5. †Position and angle of cephalic border spines. 0: at genal angles, directed posterolaterally at 45 degrees; 1: adaxial to genal angles
6. †Size of anterior border. Width of border and furrow in dorsal view as a proportion of cephalic length (sag.). 0: <0.05; 1: 0.05-0.07; 2: 0.08-0.10; 3: 0.11-0.15; 4: >0.15
7. *†Cephalic border narrower (exsag.) posteriorly than anteriorly in dorsal view. Border, not including furrow, is wider in the anteriormost portion. 0: Absent, 1: Present.
8. Cephalic border flares laterally. Border width (exsag.) increases. See *Quadragnostus*. 0: Absent, 1: Present.
9. Size of preglabellar field. Width of preglabellar field as a proportion of total cephalic length. 0: <0.08; 1: 0.08-0.14; 2: 0.14-0.23; 3: >0.23.
10. *†‡Sagittal preglabellar furrow. 0: Absent, 1: Present.
11. Preglabellar furrow meets border. 0: Absent, 1: Present.
12. *Cephalic F2 furrow development. 0: Effaced 1: Weak, shallow furrow; 2: Strong, deep furrow.
13. *†‡Basal lobe shape. 0: Short, subtriangular; 1: Elongate; 2: Complex, lobate
14. †Basal lobe size. Length of basal lobes as proportion of glabellar length.

0: <0.12; 1: 0.12-0.17; 2: 0.17-0.26; 3: >0.26.

15. †Basal lobes divided from median band of occipital ring. 0: Absent, continuous band; 1: Weakly-divided, subtle change in concavity; 2: Fully divided.
16. †Transglabellar furrow shape. 0. Straight; 1: Deflected posteriorly; 2: Deflected anteriorly.
17. †Transglabellar furrow development. 0: Effaced; 1: Interrupted; 2: Well-developed.
18. Length of glabella. Sagittal distance from base of cephalon to anterior termination of the glabella as a proportion of sagittal cephalic length (excluding anterior border), in dorsal view. 0: <0.79; 1: 0.79-1.0; 2: >1.0.
19. Length of anteroglabella. Measured as a proportion of glabellar length. 0: <0.28; 1: 0.28-0.42; 2: >0.42
20. *Posteroglabellar width. Maximum posteroglabellar width as proportion of maximum cephalic width. 0: <0.49; 1: 0.49-0.64; 2: >0.64
21. †Anterior glabella lobe expanded laterally. See Condylopygidae. 0: Absent; 1: Present.
22. Anterior glabella constricted laterally. See *Neoagnostus*. 0: Absent; 1: Present
23. †Shape of the anterior termination of glabella. 0: rounded, 1: pointed/ogival; 2: flat/truncated.
24. *Frontal sulcus on glabella. See Shergold et al., 1990, p. 12, fig. 2. N/A for character 23(1). 0: Absent; 1: Present.
25. *Definition of anterior glabella. 0: Effaced; 1: Defined.

26. †Type of cephalic border furrows. Simple change in convexity (nondeliquiate) vs. channel-like (deliquiate). 0: Nondeliquiate; 1: Deliquiate

27. †Cephalon scrobiculate. 0: Absent; 1: Present .

28. *‡Glabellar node. 0: Absent, 1. Present, weak/low relief; 2: Present, strong/high relief.

29. *‡Position of glabellar node: 0: M2; 1: M3; 2: Both.

30. ‡ Occipital posteroglabella shape. Shape of the occipital portion of the posteroglabella. 0: Rounded; 1: Tapered, pointed; 2. Flat.

31. *†‡Posteroglabellar shape. Describes the expansion of the posteroglabella. 0: cylindrical; 1: Expanded, ovate.

32. Glabellar “lobes”. F1 and F2 meet the lateral glabellar furrows, shaping the outline of the glabella. 0: Absent; 1: Weakly lobate, furrows shallow; 2: Strongly lobate, furrows deep.

33. *‡Appendiferal pits. Pits that develop at the anterior portion of the basal lobes where they meet the glabella. See *Criotypus.* 0. Absent; 1: Present.

34. †Occipital node. 0: Absent; 1: Present.

35. Deltoid depression. Depression that forms below anterior border on the sagittal axis. See *Diplagnostus*. 0: Absent; 1: Present.

36. Sagittal node/swelling on border. See *Oidalagnostus.* 0: Absent; 1: Present

37. *Glabella effaced. An extension of character 25. 0: Absent; 1: Anterior glabella effaced compared to posterior glabella (see *Euagnostus*); 2: Entirely effaced (See *Lejopyge*).

38. Shoulder angle. Angle that describes the intersection of the posterior border furrow and the lateral border furrow, measured relative to the sagittal axis. 0: <70°; 1: 70°-79°; 2: >79°.

39. †Pygidial axis reaches border furrow. 0: Absent; 1:Present.

40. †Width of pygidial border. Width of pygidial border and furrow as a proportion of length of pygidium (sag. in dorsal view). 0: <0.05; 1: 0.05-0.08; 2: 0.08-0.12; 3: 0.12-0.19; 4: >0.19.

41. *Sagittal postaxial furrow on pygidium. 0:Absent; 1: Present.

42. Postaxial furrow reaches border. Requires character 41(1). 0: Absent; 1: Present.

43. Median gap. Postaxial furrow meets the border furrow to create a triangular gap in the pygidial collar. Requires character 41(1). 0: Absent; 1: Present.

44. ‡ Development of pygidial F1. 0: Effaced, 1. weakly-developed, shallow furrow; 2: strong, deep furrow.

45. *Shape of pygidial F1 furrow. 0: Subtransverse 1: Deflected anteriorly relative to M1; 2: Anterior portion of furrow subvertical.

46. ‡Axial node divides M1. 0: Absent; 1: Present.

47. ‡ Development of pygidial F2. 0: Effaced, 1. Weakly-developed, shallow furrow; 2: Strong, deep furrow.

48. *Shape of pygidial F2 furrow: 0: Subtransverse; 1: Deflected anteriorly relative to M1; 2: Deflected posteriorly relative to M1.

49. M1 lobes. Describes the state of the exsagittal furrows on M1. 0: effaced; 1: Lobes defined, but not inflated; 2: Lobes inflated.

50. Length of M1. Measured as a proportion of total pygidial length (sag.). 0: <0.17; 1: >0.17.

51. Width of M1. Measured as a proportion of maximum pygidial width. 0: <0.4; 1: >0.4.

52. Length of M2. Measured as a proportion of total pygidial length (sag.). 0: <0.15; 1: 0.15-0.22; 2: 0.22-0.32; 3: >0.32.

53. *†‡Transverse depression. This describes the presence or absence transverse depression associated with the secondary pygidial axial node. 0: Absent, 1: Present.

54. Form of transverse depression. Describes the degree of definition of the furrow. 0: Weak, change in concavity (see *Doryagnostus*); 1: Strong, change in concavity (See *Goniagnostus*); 2: Strong, channel-like (see *Glyptagnostus*).

55. Transverse sulcus. The presence or absence of a deep, horizontal pit at the transverse depression. 0: Absent; 1: Present.

56. Posteroaxial fossae. Pair of exsagittal pits that form in the posterior axis. See *Clavagnostus*. 0: Absent; 1: Present.

57. Longitudinal furrows. Exsagittal furrows that may or may not develop from fossae. Presence or absence noted, but homology is not assumed. 0: Absent; 1:Present.

58. *Posterior axis shape. 0: Ogival; 1: Subovate; 2: Triangular/lanceolate; 3: Rectangular.

59. *Expansion of posterior axis. Lateral swelling of the axis below F2. 0: Absent; 1: Present.

60: Constricted acrolobes. Posteroaxis expanded laterally to the point of meeting lateral pygidial furrows. See *Oidalagnostus*. 0: Absent; 1: Present.

61. †Type of pygidial border furrows. 0: Nondeliquiate; 1: Deliquiate.

62. Pygidial axis width. Width of posteroaxis as a proportion of maximum width of pygidum. 0: <0.34; 1: 0.34-0.56; 2: >0.56.

63. †Postaxial space. 0: Absent, 1: Present.

64. Size of postaxial space. As a proportion of pygidial (sag.) length. Requires 63(1). 0: <0.05; 1: 0.05-0.12; 2: 0.12-0.22; 3: >0.22

65. *Axial node. 0: Absent; 1: Small (ends before F2 in dorsal view); 2: Large (overhangs F2 in dorsal view, spinelike).

66. *Pygidial border spines. 0: Absent, 1: two spines; 2: three spines.

67. Length of pygidial border spines. Requires 66(1, 2). 0: short (<25% sag. pygidial length); 1: long (>25% pygidial length).

68. Secondary axial node. If there is a secondary pygidial axial node on the posteroaxis and where it is located. 0: Absent; 1: Anterior; 2: Medial; 3: Posterior; 4: Terminal.

69. Length of pygidial axis. Length of pygidial axis (sag. distance from base of pygidium to posterior termination of the axis) as a proportion of sag. pygidial length (excluding posterior border), in dorsal view. 0: <0.87; 1: >0.87.

70. †Shape of pygidium. Sagittal length of pygidium, excluding spines, as a proportion of maximum width in dorsal view. 0: <0.82; 1: 0.82-0.98; 2: >0.98.

71. Pygidium effaced. 0: Absent; 1: Present.

72. Accessory lobules. Lateral projections from the anterior portion of the posteroaxis, as in *O. trispinifer*. 0: Absent; 1: Present.

73. Auxiliary border furrow. Secondary furrow within pygidial collar. See *Oedorhachis*. 0: Absent; 1: Present.

74. Auxiliary furrow development. Requires character 73(1). 0: short (less than half the distance from sag. axis to lateral furrow); 1: incomplete (approx. genal spines, does not meet lateral furrow); 2: full (continuous with lateral furrow).

75. Pygidial collar/ridge. Curved ridge on the inner side of posterior border. Absent; 1: Present.

76. Postaxial furrow splits collar/ridge. Does not necessarily develop a median gap. 0: Absent; 1: Present.

77. *Length of posteroaxis. Measured as a proportion of total pygidial length (sag.). 0: <0.4; 1: 0.4-0.5; 2: 0.5-0.64; 3:>0.64.

78. Truncated posteroaxis. Termination of the posteroaxis at the transverse depression. 0: Absent; 1: Present.

79. †Pygidial border narrower anteriorly than posteriorly. 0: Absent; 1: Present.

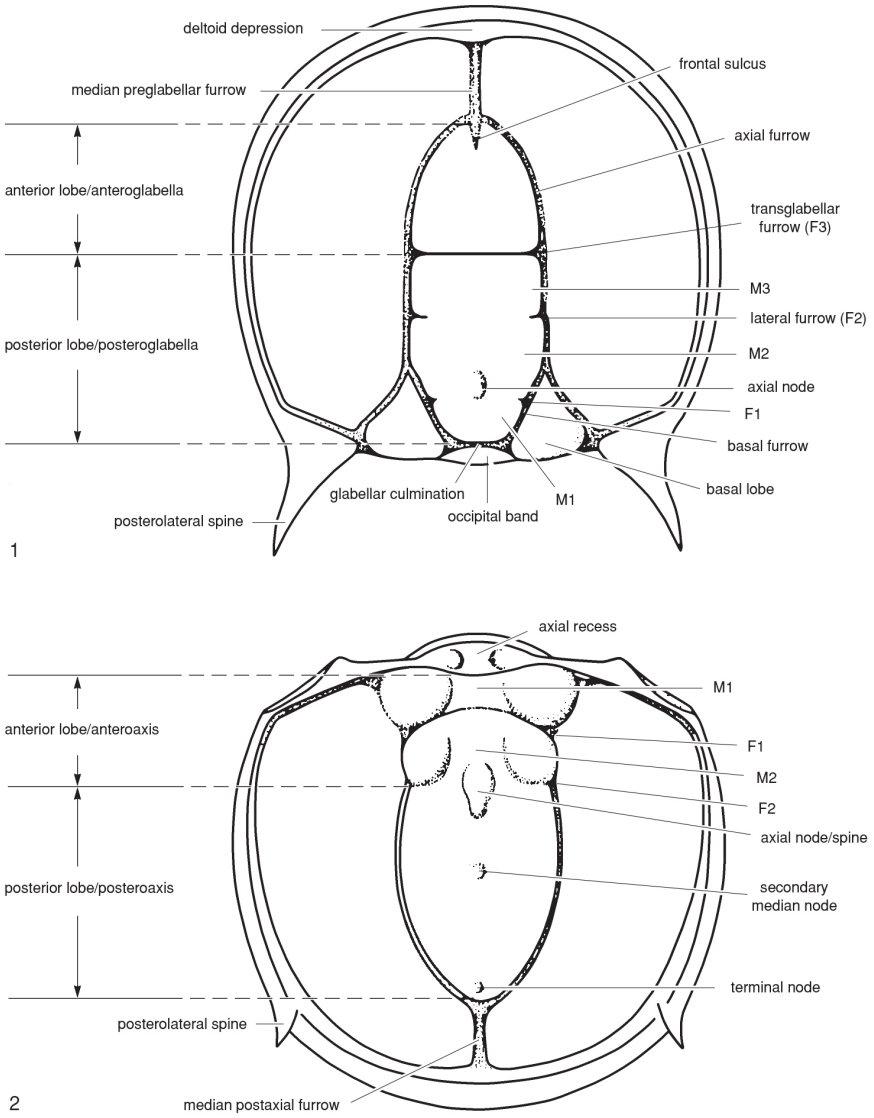

Figure A.1 —Agnostine anatomy and associated terminology, from Shergold et al., 1990 p. 18, figure 2.

Terminology—

Two characters that have previously been noted as important to species diagnosis have been excluded from this analysis. The first is the articulating device, a structure on the agnostine pygidium that joins the sclerite with the thorax, consisting of the articulating half ring, articulating furrow, and the recess in front of the axial lobe (Öpik, 1963, 1967). Four general types of this structure have been identified. The basic articulating device is seen in the Peronopsidae, Ptychagnostidae, and Spinagnostidae and consists of semicircular half ring and a narrow furrow. The glyptagnostoid structure is defined as a half-ring that is a narrow arched ridge with a furrow that is expressed as a wide elliptical depression. This type of device is noted in Diplagnostidae, Pseudagnostidae, and species of *Glyptagnostus*. The agnostoid device as seen in the Agnostidae and Clavagnostidae is described as having a broad, arching half ring and a deep articulating furrow. The final type of articulating device is one that is only seen in species of *Xestagnostus* and is described as a simple plate. This character has not been included due to a lack of published images of the structure; however future analyses should include this trait if possible.

The second trait that has been excluded is the deuterolobe, which is one of the two diagnostic traits of the Pseudagnostidae. The deuterolobe is defined as "a composite pygidial lobe consisting of confluent pleural and axial elements" (Öpik, 1963, p. 31). Kobayashi (1935) described this condition in pseudagnostids, clarifying the structure as being distinguishable from the axial furrow and thus not a simple expansion of the

posteroaxis. A pair of longitudinal depressions that appear on the pygidia of some species were interpreted to be axial furrows and, in later studies, were described as the inner part of a nested axis structure (Palmer, 1955). These inner axial furrows were later termed "notulae" by Öpik (1963) who argued that they are not representative of true axial furrows, nor are the furrows that define the deuterolobe. The accessory furrows that outline the deuterolobe were interpreted as distinct scrobiculae that represent external expressions of internal anatomy. To account for this uncertainty of axial elements, the term deuterolobe was established to unite the features as a single structure (Öpik, 1963). Following this, Shergold (1977) defined the deuterolobate condition as diagnostic for pseudagnostids, despite there being no established criteria on how to distinguish axial furrows from a deuterolobe (Peng and Robison, 2000).

Several studies have argued against the recognition of the deuterolobe as a distinct feature, instead concluding that the furrows that define the deuterolobe are homologous to axial furrows (Troedsson,1937; Rozova 1960; Pratt, 1992; Peng and Robison, 2000). A study comparing the ontogenetic trajectories of a species of *Pseudagnostus* and the ammagnostine *Kormagnostus* showed that the pseudagnostid deuterolobe was not developmentally distinct from an expanded posteroaxis, concluding that the deuterolobate condition was not unique to pseudagnostids (Pratt, 1992). Peng and Robison (2000) reviewed this trait and also concluded that there is no evidence to support the deuterolobe as a diagnostic feature of pseudagnostines, and further they suggested that terms associated with it, such as accessory furrow, axiolobate, plethoid, and pseudolobe, also lack support and should not be used in subsequent descriptions.

In these analyses, the deuterolobe is interpreted as being homologous to the posteroaxis (Troedsson,1937; Rozova 1960; Pratt, 1992; Peng and Robison, 2000), disregarding the described condition of deuterolobate and instead noting the degree of posteroaxis expansion. The deuterolobate condition is not uniformly expressed in relation to the F2 furrow. For example, in *S. securiger* (Figure A.2a), the posteroaxis is expanded widely behind the F2 furrow whereas in *N. bilobus* (Figure A.2b), the posteroaxis is short, approximately the same length as M2. In the latter condition, the deuterolobe is considered effaced.

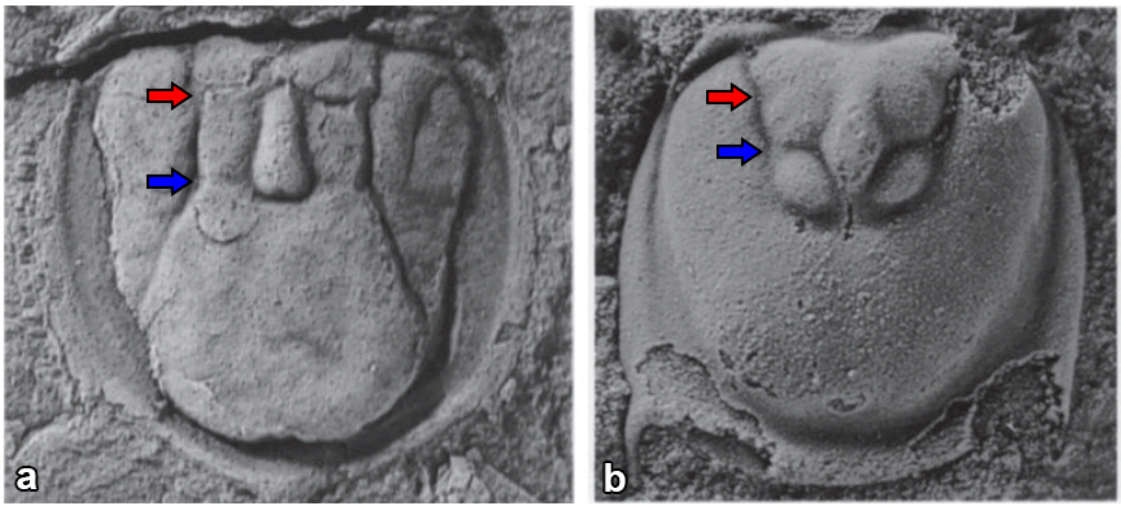

Figure A.2—Comparison of the pygidia of a. *S. securiger* (from Shergold and Laurie, 1997 p. 367 fig. 5) and b. *N. bilobus* (Shergold and Laurie, 1997, p. 369 fig. 2c). Red arrows indicate the position of the F1 furrow and blue arrows indicate the position of the F2 furrow. In *S. securiger*, the deuterolobe is the expansion of the posteroaxis below the F2 furrow; in *N. bilobus*, this trait is considered to be effaced.

Character 55, which describes the state of a transverse sulcus in the place of a transverse depression, is expressed on several agnostine taxa. This character unites *O. trispinifer* and *A. laevis* in the analyses, and the removal of the character from the analyses disassociates those taxa into pectinate arrangements. The homology with the

transverse depression cannot be determined with any degree of certainty. Moreover the comparison of this character state between taxa with vastly different pygidial complexes, such as *O. trispinifer* (Figure A.3a) and *A. laevis* (Figure A.3b), should be done with caution.

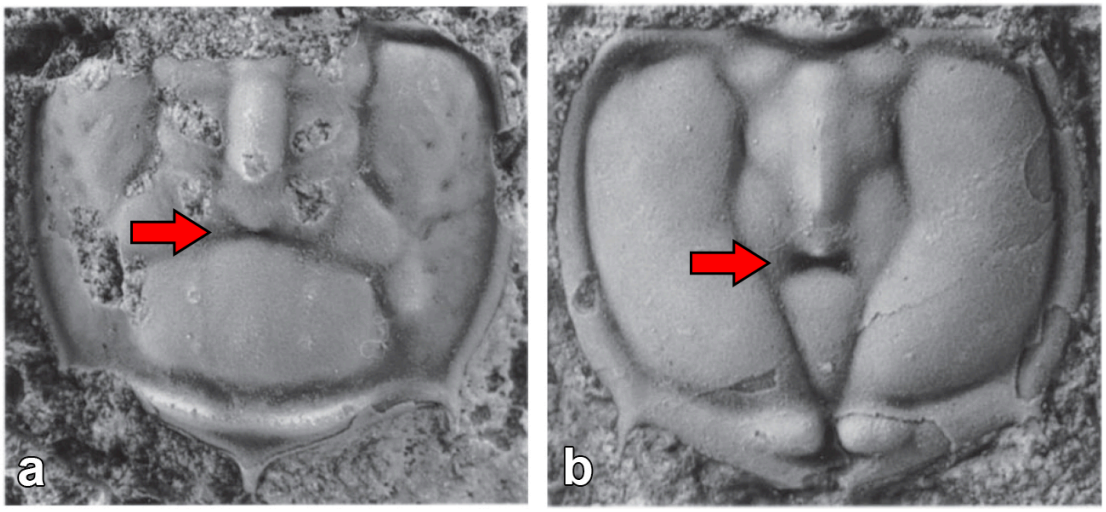

Figure A.3— Comparison of the "transverse sulcus" of a. *O. trispinifer* (from Shergold and Laurie, 1997 p. 365 fig. 2b) and b. A. *laevis* (from Shergold and Laurie, 1997 p. 372 fig. 1c:"*A. iniquilinus*"). Arrow indicates the structure in question.

Table A.1—Characters that describe traits with continuous variation and were measured as a proportion with the exception of character 38, which was measured as an angle. For these characters, the number of character states was determined by the fewest number of states with a Goodness of Variance Fit of >0.9 using Jenks Natural Breaks and visual examination of the data. Character discretization carried out with gap weighting, as described in the main text.

	char. 4		char. 6		char. 9		char. 13		char. 14		char. 18		char. 19		char. 38		char.40		char. 50		char. 51		char. 52		char. 62		char. 64		char. 69		char. 70		char. 77	
AcmTyp	0.94	2	0.09	2	0.21	2	0.25	2	0.76	0	0.31	1	0.49	1	78	1	0.15	3	0.12	0	0.37	0	0.17	1	0.4	1	0	0	0.98	1	0.83	1	0.17	2
AgnPis	0.86	1	0.1	2	0.21	2	0.29	3	0.77	0	0.31	1	0.54	1	72	1	0.09	2	0.16	0	0.38	0	0.17	1	0.4	1	0	0	0.97	1	0.83	1	0.17	2
AgtOri	0.87	1	0.09	2	0.26	3	0.25	2	0.75	0	0.25	0	0.52	1	75	1	0.08	2	0.15	0	0.44	1	0.21	1	0.59	2	0	0	0.97	1	1.04	2	0.21	3
AmmSim	1.01	2	0.14	3	0.18	2	0.26	3	0.74	0	0.33	1	0.56	1	72	1	0.15	3	0.14	0	0.45	1	0.17	1	0.49	1	0	0	1	1	0.86	1	0.17	2
ArtTar	0.99	2	0.12	3	0.23	3	0.15	1	0.67	0	0.34	1	0.64	2	75	1	0.16	3	0.26	1	0.39	0	0.39	3	0.27	0	0.44	3	0.47	0	0.82	1	0.39	0
AspLae	0.91	1	0.11	3	0.28	3	0.28	3	0.7	0	?	?	0.54	1	78	1	0.21	4	0.14	0	0.37	0	0.17	1	0.34	1	0	0	0.97	1	0.84	1	0.17	1
AtdAmp	0.83	1	0.09	2	0.23	3	0.18	2	0.71	0	0.29	1	0.46	0	74	1	0.08	2	0.15	0	0.35	0	0.2	1	0.24	0	0.08	1	0.91	1	0.78	0	0.2	3
BarBar	0.85	1	0.06	1	0.24	3	0.22	2	0.73	0	0.35	1	0.58	1	73	1	0.09	2	0.2	1	0.39	0	0.22	2	0.34	1	0.18	2	0.8	0	0.83	1	0.22	2
ClaRep	1	2	0.07	2	0.21	2	0.21	2	0.77	0	?	?	0.5	1	75	1	0.14	3	0.19	1	0.38	0	0.19	1	0.65	2	0.05	1	0.95	1	1.03	2	0.19	2
ConCar	1.08	2	0.11	3	0.08	1	0.11	0	0.87	1	0.49	2	0.43	0	70	1	0.14	3	0.17	1	0.43	1	0.17	1	0.41	1	0.08	1	0.91	1	1	2	0.17	3
ConRex	0.99	2	0.12	3	0.03	0	0.09	0	0.94	1	0.46	2	0.53	1	72	1	0.17	3	0.13	0	0.42	1	0.17	1	0.41	1	0.07	1	0.92	1	0.88	1	0.17	3
CorMor	0.96	2	0.06	1	0.26	3	0.25	2	0.64	0	0.25	0	0.69	2	76	1	0.1	2	0.2	1	0.39	0	0.31	2	0.28	0	0.45	3	0.5	0	0.87	1	0.31	1
CotLen	0.95	2	0.11	3	?	?	?	?	?	?	?	?	?	?	80	2	0.13	3	0.13	0	0.42	1	0.13	0	0.37	1	0.11	1	0.87	1	0.92	1	0.13	1
DipPla	0.85	1	0.09	2	0.23	3	0.23	2	0.7	0	0.27	0	0.59	1	82	2	0.19	4	0.22	1	0.42	1	0.22	2	0.47	1	0	1	0.95	1	0.81	0	0.22	2
DorInc	0.93	2	0.1	2	0.19	2	0.23	2	0.73	0	0.31	1	0.51	1	74	1	0.11	2	0.19	1	0.34	0	0.19	1	0.28	0	0.15	2	0.83	0	0.9	1	0.19	2
DorWas	0.9	1	0.1	2	0.15	2	0.2	2	0.79	1	0.34	1	0.53	1	76	1	0.11	2	0.17	1	0.39	0	0.21	1	0.38	1	0.08	1	0.91	1	0.88	1	0.21	2
EoaRod	1	2	0.07	2	0.17	2	0.12	1	0.82	1	0.3	1	0.49	1	65	0	0.15	3	0.18	1	0.5	1	0.2	1	0.51	1	0.15	2	0.82	0	1	2	0.2	2
EuaOpi	0.84	1	0.07	2	0.18	2	0.14	1	0.77	0	0.34	1	0.55	1	74	1	0.12	3	0.18	1	0.37	0	0.18	1	0.34	1	0.09	1	0.9	1	0.81	0	0.18	3
EurGra	0.94	2	0.1	2	0.23	3	0.2	2	0.74	0	0.42	2	0.46	0	68	0	0.09	2	0.16	0	0.38	0	0.16	1	0.31	0	0.21	2	0.77	0	0.84	1	0.16	0
GalGal	0.94	2	0.12	3	0.23	3	0.17	2	0.74	0	0.4	1	0.67	2	79	2	0.13	3	0.29	1	0.5	1	0.35	3	0.43	1	0.37	3	0.57	0	0.93	1	0.35	0
GerSid	1.07	2	0.1	2	0.2	2	0.21	2	0.75	0	0.28	1	0.5	1	79	2	0.08	2	0.23	1	0.42	1	0.23	2	0.42	1	0.32	3	0.65	0	0.9	1	0.23	2
GlyRet	0.98	2	0.05	1	0.33	3	0.2	2	0.64	0	0.24	0	0.44	0	75	1	0.04	0	0.13	0	0.39	0	0.17	1	0.3	0	0.13	2	0.86	0	0.93	1	0.17	3
GonNat	0.95	2	0.07	2	0.15	2	0.19	2	0.83	1	0.42	2	0.56	1	72	1	0.05	1	0.17	1	0.42	1	0.19	1	0.41	1	0.06	1	0.94	1	0.99	2	0.19	3
HadMod	0.94	2	0.14	3	0.14	2	0.27	3	0.82	1	0.34	1	0.55	1	71	1	0.11	2	0.15	0	0.48	1	0.29	2	0.56	2	0	0	0.97	1	0.8	0	0.29	2
HomCap	0.95	2	0.06	1	0.24	3	0.23	2	0.74	0	0.3	1	0.5	1	73	1	0.1	2	0.17	1	0.5	1	0.19	1	0.57	2	0.06	1	0.93	1	0.95	1	0.19	1
HypBre	0.94	2	0.06	1	0.19	2	0.13	1	0.78	0	0.37	1	0.51	1	76	1	0.08	2	0.2	1	0.5	1	0.22	2	0.47	1	0.18	2	0.8	0	1	2	0.22	2
HypPar	0.99	2	0.08	2	0.29	3	0.17	2	0.64	0	0.23	0	0.6	1	73	1	0.16	3	0.17	1	0.42	1	0.2	1	0.44	1	0.06	1	0.93	1	0.93	1	0.2	2
ItaInt	0.83	1	0.12	3	0.15	2	0.15	1	0.82	1	0.36	1	0.58	1	75	1	0.13	3	0.22	1	0.41	1	0.22	2	0.35	1	0.07	1	0.92	1	0.79	0	0.22	2
KorSim	0.93	2	0.18	4	0.19	2	0.2	2	0.75	0	0.26	0	0.54	1	79	2	0.18	3	0.15	0	0.44	1	0.22	2	0.52	1	0	0	1	1	0.87	1	0.22	1
LejLae	1.01	2	0.03	0	0.28	3	0.1	0	0.71	0	?	?	0.48	0	70	1	0.06	1	0.17	1	0.43	1	0.17	1	0.38	1	0.06	1	0.94	1	0.97	1	0.17	2
LinKje	0.85	1	0.11	3	0.18	2	0.28	3	0.78	0	0.23	0	0.52	1	74	1	0.23	4	0.2	1	0.43	1	0.29	2	0.36	1	0.2	2	0.74	0	0.74	0	0.29	1
LotAme	1	2	0.08	2	0.19	2	0.25	2	0.8	1	0.35	1	0.56	1	73	1	0.05	1	0.15	0	0.47	1	0.18	1	0.43	1	0.09	1	0.9	1	0.89	1	0.18	2
NeoBil	0.93	2	0.14	3	0.21	2	0.25	2	0.73	0	0.32	1	0.64	2	76	1	0.12	3	0.27	1	0.46	1	0.35	3	0.35	1	0.48	3	0.46	0	0.97	1	0.35	0
OedTyp	0.92	1	0.12	3	0.19	2	0.28	3	0.78	0	0.26	0	0.46	0	78	1	0.22	4	0.15	0	0.41	1	0.12	0	0.48	1	0	0	0.98	1	0.92	1	0.12	1
OidTri	0.53	0	0.21	4	0.15	2	0.24	2	1.45	2	0.23	0	0.47	0	83	2	0.15	3	0.17	1	0.41	1	0.22	2	0.67	2	0	0	1	1	0.86	1	0.22	2
PenBri	0.85	1	0.09	2	0.17	2	0.18	2	0.79	1	0.36	1	0.44	0	71	1	0.09	2	0.18	1	0.39	0	0.27	2	0.37	1	0.09	1	0.9	1	0.81	0	0.27	2
PenSeg	0.89	1	0.11	3	0.17	2	0.23	2	0.77	0	0.34	1	0.49	1	77	1	0.13	3	0.2	1	0.42	1	0.28	2	0.41	1	0.08	1	0.9	1	0.77	0	0.28	2
PerInt	0.93	2	0.1	2	0.17	2	0.14	1	0.8	1	0.29	1	0.51	1	71	1	0.08	2	0.19	1	0.44	1	0.3	2	0.46	1	0.18	2	0.8	0	0.87	1	0.3	2
PerOri	0.95	2	0.06	1	0.22	2	0.12	1	0.74	0	0.23	0	0.49	1	74	1	0.1	2	0.19	1	0.46	1	0.23	2	0.35	1	0.18	2	0.8	0	1.02	2	0.23	2
PleGra	0.96	2	0.08	2	0.22	2	0.14	1	0.82	1	0.33	1	0.48	0	70	1	0.07	1	0.16	0	0.46	1	0.16	1	0.37	1	0.17	2	0.81	0	0.91	1	0.16	1
ProBul	0.94	2	0.13	3	0.16	2	0.2	2	0.79	1	0.3	1	0.51	1	79	2	0.13	3	0.12	0	0.45	1	0.17	1	0.53	1	0	0	1	1	0.95	1	0.17	2
SulSec	0.88	1	0.1	2	0.17	2	0.21	2	0.78	0	0.29	1	0.5	1	79	2	0.11	2	0.16	0	0.38	0	0.22	2	0.59	2	0	0	0.98	1	0.9	1	0.22	2
PtyAta	1	2	0.05	1	0.14	2	0.27	3	0.8	1	0.42	2	0.52	1	75	1	0.07	1	0.22	1	0.47	1	0.24	2	0.45	1	0.09	1	0.9	1	0.95	1	0.24	2
PtyPra	0.89	1	0.09	2	0.18	2	0.16	1	0.8	1	0.39	1	0.44	0	76	1	0.1	2	0.15	0	0.4	1	0.26	2	0.35	1	0.16	2	0.82	0	0.87	1	0.26	2
QuaCla	0.92	1	0.09	2	0.24	3	0.31	3	0.73	0	0.28	1	0.5	1	74	1	0.18	3	0.14	0	0.38	0	0.16	1	0.36	1	0.06	1	0.93	1	0.9	1	0.16	1
QuaSub	0.93	2	0.13	3	0.15	2	0.16	1	0.8	1	0.29	1	0.46	0	70	1	0.19	4	0.1	0	0.36	0	0.18	1	0.47	1	0	0	1	1	0.77	0	0.18	2
RhoNas	0.9	1	0.1	2	0.26	3	0.2	2	0.71	0	0.35	1	0.55	1	73	1	0.07	1	0.11	0	0.36	0	0.2	1	0.28	0	0.16	2	0.82	0	0.87	1	0.2	3
TriEls	0.96	2	0.11	3	0.23	3	0.16	1	0.72	0	0.37	1	0.64	2	75	1	0.18	3	0.27	1	0.38	0	0.34	3	0.34	1	0.29	3	0.65	0	0.76	0	0.34	0
TriGib	1.01	2	0.05	1	0.2	2	0.25	2	0.76	0	0.39	1	0.49	1	71	1	0.08	2	0.21	1	0.45	1	0.21	1	0.4	1	0.1	1	0.89	1	0.9	1	0.21	2
UtaSon	0.95	2	0.13	3	0.24	3	0.27	3	0.69	0	0.27	0	0.47	0	78	1	0.2	4	0.19	1	0.43	1	0.27	2	0.35	1	0.18	2	0.77	0	0.82	1	0.27	2
UtaTri	0.82	1	0.13	3	0.21	2	0.23	2	0.76	0	0.23	0	0.47	0	78	1	0.17	3	0.09	0	0.36	0	0.2	1	0.49	1	0.05	1	0.94	1	0.89	1	0.2	3

Table A.2—Cephalic diagnostic traits for families of Agnostina from Shergold et al., 1990. Shaded cells indicate variable, uninformative, or unspecified (=N/S) character states.

Family	Cephalic definition	Border furrows	Cephalic acrolobes	Cephalic border width	Preglabellar furrow	Anteroglabella shape
Agnostidae	Variable	Variable	Usually unconstricted	Narrow	Variable	Variable
Ammagnostidae	Usually en grande tenue	Deliquiate	Usually unconstricted	Narrow	Absent or incomplete	Variable
Clavagnostidae	En grande tenue	Variable	Unconstricted	N/S	Variable	Variable
Diplagnostidae	En grande tenue	Usually deliquiate	Usually unconstricted	N/S	Variable	Variable
Doryagnostidae	En grande tenue	N/S	N/S	Moderate	N/S	Ogival or semiovate
Metagnostidae	Usually en grande tenue	Nondeliquiate	Unconstricted	N/S	Usually absent	Variable
Peronopsidae	Usually en grande tenue	Nondeliquiate	Unconstricted	N/S	Absent or weak	Variable
Phalacromidae	Variably effaced	Variable	N/S	Variable	Absent	N/S
Pseudagnostidae	Variable	Usually deliquiate	Usually unconstricted	Wide	Variable	Variable
Ptychagnostidae	Usually en grande tenue	Nondeliquiate	Unconstricted	N/S	Usually present	N/S
Spinagnostidae	En grande tenue or anterior glabella variably effaced	Nondeliquiate	Unconstricted	Narrow or moderately wide	Variable	Variable

Family	Glabellar culmination shape	F2 furrow	Transglabellar furrow	Glabellar node	Basal lobes
Agnostidae	Variable	Variable	Straight or curved	Between F1 and F2 or in front F2	Variable size, simple
Ammagnostidae	Variable	Variable	Straight or curved	Between F1 and F2 or in front F2	Small or moderate, simple
Clavagnostidae	Variably rounded or angular	Absent or weak	N/S	Elongate, near midpoint or in front of F3	Small or moderate, simple
Diplagnostidae	Variable	Variable	Straight or chevron	Behind F2 or near F3	Moderate or large, simple
Doryagnostidae	Broadly rounded	Well-defined	Straight or slightly curved	Level with F1 or between F1 and F2	N/S
Metagnostidae	Variable	Absent or chevron	Effaced	On or near F3	Small or moderate, simple
Peronopsidae	Narrowly rounded	Well-defined	Straight or curved	Between F1 and F2 or in front F2	Small, simple
Phalacromidae	N/S	Absent	Absent	N/S	N/S
Pseudagnostidae	N/S	N/S	Variable	Behind F2 or near F3	N/S
Ptychagnostidae	N/S	N/S	N/S	Variable	Usually elongate
Spinagnostidae	Usually broadly rounded	Usually defined	Variable	Level with F1 or in front of F2	Small, simple

Table A.3—Pygidial diagnostic traits for families of Agnostina from Shergold et al., 1990. Shaded cells indicate variable, uninformative, or unspecified (=N/S) character states.

Family	Pygidial definition	Pygidial border furrow	Pygidial acrolobes	Pygidial border width	Postaxial furrow	Pygidial axis
Agnostidae	Variable	Variable	Usually unconstricted	Variable	N/S	Usually long, commonly reaches border furrow
Ammagnostidae	Usually en grande tenue	Deliquiate	Usually unconstricted	Broad	N/S	Long, variably expanded
Clavagnostidae	En grande tenue	Deliquiate	Unconstricted	N/S	N/S	Long, commonly reaches border furrow
Diplagnostidae	En grande tenue	Usually deliquiate	Commonly constricted	N/S	N/S	Variable, commonly deuterolobate
Doryagnostidae	En grande tenue	N/S	N/S	Moderate	Usually present	Long, does not reach border furrow
Metagnostidae	Usually en grande tenue	Nondeliquiate	Unconstricted	N/S	Absent	Short
Peronopsidae	Usually en grande tenue	Nondeliquiate	Unconstricted	N/S	N/S	Long, does not reach border furrow
Phalacromidae	En grande tenue	Variable	N/S	Variable	N/S	Long, laterally expanded
Pseudagnostidae	Variable	Usually deliquiate	Commonly constricted	Wide	N/S	Long, commonly reaches border furrow
Ptychagnostidae	Usually en grande tenue	Nondeliquiate	Unconstricted	N/S	Usually present	Long, acuminate or rounded
Spinagnostidae	En grande tenue	Nondeliquiate	Unconstricted	Narrow or moderately wide	Usually present	Long, does not reach border furrow

Family	F1 furrow	F2 furrow	M1	Axial node	Secondary node	Pygidial spines
Agnostidae	Variable	Variable	Usually trilobate	Variable	Variable	N/S
Ammagnostidae	Variable	Variable	N/S	Usually large	Variable	Bispinose
Clavagnostidae	Variable	Variable	N/S	Long	N/S	Bispinose or trispinose
Diplagnostidae	Variable	Variable	Commonly trilobate	N/S	N/S	Bispinose or trispinose
Doryagnostidae	Effaced	Effaced	N/S	N/S	Small, posteroaxis	Nonspinose or bispinose
Metagnostidae	Defined, curved	Variable	N/S	N/S	Terminal node common	Usually bispinose
Peronopsidae	Variable	Variable	N/S	N/S	N/S	Nonspinose or bispinose
Phalacromidae	N/S	N/S	N/S	Close or midpoint	N/S	Variable
Pseudagnostidae	Effaced	Well-defined	N/S	N/S	Terminal node	Bispinose or trispinose
Ptychagnostidae	Well-defined	Rarely absent	N/S	N/S	N/S	Nonspinose or bispinose
Spinagnostidae	Usually effaced	Usually effaced	N/S	Usually moderate size	N/S	Nonspinose or bispinose

Table A.4—Geologic time series/stage and image references for each taxon included in the analyses.

Taxon code	Taxon name	Geologic Timescale 2018 Series/Stage	Image references
Agnostidae			
AgnPis	*Agnostus pisifomis*	Cambrian Miaolingian/Guzhangian	Shergold & Laurie, 1997, fig. 217 1a-b; Jackson & Budd, 2017, fig. 6; ICS 250, 2422, 2423
EurGra	*Eurudagnostus grandis*	Cambrian Furongian/Paibian	Naimark & Pegel 2017, pl. 7, fig. 7-8; ICS 2630, 2631
HomCap	*Homagnostus captiosus*	Cambrian Furongian/Paibian	Naimark & Pegel 2017, pl. 8, fig. 6-7
LotAme	*Lotagnostus americanus*	Cambrian Furongian/Jiangshanian	Shergold & Laurie, 1997, fig. 218 1a-c' Peng & Babcock 2005, fig. 2; ICS 886
BarBar	*Barrandagnostus barrandei*	Cambrian Furongian/Paibian	Naimark & Pegel 2017, pl. 8, fig. 2-3
Ammagnostidae			
AmmSim	*Ammagnostus simplexifomis*	Cambrian Miaolingian/Drumian	Shergold & Laurie, 1997, Naimark & Pegel 2017, pl.6, fig. 6
KorSim	*Kormagnostus simplex*	Cambrian Miaolingian/Guzhangian	Shergold & Laurie, 1997, fig. 220 fig. 4a-b; ICS 1760
ProBul	*Proagnostus bulbus*	Cambrian Furongian/Paibian	Shergold & Laurie, 1997, fig. 220 3a-c; Peng & Robison, 2000 fig. 25
HadMod	*Hadragnostus modestus*	Cambrian Miaolingian/Guzhangian	Peng & Robison, 2000 fig. 23
Clavagnostidae			
ClaRep	*Clavagnostus repandus*	Cambrian Miaolingian/Guzhangian	Shergold & Laurie, 1997, fig. 235 2a-b, Peng & Robison, 2000 fig. 26; ICS 758
AspLae	*Aspidagnostus laevis*	Cambrian Miaolingian/Guzhangian	Shergold & Laurie, 1997, fig. 235 1a-c; Peng & Robison, 2000 fig. 30
UtaTri	*Utagnostus trispinulus*	Cambrian Miaolingian/Drumian	Shergold & Laurie, 1997, fig. 235 3a-b; Peng & Robison, 2000 fig. 33
UtaSon	*Utagnostus songae*	Cambrian Miaolingian/Drumian	Peng & Robison, 2000 fig. 34
Condylopygidae			
ConCar	*Condylopyge carinata*	Cambrian Miaolingian/Wuliuan	Naimark & Pegel 2017, pl.2, fig. 1-2
ConRex	*Condylopyge rex*	Cambrian Series 2/Stage 4	Shergold & Laurie, 1997, fig. 240 3
PleGra	*Pleuroctenium granulatum*	Cambrian Series 2/Stage 4	Shergold & Laurie, 1997, fig. 240 4a-b
Diplagnostidae			
DipPla	*Diplagnostus planicauda*	Cambrian Miaolingian/Drumian	Shergold & Laurie, 1997, fig. 230 1a-b; Peng & Robison, 2000 fig. 35; ICS 289, 290
OidTri	*Oidalagnostus trispinifer*	Cambrian Miaolingian/Guzhangian	Shergold & Laurie, 1997, fig. 231 2a-b; Peng & Robison, 2000 fig. 42; ICS 291, 292, 1023
LinKje	*Linguagnostus kjerulfi*	Cambrian Miaolingian/Drumian	Shergold & Laurie, 1997, fig. 230 5a-b; Peng & Robison, 2000 fig. 38; ICS 334
OedTyp	*Oedorhachis typicalis*	Cambrian Miaolingian/Guzhangian	Shergold & Laurie, 1997, fig. 230 3a-b
Doryagnosidae			
DorInc	*Doryagnostus incertus*	Cambrian Miaolingian/Drumian	Shergold & Laurie, 1997, fig. 228 1a-b; Peng & Robison, 2000 fig. 44; ICS 304
RhoNas	*Rhodotypiscus nasonis*	Cambrian Miaolingian/Drumian	Shergold & Laurie, 1997, fig. 228 3
DorWas	*Doryagnostus wasatchensis*	Cambrian Miaolingian/Wuliuan	Robison 1978, pl. 1 fig. 1-4, 6. pl. 2 fig. 6, 9-13
EuaOpi	*Euagnostus opimus*	Cambrian Miaolingian/Drumian	Shergold & Laurie, 1997, fig. 226 7a-b
Metagnostidae			
GerSid	*Geragnostus sidenbladhi*	Ordovician Lower/Tremadocian	Shergold & Laurie, 1997, fig. 237 4a-b; ICS 388, 389
TriEls	*Trinodus elspethi*	Ordovician Upper/Sandbian	Bruton & Nakrem 2005, fig. 2
GalGal	*Galbagnostus galba*	Ordovician Middle/Dapingian	Shergold & Laurie, 1997, fig. 236 3a-b
ArtTar	*Arthrorhachis tarda*	Ordovician Upper/Hirnantian	Ahlberg 1989, fig. 2-4; Shergold & Laurie, 1997, , 1997 fig. 236-2
CorMor	*Corrugatagnostus morea*	Ordovician Middle/Darriwilian	Shergold & Laurie, 1997, fig. 236 5a-c
Peronopsidae			
EoaRod	*Eoagnostus roddyi*	Cambrian Series 2/Stage 4	Geyer & Peel, 2011 fig. 11
ItaInt	*Itagnostus interstricta*	Cambrian Miaolingian/Wuliuan	Robison 1982, pl. 6 fig. 9-11
PenBri	*Pentagnostus brighamensis*	Cambrian Miaolingian/Wuliuan	Robison 1978, pl. 1 fig. 7, 11, 14; Naimark & Pegel 2017, pl.3, fig. 1-2; ICS 2325
PerInt	*Peronopsis integer*	Cambrian Miaolingian/Drumian	Shergold & Laurie, 1997, fig. 229 1a-b; Naimark 2012, fig. 6
QuaCla	*Quadragnostus clarus*	Cambrian Miaolingian/Drumian	Naimark & Pegel 2017, pl. 4, fig. 5-6
PenSeg	*Pentagnostus segmenta*	Cambrian Miaolingian/Wuliuan	Robison 1982, pl. 6 fig. 1-4
Pseudagnostidae			
AgtOri	*Agnostotes orientalis*	Cambrian Furongian/Jiangshanian	Shergold & Laurie, 1997, fig. 232 3a-b
SulSec	*Sulcagnostus securiger*	Cambrian Miaolingian/Guzhangian	Shergold & Laurie, 1997, fig. 232 5
AcmTyp	*Acmarhachis typicalis*	Cambrian Miaolingian/Guzhangian	Shergold & Laurie, 1997, , 1997 fig. 222 4a-c; Peng & Robison fig. 13
NeoBil	*Neoagnostus bilobus*	Cambrian Furongian/Stage 10	Shergold & Laurie, 1997, fig. 233 2a-c
Ptychagnostidae			
GonNat	*Goniagnostus nathorsti*	Cambrian Miaolingian/Drumian	Shergold & Laurie, 1997, fig. 223 3a-c; Peng & Robison, 2000 fig. 56; ICS 302, 303, 1299
PtyAta	*Ptychagnostus atavus*	Cambrian Miaolingian/Wuliuan	Robison 1982, pl. 1 fig. 1-9; Peng & Robison, 2000 fig. 52; ICS 295, 296, 301
TriGib	*Triplagnostus gibbus*	Cambrian Miaolingian/Wuliuan	Robison 1982, pl. 2 fig. 1-13;Peng & Robison, 2000 fig. 54; ICS 293, 294
LejLae	*Lejopyge laevigata*	Cambrian Miaolingian/Guzhangian	Shergold & Laurie, 1997, fig. 224 5a-b; Peng & Robison, 2000 fig. 60; ICS 307
PtyPra	*Ptychagnostus praecurrens*	Cambrian Miaolingian/Wuliuan	Robison 1978, pl. 1 fig. 5,8; Robison 1982, pl. 4 fig. 7-10; ICS 299
Spinagnostidae			
HypPar	*Hypagnostus parvifrons*	Cambrian Miaolingian/Drumian	Peng & Robison, 2000 fig. 45; ICS 282, 283
PerOri	*Peratagnostus orientalis*	Cambrian Furongian/Paibian	Naimark & Pegel 2017, pl.6, fig. 4-5; ICS 2531, 2532
CotLen	*Cotalagnostus lens*	Cambrian Miaolingian/Wuliuan	Shergold & Laurie, 1997, fig. 226, 1a-b; ICS 287, 288
HypBre	*Hypagnostus brevifrons*	Cambrian Miaolingian/Drumian	Peng & Robison, 2000 fig. 46; ICS 328
Unassigned/Uncertain			
GlyRet	*Glyptagnostus reticulatus*	Cambrian Furongian/Paibian	Shergold & Laurie, 1997, fig. 222 1a-b; Peng & Robison, 2000 fig. 71; ICS 332, 333, 1189-1191
QuaSub	*Quadrahomagnostus subquadratu*	Cambrian Miaolingian/Guzhangian	Shergold & Laurie, 1997, fig. 222 5a-b
AtdAmp	*Agnostardis amplinatus*	Cambrian Miaolingian/Guzhangian	Shergold & Laurie, 1997, fig. 222 2a-b; Peng & Robison, 2000 fig. 73

Table A.5—The fully discretized matrix used in BEAST and PAUP*. The matrix used in the TNT analysis is the same with the exception of the seventeen continuous characters, which were coded as their raw values. Inapplicable character states are coded as "?". (Table A.1).

Taxon \ Character	char. 1	char. 2	char. 3	char. 4	char. 5	char. 6	char. 7	char. 8	char. 9	char. 10	char. 11	char. 12	char. 13	char. 14	char. 15	char. 16	char. 17	char. 18	char. 19	char. 20	char. 21	char. 22	char. 23	char. 24	char. 25	char. 26	char. 27	char. 28	char. 29	char. 30	char. 31	char. 32	char. 33	char. 34	char. 35	char. 36	char. 37	char. 38	char. 39	char. 40
AcmTyp	1	0	0	2	1	2	0	1	2	1	0	0	1	2	2	0	1	0	1	1	0	0	1	0	1	1	0	1	1	0	0	0	0	0	0	0	0	1	1	3
AgnPis	0	?	1	1	?	2	0	0	2	1	1	1	1	3	2	1	1	0	1	1	0	0	1	0	1	1	0	1	0	1	1	0	0	0	0	0	0	1	0	2
AgtOri	1	0	0	1	1	2	0	0	3	1	1	1	1	2	2	2	1	0	0	1	0	0	2	1	1	1	1	1	1	2	0	2	0	0	1	0	0	1	0	2
AmmSim	1	0	0	3	1	3	1	0	2	0	?	0	1	3	2	1	1	0	1	1	0	0	0	0	1	0	0	0	?	0	1	0	0	0	0	0	0	1	1	3
ArtTar	1	0	0	3	1	3	1	0	3	0	?	0	0	1	2	1	0	0	1	2	0	0	0	0	1	0	0	1	1	1	0	0	0	0	0	0	0	1	0	3
AspLae	1	0	2	1	1	3	0	0	3	1	1	0	1	3	2	?	0	0	?	1	0	1	1	0	1	1	0	1	1	1	0	0	0	0	0	1	0	1	1	4
AtdAmp	1	0	1	1	0	2	0	0	3	1	1	1	1	2	2	0	1	0	1	0	0	0	1	0	1	1	0	1	0	0	1	0	0	1	1	0	0	1	1	2
BarBar	1	0	1	1	1	1	0	0	3	1	0	2	1	2	2	0	1	0	1	1	0	0	2	1	1	0	1	1	0	0	1	2	0	0	1	0	0	1	0	2
ClaRep	1	0	2	3	1	2	0	0	2	0	?	0	1	2	2	?	0	0	?	1	0	0	1	0	1	0	0	1	1	0	0	0	0	0	0	0	0	1	1	3
ConCar	0	?	1	0	?	3	0	1	1	0	?	1	0	0	2	0	1	1	2	0	1	0	1	0	1	1	0	1	0	2	0	0	0	1	0	0	0	1	0	3
ConRex	1	0	1	3	1	3	0	1	0	0	?	1	0	0	2	0	1	1	2	1	1	0	1	0	1	1	0	1	0	2	0	0	0	1	0	0	0	1	0	3
CorMor	1	0	2	2	1	1	1	1	3	0	?	2	1	2	2	2	0	0	0	2	0	0	0	0	1	1	1	1	1	1	0	0	0	0	0	0	0	1	0	2
CotLen	1	0	1	2	1	3	1	0	?	0	?	0	0	?	1	?	0	?	?	?	0	0	?	?	0	1	0	1	1	1	1	0	0	0	0	0	1	2	0	3
DipPla	1	0	0	1	1	2	0	0	3	1	1	1	1	2	2	2	1	0	0	1	0	0	2	1	1	1	1	0	?	0	0	1	1	1	1	0	0	2	0	4
DorInc	0	?	0	2	?	2	0	0	2	1	1	0	1	2	1	0	1	0	1	1	0	0	1	0	1	1	0	0	?	0	1	0	0	0	1	0	0	1	0	2
DorWas	0	?	2	1	?	2	0	0	2	1	1	1	1	2	1	0	1	1	1	1	0	0	0	0	1	1	0	0	?	0	1	0	0	0	1	0	0	1	0	2
EoaRod	0	?	1	3	?	2	0	0	2	0	?	0	1	1	2	0	1	1	1	1	0	0	0	0	0	1	0	0	?	0	1	0	0	0	0	0	1	0	0	3
EuaOpi	0	?	2	1	?	2	0	0	2	0	?	0	1	1	2	0	1	0	1	1	0	0	0	0	0	1	0	1	0	0	1	0	0	0	?	0	1	1	0	3
EurGra	0	?	1	2	?	2	0	0	3	0	?	2	1	2	2	1	1	0	2	0	0	0	0	0	1	1	0	1	0	1	1	1	0	1	0	0	0	0	0	2
GalGal	1	0	0	2	1	3	1	0	3	0	?	0	0	2	2	1	0	0	1	2	0	0	0	0	1	1	0	1	1	1	0	0	0	0	0	0	0	2	0	3
GerSid	1	0	2	0	1	2	1	1	2	0	?	0	1	2	2	1	0	0	1	1	0	0	2	0	1	0	0	1	1	1	0	1	0	0	0	0	0	2	0	2
GlyRet	0	?	0	3	?	1	0	0	3	1	1	1	2	2	2	2	1	0	0	0	0	0	2	0	1	1	1	1	0	0	0	2	1	0	0	0	0	1	0	0
GonNat	1	0	1	2	0	2	0	0	2	1	1	1	1	2	2	0	1	1	2	1	0	0	1	0	1	1	1	1	0	2	1	2	0	0	1	0	0	1	0	1
HadMod	0	?	0	2	?	3	1	0	2	1	1	0	1	3	2	1	1	1	1	1	0	0	0	0	0	1	1	0	1	1	0	1	0	0	0	0	0	1	1	2
HomCap	0	?	0	2	?	1	0	0	3	1	0	2	1	2	2	0	1	0	1	1	0	0	1	0	1	0	2	1	0	0	1	1	0	0	0	0	0	1	0	2
HypBre	1	0	1	2	1	1	1	0	2	0	?	0	0	1	1	2	1	0	1	1	0	0	0	0	0	0	1	0	1	1	0	1	0	0	0	0	0	1	1	2
HypPar	1	0	1	3	1	2	1	0	3	0	?	0	1	2	1	2	1	0	0	1	0	0	0	0	0	1	0	1	1	1	0	1	0	0	0	0	0	1	1	3
ItaInt	1	0	1	1	1	3	0	0	2	0	?	0	1	1	2	0	1	1	1	1	0	0	0	0	0	1	1	0	1	0	0	1	0	0	0	0	0	1	0	3
KorSim	0	?	1	2	?	4	1	0	2	0	?	0	1	2	2	1	1	0	0	1	0	0	?	?	0	0	0	0	?	0	1	0	0	0	0	0	1	2	1	3
LejLae	1	1	1	3	1	0	0	0	3	1	1	0	1	0	2	?	0	0	?	0	0	0	?	?	0	1	0	0	?	0	1	0	0	0	1	0	1	1	0	1
LinKje	1	0	0	1	1	3	0	0	2	1	0	1	1	3	2	1	1	0	0	1	0	0	2	1	1	1	1	1	1	1	0	1	1	1	1	0	0	1	0	4
LotAme	0	?	0	3	?	2	0	0	2	1	0	2	1	2	2	0	1	1	1	1	0	0	1	0	1	0	1	1	0	1	1	2	0	1	0	0	0	1	0	1
NeoBil	1	0	2	2	1	3	1	1	2	1	1	2	0	2	2	1	0	0	1	2	0	0	0	0	1	0	0	1	1	1	0	0	0	0	0	0	0	1	0	3
OedTyp	1	0	2	2	1	3	1	0	2	1	0	0	1	3	2	2	1	0	0	0	0	0	2	0	1	1	1	1	1	1	0	1	1	1	0	1	0	1	1	4
OidTri	1	0	0	0	1	4	0	0	2	1	1	0	1	2	2	0	1	2	0	0	0	0	0	0	1	1	1	1	1	0	0	1	1	1	0	1	0	2	1	3
PenBri	1	0	1	1	1	2	0	0	2	0	?	0	1	2	2	0	1	1	1	0	0	0	0	0	1	1	0	1	0	0	1	1	0	0	0	0	0	1	0	2
PenSeg	1	0	1	1	1	3	0	0	2	0	?	0	1	2	2	0	1	0	1	1	0	0	0	0	0	1	1	0	1	0	0	0	0	0	0	0	0	1	0	3
PerInt	1	0	1	2	1	2	0	0	2	0	?	0	1	1	2	0	1	1	1	1	0	0	0	0	0	1	0	0	0	?	0	0	0	0	0	0	0	1	1	2
PerOri	1	0	1	2	1	1	1	0	2	0	?	0	0	1	1	?	0	0	0	1	0	0	?	?	0	1	0	1	1	0	1	0	0	0	0	0	1	1	0	2
PleGra	0	?	1	2	?	2	1	0	2	0	?	0	0	1	2	2	1	1	1	0	1	0	0	1	1	1	0	0	?	2	0	0	0	1	0	0	0	1	0	1
ProBul	1	0	0	2	1	3	1	0	2	1	1	0	1	2	2	2	1	1	1	1	0	0	0	0	0	1	1	0	1	1	1	1	0	0	0	?	0	0	2	1	3
SulSec	1	0	0	1	0	2	1	1	2	1	1	0	1	2	2	0	0	0	1	1	0	0	1	0	1	1	1	1	1	2	0	0	0	0	1	0	0	2	1	2
PtyAta	1	0	1	3	0	1	0	0	2	1	1	1	1	3	2	0	1	1	2	1	0	0	1	0	1	1	1	1	0	2	1	2	0	0	1	0	0	1	0	1
PtyPra	1	0	1	1	0	2	0	0	2	1	1	0	1	1	2	0	1	1	1	0	0	0	1	0	1	1	0	1	0	2	1	1	0	0	0	0	0	1	0	2
QuaCla	1	0	2	2	1	2	0	1	3	1	1	1	1	3	2	1	2	0	1	1	0	0	2	1	1	1	1	0	?	0	0	1	0	0	0	0	0	1	0	3
QuaSub	1	0	2	2	1	3	1	1	2	1	0	1	0	1	1	1	1	1	1	0	0	1	1	0	1	1	0	1	0	1	0	1	0	1	0	0	0	0	1	1	4
RhoNas	1	0	2	1	1	2	0	0	3	1	0	1	1	2	1	0	1	0	1	1	0	0	1	0	1	1	1	0	0	?	0	1	0	0	0	0	0	1	0	1
TriEls	1	0	2	2	1	3	1	1	3	0	?	0	0	1	2	1	0	0	1	2	0	0	0	0	1	0	0	1	1	1	0	0	0	0	0	0	0	1	0	3
TriGib	1	1	1	3	0	1	1	1	2	1	1	0	1	2	2	0	1	0	1	1	0	0	0	0	0	1	1	0	1	0	0	0	1	0	0	1	0	0	1	0	2
UtaSon	1	0	0	2	1	3	0	0	3	1	0	0	1	3	2	1	1	0	0	0	0	0	1	1	0	1	1	1	1	0	1	0	0	0	0	0	0	1	0	4
UtaTri	1	1	0	1	1	3	0	0	2	0	?	0	1	2	2	0	0	0	0	0	0	1	1	0	1	0	0	1	1	1	0	0	0	0	0	1	0	1	1	3

Table A.5 (cont.)—The fully discretized matrix used in BEAST and PAUP*. The matrix used in the TNT analysis is the same with the exception of the seventeen continuous characters, which were coded as their raw values (Table A.1).

Taxon \ Character	char. 41	char. 42	char. 43	char. 44	char. 45	char. 46	char. 47	char. 48	char. 49	char. 50	char. 51	char. 52	char. 53	char. 54	char. 55	char. 56	char. 57	char. 58	char. 59	char. 60	char. 61	char. 62	char. 63	char. 64	char. 65	char. 66	char. 67	char. 68	char. 69	char. 70	char. 71	char. 72	char. 73	char. 74	char. 75	char. 76	char. 77	char. 78	char. 79
AcmTyp	1	1	1	2	1	1	2	2	1	0	0	1	0	?	0	0	?	0	1	0	1	1	0	0	2	1	0	2	1	1	0	0	0	?	0	0	2	0	0
AgnPis	0	?	0	1	1	0	0	0	1	0	0	1	0	?	0	0	?	0	0	0	1	1	1	0	2	1	0	0	1	1	0	0	0	?	0	0	2	0	0
AgtOri	0	?	0	2	1	1	2	2	1	0	1	1	0	?	0	1	1	1	1	0	1	2	1	0	2	1	0	0	1	2	0	0	1	1	1	0	3	0	0
AmmSim	0	?	0	0	0	0	0	0	1	0	1	1	0	?	0	0	?	1	1	1	0	1	0	0	1	1	0	0	1	1	0	0	0	?	0	0	2	0	0
ArtTar	0	?	0	1	1	1	1	1	1	1	0	3	0	?	0	0	?	3	0	0	0	0	1	3	2	1	0	2	0	1	0	0	0	?	0	0	0	1	0
AspLae	1	1	1	0	0	1	1	0	1	0	0	1	1	2	1	1	1	2	1	0	1	1	0	0	2	2	0	1	1	1	0	0	1	?	1	1	1	0	1
AtdAmp	1	1	0	0	1	0	1	2	1	0	0	1	1	2	0	0	?	2	0	0	1	0	1	1	2	1	0	1	1	0	0	0	0	?	0	0	3	0	0
BarBar	0	?	0	2	1	1	1	2	1	1	0	2	0	?	0	0	?	0	0	0	0	1	1	2	2	1	0	2	0	1	0	0	0	?	0	0	2	0	0
ClaRep	1	1	1	0	0	0	0	0	1	1	0	1	1	1	0	1	0	2	1	0	0	2	0	1	2	1	0	0	1	2	0	0	0	?	0	0	2	0	1
ConCar	0	?	0	2	1	1	2	1	1	1	1	1	1	2	0	0	?	0	0	0	1	1	1	1	2	0	?	1	1	2	0	0	0	?	0	0	3	0	0
ConRex	0	?	0	2	1	1	2	1	1	0	1	1	1	2	0	0	?	0	0	0	1	1	1	1	2	0	?	1	1	1	0	0	0	?	0	0	3	0	0
CorMor	0	?	0	2	1	1	2	1	1	1	0	2	0	?	0	0	?	3	0	0	0	0	1	3	2	1	1	2	0	1	0	0	0	?	0	0	1	1	0
CotLen	1	0	0	0	1	0	0	2	1	0	1	0	1	0	0	1	0	0	0	0	0	1	1	1	1	1	0	?	0	1	1	0	0	0	?	0	0	1	0	0
DipPla	0	?	0	1	1	1	1	0	1	1	1	2	1	0	0	1	0	0	1	0	1	1	1	1	2	1	0	0	1	0	0	0	1	2	1	0	2	0	0
DorInc	1	1	0	0	1	0	0	1	1	1	0	1	1	1	0	0	?	2	1	0	1	0	1	2	1	1	0	0	0	1	0	0	0	?	0	0	2	0	0
DorWas	1	1	0	0	1	0	0	1	1	1	0	1	1	0	0	0	?	2	1	0	1	1	1	1	1	1	0	0	1	1	0	0	0	?	0	0	2	0	0
EoaRod	1	0	1	0	1	0	0	1	0	1	1	1	0	?	0	0	?	0	0	0	1	1	1	2	1	0	?	0	0	2	0	0	0	?	0	0	2	0	0
EuaOpi	1	1	1	0	1	0	0	1	1	1	0	1	1	0	0	0	?	2	1	0	1	1	1	1	1	1	0	0	1	0	0	0	0	?	0	0	3	0	0
EurGra	0	?	0	2	1	1	2	1	1	0	0	1	0	?	0	0	?	0	0	0	1	0	1	2	2	1	1	0	0	1	0	0	0	?	0	0	0	0	0
GalGal	0	?	0	1	1	1	1	1	1	1	1	3	0	?	0	0	?	3	0	0	1	1	1	3	2	?	?	2	0	1	0	0	0	?	0	0	0	1	0
GerSid	0	?	0	1	1	1	1	0	1	1	1	2	0	?	0	0	?	3	0	0	0	1	1	3	2	1	0	0	0	1	0	0	0	?	0	0	2	1	0
GlyRet	1	1	0	2	1	1	2	2	1	0	0	1	1	2	0	1	1	2	0	0	1	0	1	2	2	1	0	0	0	1	0	0	0	?	0	0	3	0	0
GonNat	1	1	0	2	1	0	2	2	1	1	1	1	1	1	0	0	?	2	1	0	1	1	1	1	2	1	0	1	1	2	0	0	0	?	0	0	3	0	0
HadMod	0	?	0	1	1	0	1	0	1	0	1	2	0	?	0	0	?	1	1	1	1	2	0	0	2	1	0	0	1	0	0	0	0	?	0	0	2	0	0
HomCap	0	?	0	2	1	0	1	2	1	1	1	1	0	?	0	0	?	0	1	0	0	2	1	1	2	1	1	2	1	1	0	0	0	?	0	0	1	0	0
HypBre	1	0	0	0	1	0	0	2	1	1	1	2	1	0	0	1	0	0	0	0	0	1	1	1	2	1	0	?	0	0	2	0	0	0	?	0	0	2	0	0
HypPar	1	1	1	0	1	0	0	?	1	1	1	1	0	?	0	1	0	0	0	0	0	1	1	1	1	1	0	?	0	1	1	0	0	0	?	0	0	2	0	1
ItaInt	1	1	1	0	1	0	0	1	0	1	1	2	1	0	0	0	?	0	0	0	0	1	1	1	1	1	0	?	0	1	0	0	0	0	?	0	0	2	0	0
KorSim	0	?	0	0	0	0	0	0	0	0	1	2	0	?	0	0	?	1	1	1	0	1	0	0	1	1	0	0	1	1	0	0	0	?	0	0	1	0	0
LejLae	1	1	0	0	1	0	0	2	1	1	1	1	1	0	0	1	0	2	0	0	1	1	1	1	1	1	0	?	0	1	1	1	0	0	?	0	0	2	0	0
LinKje	1	1	1	1	1	1	1	1	1	1	1	2	1	2	1	0	?	0	0	0	1	1	1	2	2	2	0	1	0	0	0	0	0	?	1	0	1	0	0
LotAme	0	?	0	2	1	1	2	1	1	0	1	1	1	0	0	1	1	0	0	0	1	1	1	1	2	1	0	2	1	1	0	0	0	?	0	0	2	0	0
NeoBil	0	?	0	1	1	1	1	2	1	1	1	3	0	?	0	0	?	3	0	0	0	1	1	3	2	1	0	0	0	1	0	0	0	?	0	0	0	1	1
OedTyp	0	?	0	1	1	1	1	1	1	0	1	0	1	0	0	1	0	0	1	0	1	1	1	0	2	2	0	0	1	1	0	0	1	1	1	0	1	0	0
OidTri	0	?	1	1	0	1	1	2	1	1	1	2	1	2	1	1	1	1	1	1	1	2	0	0	2	2	0	1	1	1	0	1	1	1	1	0	2	0	0
PenBri	0	?	0	2	1	0	1	0	1	1	0	2	1	0	0	0	?	0	0	0	1	1	1	1	1	0	?	0	1	0	0	0	0	?	0	0	2	0	0
PenSeg	1	1	1	2	1	0	0	0	1	1	1	2	1	0	0	0	?	0	0	0	1	1	1	1	2	1	1	0	1	0	0	0	0	?	0	0	2	0	0
PerInt	0	?	0	0	1	0	0	0	1	1	1	2	1	0	0	0	?	0	1	0	0	1	1	2	1	0	?	0	0	1	0	0	0	?	0	0	2	0	0
PerOri	1	0	0	0	1	0	0	2	1	1	1	2	1	0	0	1	0	2	0	0	1	1	1	2	1	0	?	0	0	2	1	0	0	?	0	0	2	0	0
PleGra	0	?	0	2	1	1	2	1	1	0	1	1	1	2	0	0	?	1	1	0	1	1	1	2	2	0	?	1	0	1	0	0	0	?	0	0	1	0	0
ProBul	0	?	0	0	0	0	0	0	1	0	1	1	0	?	0	0	?	1	1	1	1	1	0	0	2	1	0	1	1	1	0	0	0	?	0	0	2	0	0
SulSec	0	?	0	1	1	0	0	0	1	0	0	2	0	?	0	1	1	1	1	1	1	2	0	0	2	2	0	0	1	1	0	0	0	?	0	0	2	0	0
PtyAta	1	1	0	2	1	0	2	2	1	1	1	2	1	0	0	0	?	0	0	0	1	1	1	1	2	0	?	0	1	1	0	0	0	?	0	0	2	0	0
PtyPra	1	1	0	2	1	0	2	2	1	0	1	2	1	0	0	0	?	2	1	0	1	1	1	2	2	0	?	0	0	1	0	0	0	?	0	0	2	0	0
QuaCla	1	1	1	0	1	0	0	1	1	0	0	1	1	0	0	0	?	0	0	0	1	1	1	1	2	1	0	1	1	1	0	0	0	?	0	0	1	0	1
QuaSub	0	?	1	1	1	1	1	0	0	0	0	1	1	0	0	0	?	1	0	0	1	1	0	0	1	0	?	0	1	0	0	0	0	?	0	0	2	0	0
RhoNas	1	1	0	0	1	0	0	1	1	0	0	1	1	1	0	0	?	2	1	0	1	0	1	2	1	1	0	0	0	1	0	0	0	?	0	0	3	0	0
TriEls	0	?	0	1	1	1	1	1	1	1	0	3	0	?	0	0	?	1	0	0	0	1	1	3	2	1	0	0	0	0	0	0	0	?	0	0	0	1	0
TriGib	1	1	0	2	1	0	2	2	1	1	1	1	1	0	0	0	?	2	1	0	1	1	1	1	2	0	?	0	1	1	0	0	0	?	0	0	2	0	0
UtaSon	1	1	1	0	0	1	0	0	1	1	1	2	1	0	0	1	0	1	0	0	1	1	1	2	2	1	0	0	0	1	0	0	0	?	0	0	2	0	1
UtaTri	1	1	1	0	0	0	1	0	1	0	0	1	1	0	0	0	?	1	1	0	0	1	0	1	2	2	0	0	1	1	0	0	0	?	0	0	3	0	1

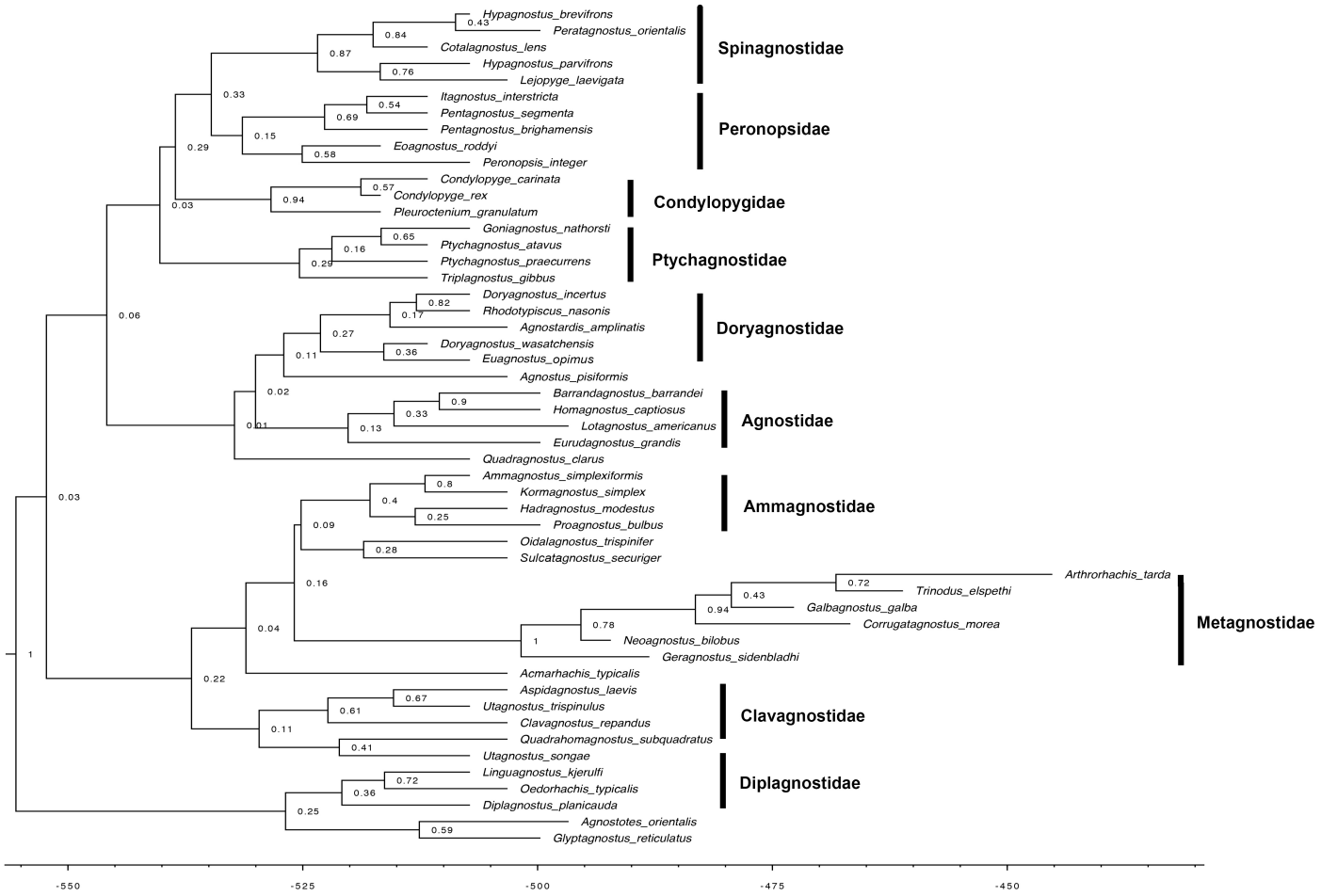

Figure A.4—MCC tree as in Figure 1.1, with posterior values provided on the nodes.

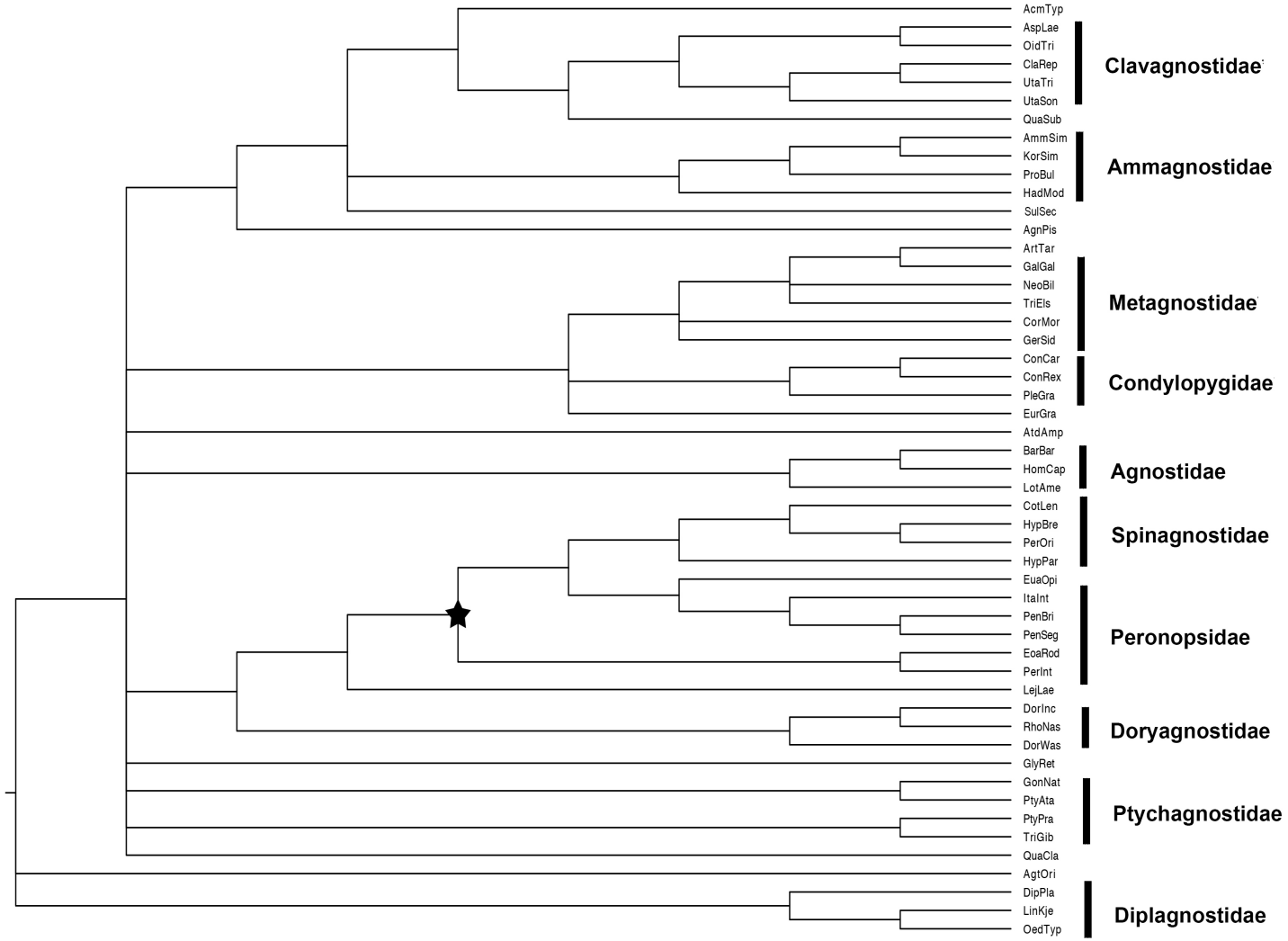

Figure A.5—Cladogram rooted with diplagnostine taxa as an outgroup. The star indicates the node of the relatively derived [Peronopsidae + Spinagnostidae] clade.

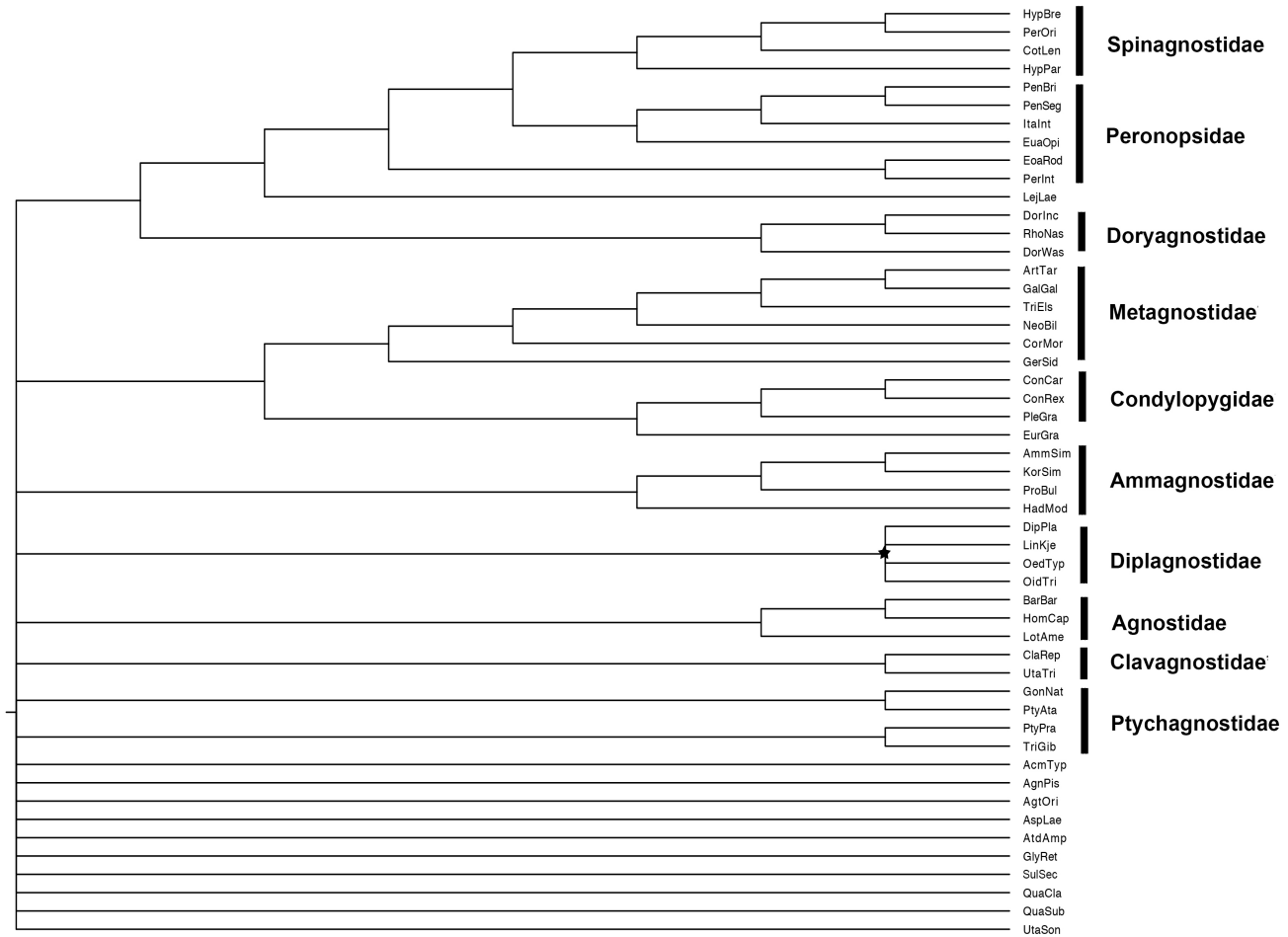

Figure A.6—Cladogram resulting from the removal of character 55 (transverse sulcus). The star notes the pectinate arrangement of diplagnostine taxa, including *O. trispinifer*.

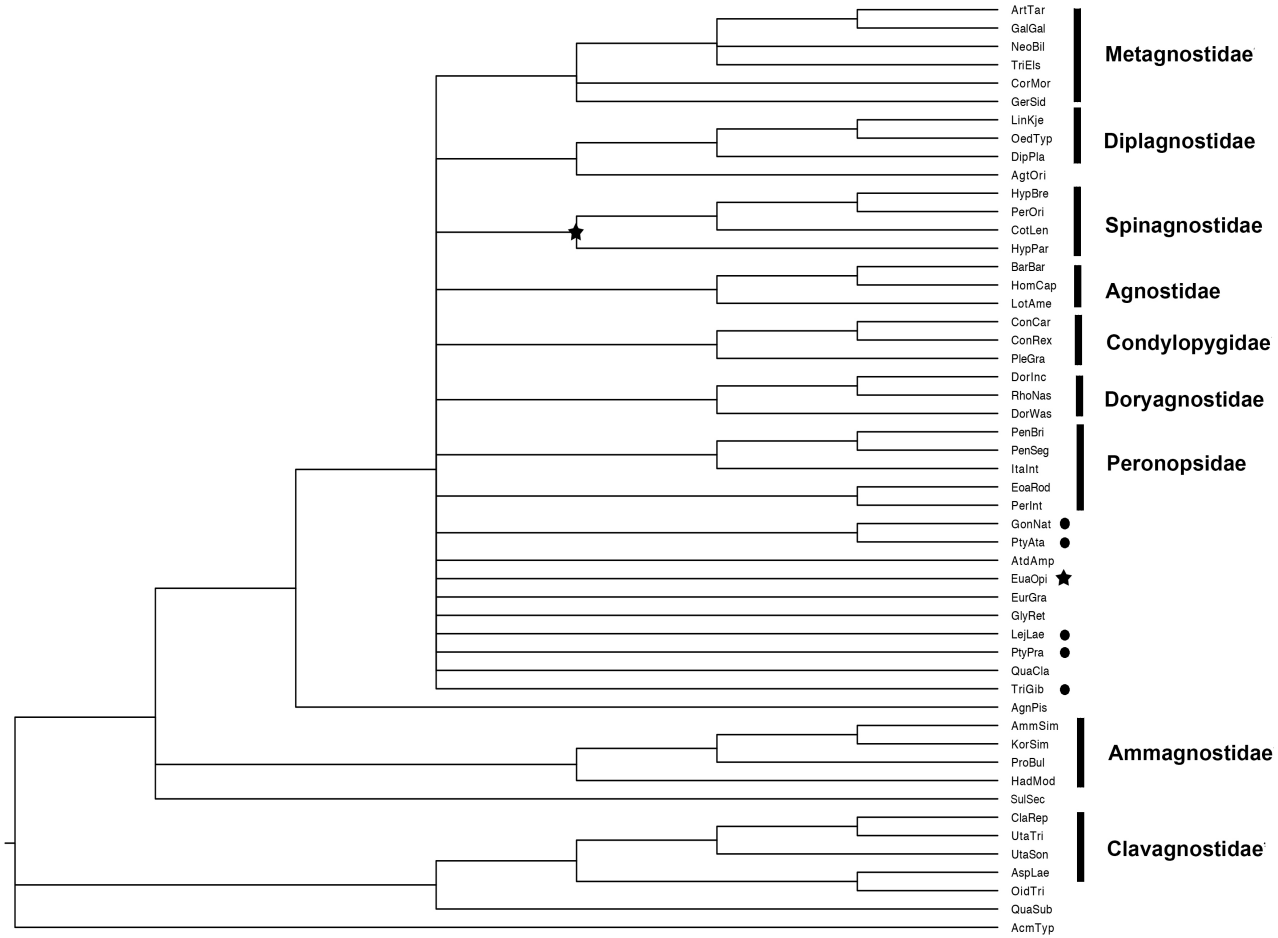

Figure A.7—Cladogram resulting from the removal of characters 25 and 37, which describe glabellar effacement. Stars indicate the position of spinagnostine taxa and circles indicate the position of ptychagnostine taxa.

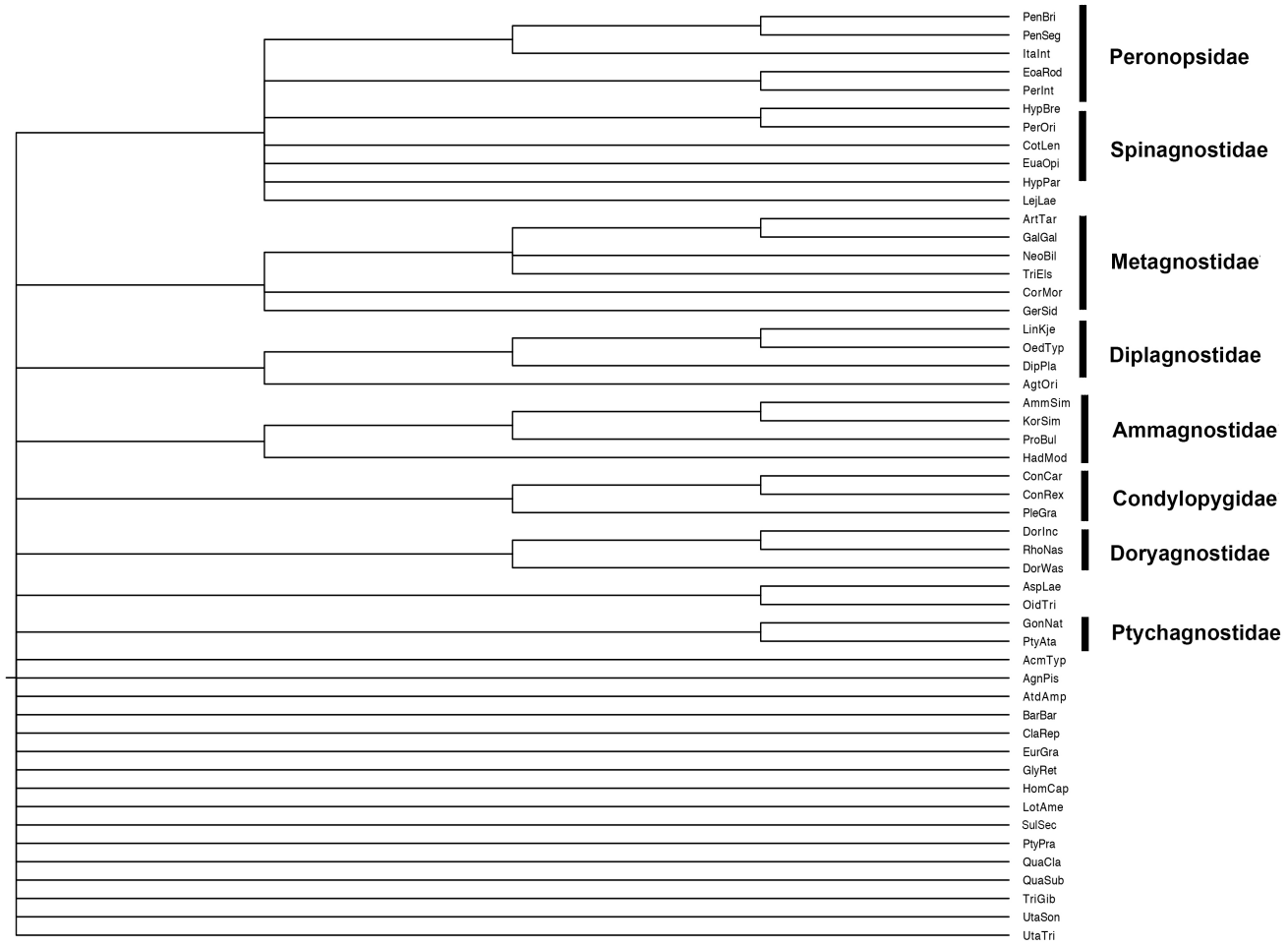

Figure A.8—Cladogram resulting from the removal of character 14, a quantitative character that describes the size of the basal lobes. This collapses many taxa into a polytomy at the base of the tree, namely all of the taxa that are historically classified within Agnostidae.

APPENDIX B:

SUPPLEMENTAL INFORMATION FOR CHAPTER TWO

This appendix contains a map detailing the geographic location of the Miners Hollow site in the Wellsville Mountains of northeastern Utah (Figure B.1), a measured stratigraphic section of the Spence Shale member of the Langston Formation at the Miners Hollow site (Figure B.2), the table of p-values for the among-partition correlation matrix for *P. brighamensis* (Table B.1), the partial correlation coefficients (Table B.2), precision matrices (Table B.3), derived edge strengths (Table B.4) used in graphical modeling analyses on *P. brighamensis*, and the test statistics resulting from those graphical modeling analyses (Table B.5).

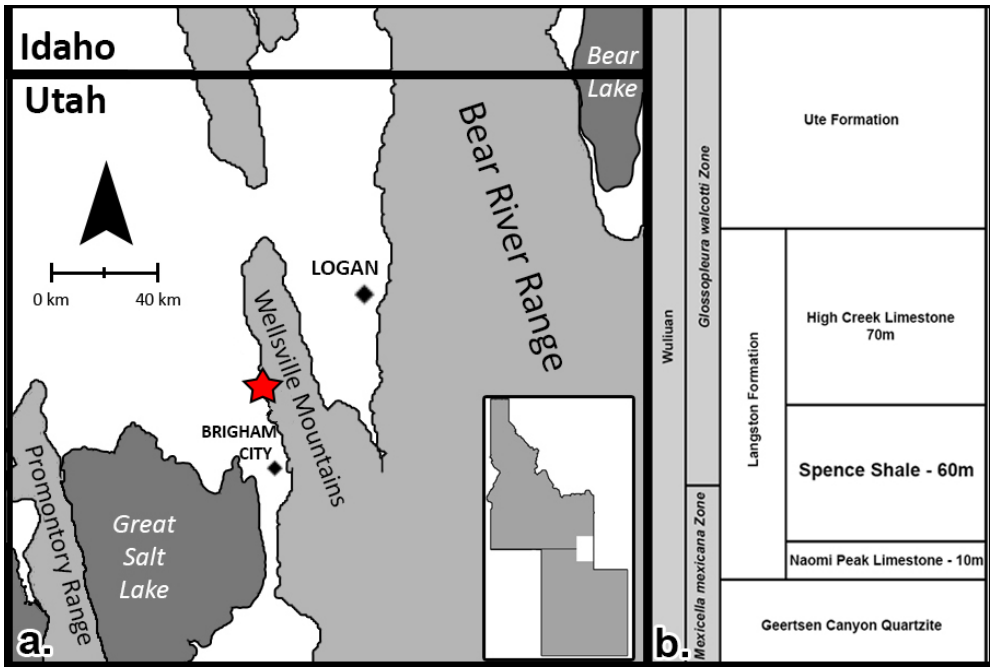

Figure B.1— a) Map showing the area of northeastern Utah in which the Spence Shale member of the Langston Formation outcrops. The red star marks the location of the Miners Hollow site in the Wellsville Mountains (41°36'07" N, 112° 02'10" W). b) General stratigraphy of the Langston Formation and adjacent units. Modified from Liddell et al., 1997.

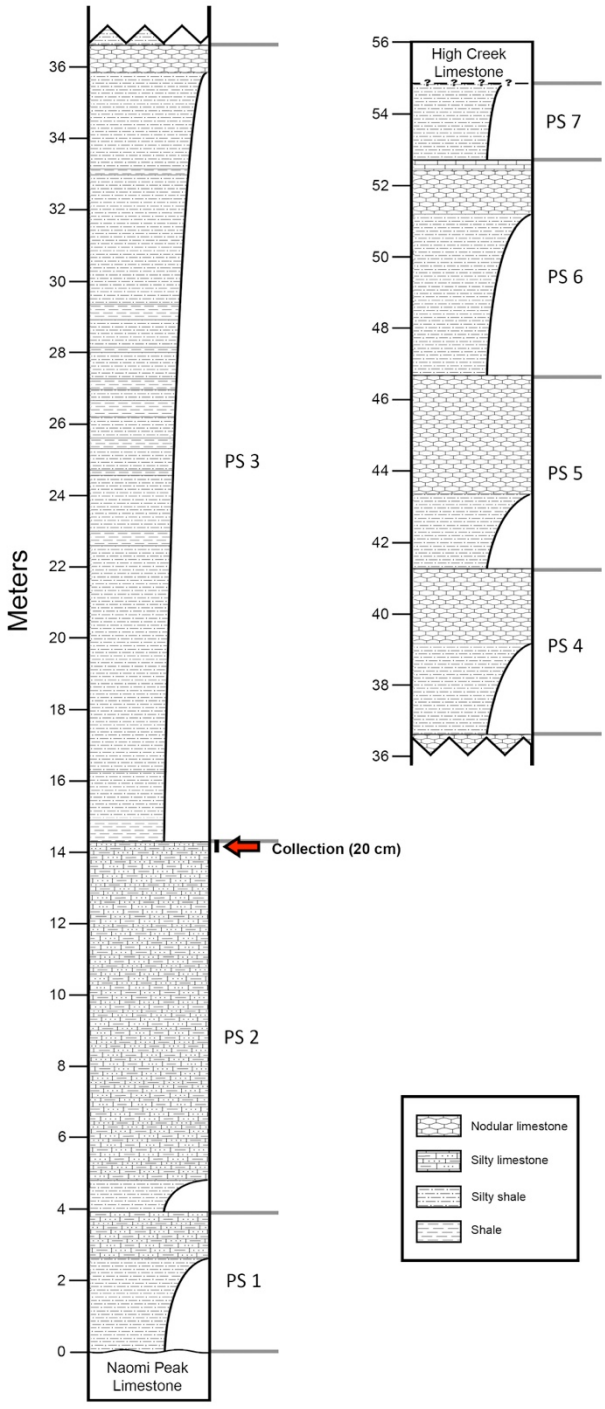

Figure B.2— Measured stratigraphic section of the Spence Shale in Miners Hollow. Red arrow indicates sample collection.

Table B.1— Mantel test p-values for the among partition correlations for *P. brighamensis* (1000 permutations). Upper triangle represents the FA component of variation, lower triangle represents the Individuals component of variation. Significant values are bolded.

	Anterior glabella	Transglabellar furrow	Anterior posteroglabella	Medial posteroglabella	Posterior posteroglabella	Basal lobes
Anterior glabella		0.322	**0.001**	**0.001**	**0.004**	0.065
Transglabellar furrow	**0.034**		0.119	0.071	**0.039**	0.273
Anterior posteroglabella	**0.001**	0.107		**0.001**	0.171	**0.001**
Medial posteroglabella	**0.001**	0.488	**0.001**		**0.001**	**0.001**
Posterior posteroglabella	**0.041**	0.643	**0.013**	**0.001**		**0.018**
Basal lobes	0.236	0.079	**0.003**	**0.001**	**0.001**	

Table B.2— Partial correlation coefficients for the FA component (upper triangle) and Individuals component (lower triangle) of variation for *P. brighamensis*. Bolded values indicate edges that are deemed strong (>0.025; Table B.3).

	Anterior glabella	Transglabellar furrow	Anterior posteroglabella	Medial posteroglabella	Posterior posteroglabella	Basal lobes
Anterior glabella		0.203	**0.343**	**0.455**	0.096	-0.204
Transglabellar furrow	0.189		-0.104	-0.120	-0.075	0.045
Anterior posteroglabella	**0.651**	-0.005		0.105	-0.133	**0.421**
Medial posteroglabella	-0.179	-0.062	**0.616**		**0.391**	**0.278**
Posterior posteroglabella	0.143	-0.025	**-0.233**	**0.454**		0.091
Basal lobes	-0.077	0.160	0.079	0.093	0.200	

Table B.3— Edge strengths calculated for the partial correlation coefficients of Table B.2 for the FA component (upper triangle) and Individuals component (lower triangle) of variation. Bolded values indicate edges that are deemed strong (>0.025), calculated as $E_{ij} = -0.5*\ln(1-(p_{ij}^2))$ where p = the partial correlation coefficient. Edge strength values larger than 0.025 are deemed strong according to Lawler (2008, p. 208).

	Anterior glabella	Transglabellar furrow	Anterior posteroglabella	Medial posteroglabella	Posterior posteroglabella	Basal lobes
Anterior glabella		0.021	**0.062**	**0.116**	0.005	0.021
Transglabellar furrow	0.018		0.005	0.007	0.003	0.001
Anterior posteroglabella	**0.275**	0.000		0.006	0.009	**0.097**
Medial posteroglabella	0.016	0.002	**0.239**		**0.083**	**0.040**
Posterior posteroglabella	0.010	0.000	**0.028**	**0.115**		0.004
Basal lobes	0.003	0.013	0.003	0.004	0.020	

Table B.4 — The inverted, or "precision", among-partition correlation matrices for the FA component (upper triangle) and Individuals component (lower triangle) of variation that were used in the graphical modeling analyses on *P. brighamensis*. The among partition correlation matrix was inverted and the diagonals were rescaled to 1 in the same manner that is described in Magwene, 2001.

	Anterior glabella	Transglabellar furrow	Anterior posteroglabella	Medial posteroglabella	Posterior posteroglabella	Basal lobes
Anterior glabella		-0.203	-0.343	-0.455	-0.096	0.204
Transglabellar furrow	-0.189		0.104	0.120	0.075	-0.045
Anterior posteroglabella	-0.651	0.005		-0.105	0.133	-0.421
Medial posteroglabella	0.179	0.062	-0.616		-0.391	-0.278
Posterior posteroglabella	-0.143	0.025	0.233	-0.454		-0.091
Basal lobes	0.077	-0.160	-0.079	-0.093	-0.200	

Table B.5— Edge support from F-tests during graphical modeling analyses for the a) FA component and b) Individuals component of variation for *P. brighamensis*. Abbreviations: AG=anterior glabella; TF=transglabellar furrow; AP=anterior posteroglabella; MP=medial posteroglabella; PP=posterior posteroglabella; BL=basal lobes.

a.

Model:	[AG+AP+MP][AG+MP+PP][TF][AP+MP+BL]		
dev	7.4972		
df	8		
Edge	**F**	**df**	**P**
AG-PP	5.711	1	0.0169
MP-BL	6.542	1	0.0105
MP-PP	13.245	1	0.0003
AG-MP	20.937	1	0
AP-MP	9.048	1	0.0026
AP-BL	12.038	1	0.0005
AG-AP	10.3972	1	0.0013

b.

Model:	[AG+AP+MP][TF][MP+PP][BL]		
dev	12.1796		
df	11		
Edge	**F**	**df**	**P**
AG-AP	32.0262	1	0
MP-PP	11.0632	1	0.0009
AP-MP	28.4952	1	0
AG-MP	7.1407	1	0.0075

APPENDIX C:

SUPPLEMENTAL INFORMATION FOR CHAPTER THREE

This appendix contains a map detailing the geographic location of the collection site in the House Range of western Utah (Figure C.1), a scree plot from the PCA of Agnostina showing the variance explained by each principal component (Figure C.2), the individual CR plots for P. brighamensis and P. segmenta (Figures C.3a and C.3b), the table of p-values for the among-partition correlation matrix for *P. segmenta* (Table C.1), the partial correlation coefficients, (Table C.2), precision matrices (Table C.3), derived edge strengths (Table C.4) used in graphical modeling analyses on *P. segmenta*, and the test statistics resulting from those graphical modeling analyses (Table C.5). Figure C.4 shows the results from the hierarchical cluster analyses conducted on *P. segmenta.*

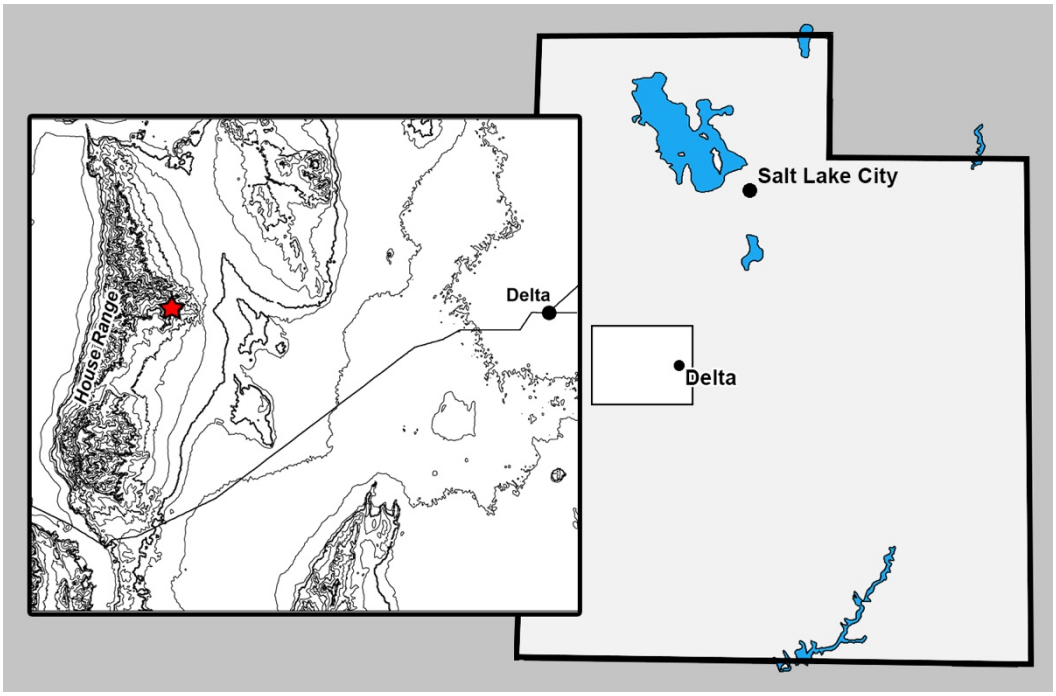

Figure C.1—Contour map showing the area of western Utah in which the Marjum Formation outcrops in the Wheeler Amphitheater, west of Delta, Utah (Millard County). The red star marks the location of collection (39°21’ 46”' N, 113°15’ 57” W).

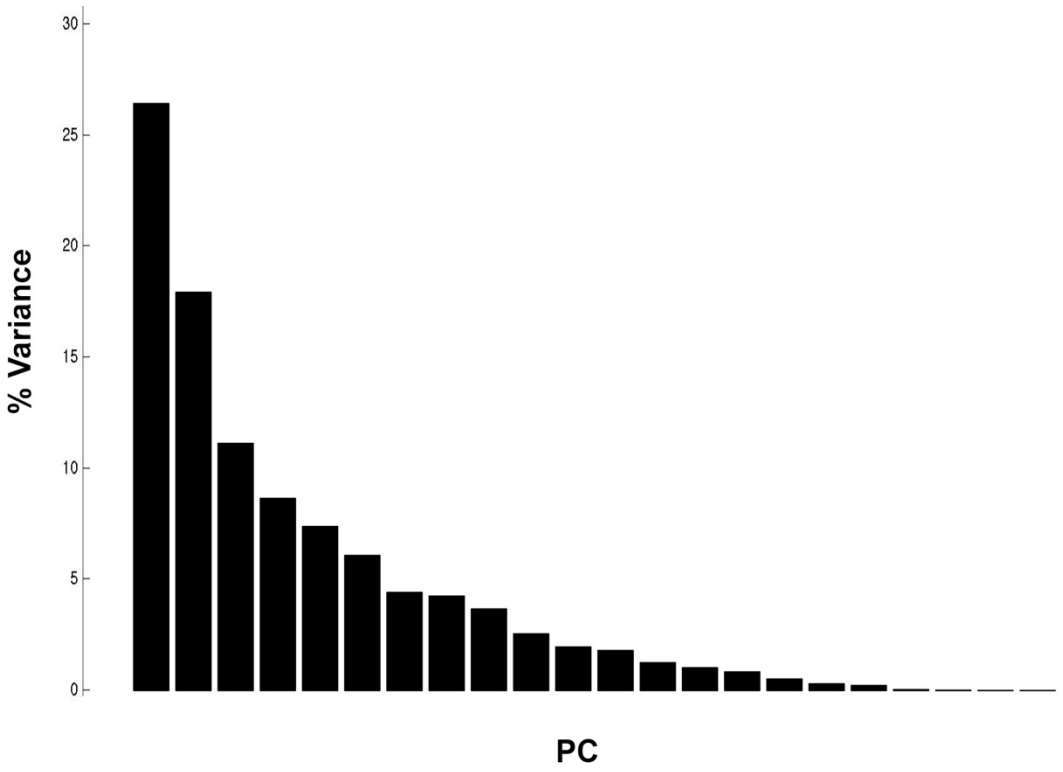

Figure C.2—Scree plot from the PCA of Agnostina showing the variance explained by each principal component.

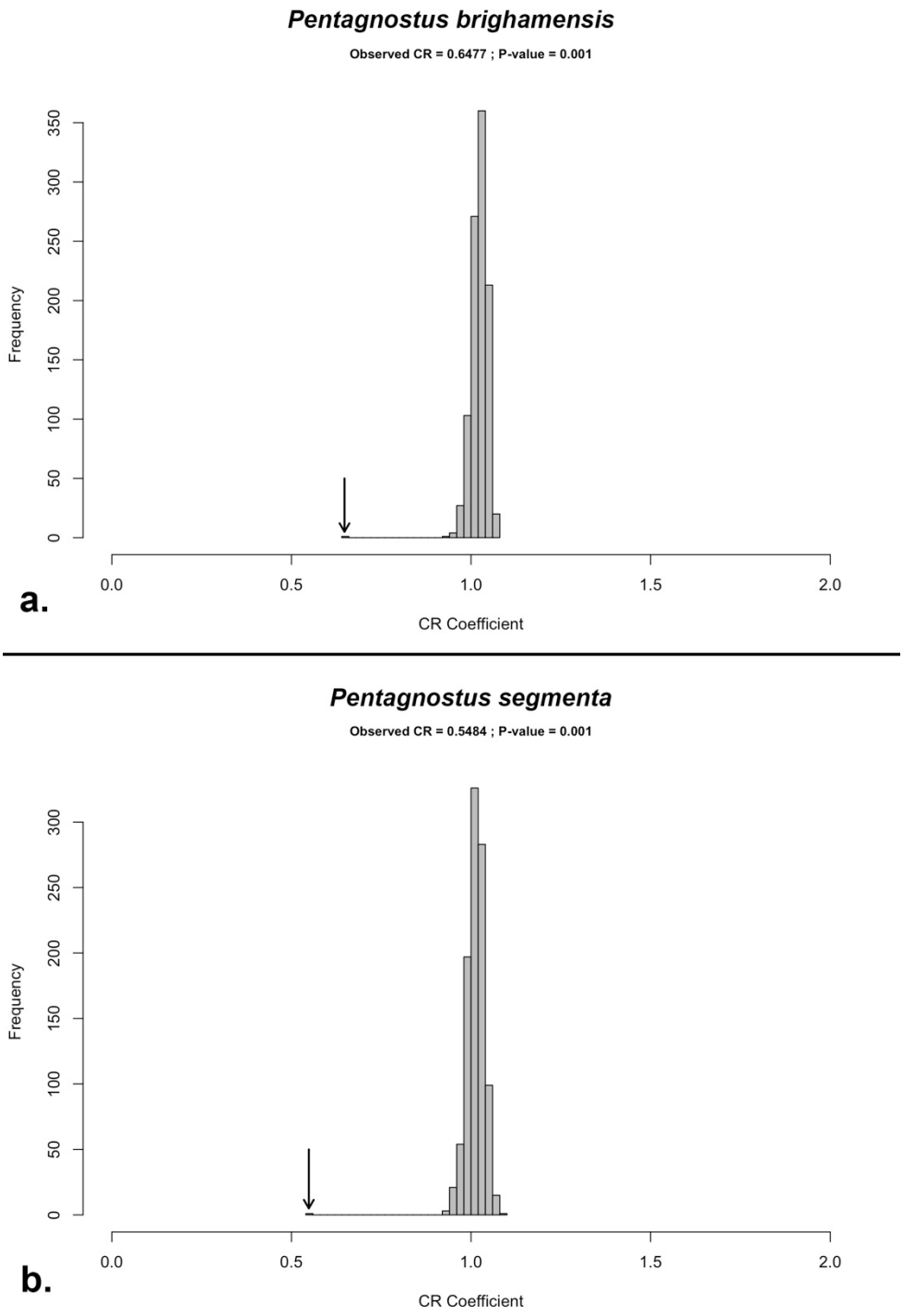

Figure C.3—CR plots for a) *P. brighamensis* and; *P. segmenta*. Both graphs show a CR value less than the null of 1, indicating a more modular structure for both species.

Table C.1— Mantel test p-values for the among partition correlations for *P. segmenta* (1000 permutations). Upper triangle represents the FA component of variation, lower triangle represents the Individuals component of variation. Significant values are bolded.

	Anterior glabella	Transglabellar furrow	Anterior posteroglabella	Medial posteroglabella	Posterior posteroglabella	Basal lobes
Anterior glabella		**0.001**	**0.002**	0.082	**0.001**	**0.019**
Transglabellar furrow	**0.001**		**0.004**	0.668	**0.001**	0.158
Anterior posteroglabella	**0.005**	**0.002**		**0.001**	0.123	**0.036**
Medial posteroglabella	**0.002**	**0.015**	**0.001**		0.100	**0.001**
Posterior posteroglabella	**0.001**	0.107	0.078	**0.001**		0.388
Basal lobes	0.105	0.232	**0.029**	0.148	**0.002**	

Table C.2— Partial correlation coefficients for the FA component (upper triangle) and Individuals component (lower triangle) of variation for *P. segmenta*. Bolded values indicate edges that are deemed strong (>0.025; Table B.3).

	Anterior glabella	Transglabellar furrow	Anterior posteroglabella	Medial posteroglabella	Posterior posteroglabella	Basal lobes
Anterior glabella		**0.302**	0.209	-0.033	**0.440**	**0.248**
Transglabellar furrow	**0.381**		**0.232**	-0.216	**0.303**	0.125
Anterior posteroglabella	0.094	0.154		**0.420**	-0.143	-0.050
Medial posteroglabella	0.090	0.062	**0.424**		**0.239**	**0.424**
Posterior posteroglabella	0.137	0.001	-0.114	**0.374**		**-0.223**
Basal lobes	0.032	0.036	0.185	-0.068	**0.312**	

Table C.3— Edge strengths calculated for the partial correlation coefficients of Table C.2 for the FA component (upper triangle) and Individuals component (lower triangle) of variation. Bolded values indicate edges that are deemed strong (>0.025), calculated as $E_{ij} = -0.5*\ln(1-(p_{ij}^2))$ where p = the partial correlation coefficient. Edge strength values larger than 0.025 are deemed strong according to Lawler (2008, p. 208).

	Anterior glabella	Transglabellar furrow	Anterior posteroglabella	Medial posteroglabella	Posterior posteroglabella	Basal lobes
Anterior glabella		**0.048**	0.022	0.001	**0.108**	**0.032**
Transglabellar furrow	**0.078**		**0.028**	0.024	**0.048**	0.008
Anterior posteroglabella	0.004	0.012		**0.097**	0.010	0.001
Medial posteroglabella	0.004	0.002	**0.099**		**0.029**	**0.099**
Posterior posteroglabella	0.009	0.000	0.007	**0.076**		**0.025**
Basal lobes	0.001	0.001	0.017	0.002	**0.051**	

Table C.4 — The inverted, or "precision", among-partition correlation matrices for the FA component (upper triangle) and Individuals component (lower triangle) of variation that were used in the graphical modeling analyses on *P. segmenta*. The among partition correlation matrix was inverted and the diagonals were rescaled to 1 in the same manner that is described in Magwene, 2001.

	Anterior glabella	Transglabellar furrow	Anterior posteroglabella	Medial posteroglabella	Posterior posteroglabella	Basal lobes
Anterior glabella		-0.302	-0.209	0.033	-0.440	-0.248
Transglabellar furrow	-0.381		-0.232	0.216	-0.303	-0.125
Anterior posteroglabella	-0.094	-0.154		-0.420	0.143	0.050
Medial posteroglabella	-0.090	-0.062	-0.424		-0.239	-0.424
Posterior posteroglabella	-0.137	-0.001	0.114	-0.374		0.223
Basal lobes	-0.032	-0.036	-0.185	0.068	-0.312	

Table C.5— Edge support from F-tests during graphical modeling analyses for the a) FA component and b) Individuals component of variation of *P. segmenta*. Abbreviations: AG=anterior glabella; TF=transglabellar furrow; AP=anterior posteroglabella; MP=medial posteroglabella; PP=posterior posteroglabella; BL=basal lobes.

a.

Model: [AG+TF+PP][AP+MP][MP+BL]			
dev	16.989		
df	10		
Edge	**F**	**df**	**P**
TF-PP	12.5532	1	0.0004
AG-TF	12.5243	1	0.0004
MP-BL	8.3138	1	0.0039
AP-MP	8.1422	1	0.0043
AG-PP	17.5541	1	0

b.

Model:	[AG+TF][AP+MP][MP+PP][PP+BL]		
dev	11.303		
df	11		
Edge	**F**	**df**	**P**
MP-PP	6.3439	1	0.0118
AP-MP	8.3418	1	0.0039
AG-TF	6.5721	1	0.0104
PP-BL	4.3104	1	0.0379

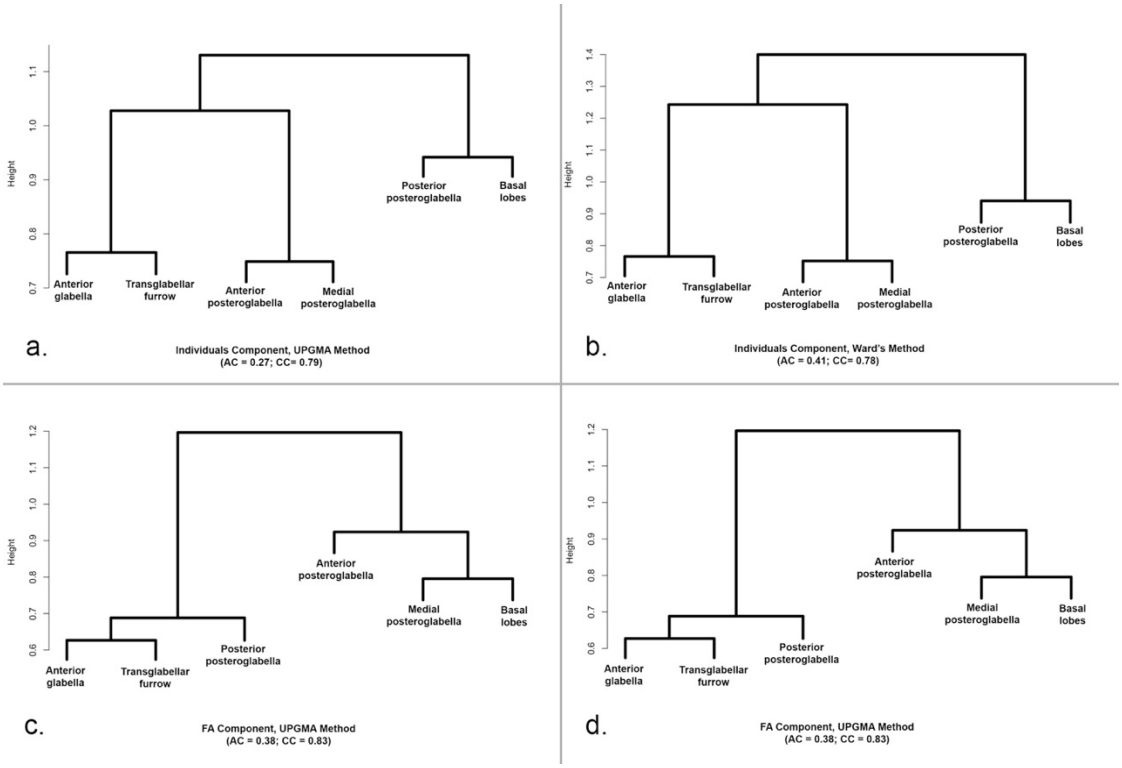

Figure C.4—Results from hierarchical cluster analyses for the Individuals component using a) UPGMA and b) Ward's method; and the FA component using c) UPGMA and d) Ward's method. Dendrograms for both components show AC values that are less than 0.55 across methods, which indicates that the hierarchical structure is weak in all cases. The highest CC value (0.83) is shown in the FA dendrograms calculated using both method (Fig. 3.8), which is below the threshold (0.85) at which the dendrograms would be considered as adequately reflective of the data.

Table C.6—Disparity metrics associated with Agnostina. PV=Procrusted variance, PD=partial disparity, %MD= percent of morphological diversity represented.

	PV	PD	%MD
Agnostidae	0.0042	0.0004	6.3%
Ammagnostidae	0.0054	0.0004	6.4%
Clavagnostidae	0.0084	0.0007	10.1%
Condylopygidae	0.0238	0.0015	21.4%
Diplagnostidae	0.0054	0.0005	6.5%
Doryagnostidae	0.0038	0.0003	4.5%
Metagnostidae	0.0054	0.0006	8.1%
Peronopsidae	0.0036	0.0005	6.5%
Pseudagnostidae	0.0062	0.0005	7.4%
Ptychagnostidae	0.0057	0.0005	6.8%
Spinagnostidae	0.0096	0.0006	8.7%
Unknown	0.0081	0.0005	7.3%

LITERATURE CITED

Adams, D. C. (2016). Evaluating modularity in morphometric data: challenges with the RV coefficient and a new test measure. *Methods in Ecology and Evolution*, *7*(5), 565-572.

Adams, D. C., and Collyer, M. L. (2016). On the comparison of the strength of morphological integration across morphometric datasets. *Evolution, 70*(11), 2623-2631.

Adams, D. C., Collyer, M., Kaliontzopoulou, A., and Sherratt, E. (2019). Geomorph: Software for geometric morphometric analyses. R package version 3.1.0. Retrieved from https://cran.r-project.org/web/packages/geomorph/index.html

Adrain, J. M. (2011). Class Trilobita Walch, 1771. In: Zhang, Z.-Q. (Ed.) Animal biodiversity: An outline of higher-level classification and survey of taxonomic richness. *Zootaxa*, *3148*(1), 104-109.

Atchley, W. R. (1993). Genetic and developmental aspects of variability in the mammalian mandible. *The skull*, 1, 207-247.

Auffray, J. C., Alibert, P., Renaud, S., Orth, A., and Bonhomme, F. (1996). Fluctuating asymmetry in *Mus musculus* subspecific hybridization. In *Advances in morphometrics* (pp. 275-283). Boston, MA: Springer.

Bapst, D. W., Wright, A. M., Matzke, N. J., and Lloyd, G. T. (2016). Topology, divergence dates, and macroevolutionary inferences vary between different tip-dating approaches applied to fossil theropods (Dinosauria). *Biology Letters, 12*(7), 20160237.

Baum, B. R. (1988). A simple procedure for establishing discrete characters from measurement data, applicable to cladistics. *Taxon*, 63-70.

Benton, M. J. (2000). Stems, nodes, crown clades, and rank-free lists: is Linnaeus dead?. *Biological Reviews, 75*(4), 633-648.

Benton, M. J. (2007). The Phylocode: Beating a dead horse?. *Acta Palaeontologica Polonica, 52*(3).

Bininda-Emonds, O. R., Gittleman, J. L., and Steel, M. A. (2002). The (super) tree of life: procedures, problems, and prospects. *Annual Review of Ecology and Systematics, 33*(1), 265-289.

Bookstein, F. L. (2015). Integration, disintegration, and self-similarity: characterizing the scales of shape variation in landmark data. *Evolutionary biology*, *42*(4), 395-426.

Bookstein, F. L., Gunz, P., Mitteroecker, P., Prossinger, H., Schaefer, K., and Seidler, H. (2003). Cranial integration in Homo: singular warps analysis of the midsagittal plane in ontogeny and evolution. *Journal of Human Evolution, 44*(2), 167-187.

Bouckaert, R., Heled, J., Kühnert, D., Vaughan, T., Wu, C-H., Xie, D., Suchard, MA., Rambaut, A., and Drummond, A. J. (2014). BEAST 2: A Software Platform for Bayesian Evolutionary Analysis. *PLoS Computational Biology, 10*(4), e1003537. doi:10.1371/journal.pcbi.1003537.

Breuker, C. J., Gibbs, M., Van Dyck, H., Brakefield, P. M., Klingenberg, C. P., and Van Dongen, S. (2007). Integration of wings and their eyespots in the speckled wood butterfly Pararge aegeria. *Journal of Experimental Zoology Part B: Molecular and Developmental Evolution, 308*(4), 454-463.

Brochu, C. A. (2003). Phylogenetic approaches toward crocodylian history. *Annual Review of Earth and Planetary Sciences, 31*(1), 357-397.

Brown, J. W., Parins-Fukuchi, C., Stull, G. W., Vargas, O. M., and Smith, S. A. (2017). Bayesian and likelihood phylogenetic reconstructions of morphological traits are not discordant when taking uncertainty into consideration: a comment on Puttick et al. *Proceedings of the Royal Society B: Biological Sciences, 284*(1864), 20170986.

Bürger, R. (1986). Constraints for the evolution of functionally coupled characters: a nonlinear analysis of a phenotypic model. *Evolution*, 40(1), 182-193.

Butler, R. J., Upchurch, P., and Norman, D. B. (2008). The phylogeny of the ornithischian dinosaurs. *Journal of Systematic Palaeontology, 6*(1), 1-40.

Carlson, S. J. (2001). Ghosts of the past, present, and future in brachiopod systematics. *Journal of Paleontology, 75*(6), 1109-1118.

Carlson, S. J., and Leighton, L. R. (2001). The phylogeny and classification of Rhynchonelliformea. *The Paleontological Society Papers, 7*, 27-52.

Chappill, J. A. (1989). Quantitative characters in phylogenetic analysis. *Cladistics, 5*(3), 217-234.

Cheverud, J. M. (1982). Phenotypic, genetic, and environmental morphological integration in the cranium. *Evolution*, *36*(3), 499-516.

Cheverud, J. M. (1996). Quantitative genetic analysis of cranial morphology in the cotton-top (*Saguinus oedipus*) and saddle-back (*S. fuscicollis*) tamarins. *Journal of Evolutionary Biology, 9*(1), 5-42.

Cohen, K. M., Finney, S. C., Gibbard, P. L., and Fan, J. X. (2013). The ICS international chronostratigraphic chart. *Episodes, 36*(3), 199-204.

Cotton, T. J., and Fortey, R. A. (2005). Comparative morphology and relationships of the Agnostida. In Koenemann, S. and Jenner, R.A. (Eds.), *Crustacea and Arthropod Relationships* (pp. 95-136). Boca Raton, FL: CRC Press.

Davidson, E. H., and Erwin, D. H. (2006). Gene regulatory networks and the evolution of animal body plans. *Science, 311*(5762), 796-800.

De Queiroz, K., and Gauthier, J. (1990). Phylogeny as a central principle in taxonomy: phylogenetic definitions of taxon names. *Systematic zoology, 39*(4), 307-322.

Drake, A. G., and Klingenberg, C. P. (2010). Large-scale diversification of skull shape in domestic dogs: disparity and modularity. *The American Naturalist, 175*(3), 289-301.

Edwards, D. (2008). MIM: A program for graphical modeling, version 3.2. 0.6. HyperGraph software. Retrieved from http://www.hypergraph.dk.

Escoufier, Y. (1973). Le traitement des variables vectorielles. *Biometrics*, *29*, 751–760.

Farris, J. S. (1969). On the cophenetic correlation coefficient. *Systematic Zoology*, *18*(3), 279-285.

Foote, M. (1993). Contributions of individual taxa to overall morphological disparity. *Paleobiology*, 19(4), 403-419.

Forey, P. L., Fortey, R. A., Kenrick, P., and Smith, A. B. (2004). Taxonomy and fossils: a critical appraisal. *Philosophical Transactions of the Royal Society of London. Series B: Biological Sciences, 359*(1444), 639-653.

Fortey, R. A., and Theron, J. N. (1994). A new Ordovician arthropod, Soomaspis, and the agnostid problem. *Palaeontology, 37*(4), 841-862.

Garcia-Cruz, J., and Sosa, V. (2006). Coding quantitative character data for phylogenetic analysis: a comparison of five methods. *Systematic Botany, 31*(2), 302-309.

Gavryushkina, A., Welch, D., Stadler, T., and Drummond, A. J. (2014). Bayesian inference of sampled ancestor trees for epidemiology and fossil calibration. *PLoS computational biology, 10*(12), E1003919.

Goloboff, P. A., and Catalano, S. A. (2016). TNT version 1.5, including a full implementation of phylogenetic morphometrics. *Cladistics, 32*(3), 221-238.

Goswami, A. (2006a). Cranial modularity shifts during mammalian evolution. *The American Naturalist*, *168*(2), 270-280.

Goswami, A. (2006b). Morphological integration in the carnivoran skull. *Evolution*, *60*(1), 169-183.

Goswami, A. (2007). Phylogeny, diet, and cranial integration in australodelphian marsupials. *PLoS One*, *2*(10), E995.

Goswami, A., and Polly, P. D. (2010a). Methods for studying morphological integration and modularity. *The Paleontological Society Papers, 16*, 213-243.

Goswami, A., and Polly, P. D. (2010b). The influence of modularity on cranial morphological disparity in Carnivora and Primates (Mammalia). *PloS One, 5*(3), e9517.

Goswami, A., Weisbecker, V., and Sánchez-Villagra, M. R. (2009). Developmental modularity and the marsupial–placental dichotomy. *Journal of Experimental Zoology Part B: Molecular and Developmental Evolution, 312*(3), 186-195.

Gould, S. J. (1989). A developmental constraint in Cerion, with comments on the definition and interpretation of constraint in evolution. *Evolution, 43*, 516–539.

Gould, S. J. (2002). *The Structure of Evolutionary Theory*. Cambridge, MA: Harvard University Press.

Gradstein, F. M., Ogg, J. G., Schmitz, M., and Ogg, G. (Eds.). (2012). *The geologic time scale 2012*. Boston, MA: Elsevier.

Graham, J.H., Raz, S., Hel-Or, H. and Nevo, E., (2010). Fluctuating asymmetry: methods, theory, and applications. *Symmetry, 2*(2), 466-540.

Hallgrímsson, B., Lieberman, D. E., Liu, W., Ford-Hutchinson, A. F., and Jirik, F. R. (2007). Epigenetic interactions and the structure of phenotypic variation in the cranium. *Evolution and development, 9*(1), 76-91.

Hallgrímsson, B., Willmore, K., Dorval, C., and Cooper, D. M. (2004). Craniofacial variability and modularity in macaques and mice. *Journal of Experimental Zoology Part B: Molecular and Developmental Evolution, 302*(3), 207-225.

Harris, J. E., and Mason, P. (1956). Vertical migration in eyeless Daphnia. *Proceedings of the Royal Society of London. Series B-Biological Sciences, 145*(919), 280-290.

Hawle, I., and Corda, A. J. (1847). *Prodrom einer Monographie der böhmischen Trilobiten*. JG Calve.

Heath, T. A., Huelsenbeck, J. P., and Stadler, T. (2014). The fossilized birth–death process for coherent calibration of divergence-time estimates. *Proceedings of the National Academy of Sciences, 111*(29), E2957-E2966.

Holtz, T. R. (1996). Phylogenetic taxonomy of the Coelurosauria (Dinosauria: Theropoda). *Journal of Paleontology, 70*(3), 536-538.

Holtz, T. R. (2000). A new phylogeny of the carnivorous dinosaurs. *Gaia*, 15, 5-61.

Hopkins, M. J., and Webster, M. (2009). Ontogeny and geographic variation of a new species of the corynexochine trilobite Zacanthopsis (Dyeran, Cambrian). *Journal of Paleontology*, *83*(4), 524-547.

Howell, B. F. (1935). New Middle Cambrian agnostian trilobites from Vermont. *Journal of Paleontology*, 218-221.

Howell, B. F. (1937). Cambrian Centropleura vermontensis fauna of northwestern Vermont. *Bulletin of the Geological Society of America, 48*(8), 1147-1210.

Hughes, N. C. (2003). Trilobite tagmosis and body patterning from morphological and developmental perspectives. *Integrative and Comparative Biology*, *43*(1), 185-206.

Hunt, G. (2007). Evolutionary divergence in directions of high phenotypic variance in the ostracode genus Poseidonamicus. *Evolution: International Journal of Organic Evolution*, *61*(7), 1560-1576.

Ivanović, A., and Kalezić, M. L. (2010). Testing the hypothesis of morphological integration on a skull of a vertebrate with a biphasic life cycle: a case study of the alpine newt. *Journal of Experimental Zoology Part B: Molecular and Developmental Evolution, 314*(7), 527-538.

Jaekel, O. (1909). Über die Agnostiden. *Zeitschrift der deutschen geologischen Gesellschaft*, 380-401.

Jamniczky, H. A., and Hallgrímsson, B. (2011). Modularity in the skull and cranial vasculature of laboratory mice: implications for the evolution of complex phenotypes. *Evolution and development, 13*(1), 28-37.

Jell, P. A. (1997). Introduction to suborder Eodiscina. In Moore, R.C. and Kaesler (Eds.) *Treatise on Invertebrate Paleontology, Part O, Arthropoda* (pp. 384-404). Lawrence, KS: The University of Kansas.

Jojić, V., Blagojević, J., and Vujošević, M. (2011). B chromosomes and cranial variability in yellow-necked field mice (Apodemus flavicollis). *Journal of Mammalogy, 92*(2), 396-406.

Jojić, V., Blagojević, J., and Vujošević, M. (2012). Two-module organization of the mandible in the yellow-necked mouse: a comparison between two different morphometric approaches. *Journal of Evolutionary Biology, 25*(12), 2489-2500.

Jukes, T. H., and Cantor, C. R. (1969). Evolution of protein molecules. *Mammalian protein metabolism, 3*(21), 132.

Kass, R. E., and Raftery, A. E. (1995). Bayes factors. *Journal of the American Statistical Association, 90*(430), 773-795.

Kaufman, L., and Rousseeuw, P. J. (2009). *Finding groups in data: an introduction to cluster analysis*. Hoboken, NJ: Wiley Publishing.

Kimmig, J. and Pratt, B.R. 2018. Coprolites in the Ravens Throat River Lagerstätte of northwestern Canada: Implications for the middle Cambrian food web. *PALAIOS, 33*, 125–140

Kimmig, J., Strotz, L. C., Kimmig, S. R., Egenhoff, S. O., and Lieberman, B. S. (2019). The Spence Shale Lagerstätte: an important window into Cambrian biodiversity. *Journal of the Geological Society, 176*(4), 609-619.

Klingenberg, C. P. (2009). Morphometric integration and modularity in configurations of landmarks: tools for evaluating a priori hypotheses. *Evolution and development, 11*(4), 405-421.

Klingenberg, C. P. (2011). MorphoJ: an integrated software package for geometric morphometrics. *Molecular ecology resources*, *11*(2), 353-357.

Klingenberg, C. P. (2004). Integration, modules, and development: molecules to morphology to evolution. In M. Pigliucci and K. A. Preston (Eds.), *Phenotypic Integration: Studying the Ecology and Evolution of Complex Phenotypes*. (pp. 213-230), Oxford, England: Oxford University Press.

Klingenberg, C. P. 2005. Developmental constraints, modules, and evolvability. In B.Hallgrímsson, and Hall, B.K. (Eds.), *Variation: A Central Concept in Biology*. (pp. 219-247). Burlington, MA: Elsevier Academic Press.

Klingenberg, C. P., A. V. Badyaev, S. M. Sowry, and N. J. Beckwith. 2001. Inferring developmental modularity from morphological integration: Analysis of individual variation and asymmetry in bumblebee wings. *American Naturalist, 157* (1): 11-23.

Klingenberg, C. P., and McIntyre, G. S. (1998). Geometric morphometrics of developmental instability: analyzing patterns of fluctuating asymmetry with Procrustes methods. *Evolution, 52*(5), 1363-1375.

Klingenberg, C. P., and S. D. Zaklan. 2000. Morphological integration between developmental compartments in the Drosophila wing. *Evolution 54*(4): 1273- 1285.

Klingenberg, C. P., Debat, V., and Roff, D. A. (2010). Quantitative genetics of shape in cricket wings: developmental integration in a functional structure. *Evolution: International Journal of Organic Evolution, 64*(10), 2935-2951.

Klingenberg, C. P., K. Mebus, and J.-C. Auffray. 2003. Developmental integration in a complex morphological structure: how distinct are the modules in the mouse mandible? *Evolution and Development, 5*(5): 522-531.

Kobayashi, T. (1939). On the agnostids (Part 1). *Journal of the Faculty of Science, Imperial University of Tokyo, Section II, 5*(5), 69-198.

Laffont, R., Renvoisé, E., Navarro, N., Alibert, P., and Montuire, S. (2009). Morphological modularity and assessment of developmental processes within the vole dental row (Microtus arvalis, Arvicolinae, Rodentia). *Evolution and development, 11*(3), 302-311.

Laurie, J.R. (2008), Species relationships in the Ptychagnostidae (Cambrian, Agnostina), In Rábano, I., Gozalo, R., and García-Bellido, D. (Eds.) *Publicaciones del Instituto Geologico y Minero de Espana No. 9: Advances in trilobite research*. (pp.211-218), Madrid: Instituto Geológico y Minero de España.

Lawler, R. R. (2008). Morphological integration and natural selection in the postcranium of wild Verreaux's sifaka (Propithecus verreauxi verreauxi). *American Journal of Physical Anthropology: The Official Publication of the American Association of Physical Anthropologists*, *136*(2), 204-213.

Leamy, L., (1984). Morphometric studies in inbred and hybrid house mice. V. Directional and fluctuating asymmetry. *The American Naturalist, 123*(5), 579-593.

Lee, M. S., and Palci, A. (2015). Morphological phylogenetics in the genomic age. *Current Biology, 25*(19), R922-R929.

Legg, D. A., Sutton, M. D., and Edgecombe, G. D. (2013). Arthropod fossil data increase congruence of morphological and molecular phylogenies. *Nature communications, 4*, 2485.

Lewis, P. O. (2001). A likelihood approach to estimating phylogeny from discrete morphological character data. *Systematic biology, 50*(6), 913-925.

M'Coy, F. (1849). XLI.—On the classification of some British fossil Crustacea, with notices of new forms in the University Collection at Cambridge. *Annals and Magazine of Natural History, 4*(24), 392-414.

Maechler, M., Rousseeuw, P., Struyf, A., Hubert, M., Hornik, K.(2018). cluster: Cluster Analysis Basics and Extensions. R package version 2.0.7-1. Retrieved from https://cran.r-project.org/web/packages/cluster/index.html.

Magwene, P. M. (2001). New tools for studying integration and modularity. *Evolution*, *55*(9), 1734-1745.

Magwene, P. M. (2008). Using correlation proximity graphs to study phenotypic integration. *Evolutionary Biology*, *35*(3), 191-198.

Magwene, P. M. (2009). Statistical methods for studying modularity: a reply to Mitteroecker and Bookstein. *Systematic biology*, *58*(1), 146-149.

Makarenkov, V. (2001). T-REX: reconstructing and visualizing phylogenetic trees and reticulation networks. *Bioinformatics*, *17*(7), 664-668.

Makarenkov, V., and Legendre, P. (2004). From a phylogenetic tree to a reticulated network. Journal of Computational Biology, 11(1), 195-212.

Makarenkov, V., Legendre, P., and Desdevises, Y. (2004). Modelling phylogenetic relationships using reticulated networks. *Zoologica scripta, 33*(1), 89-96.

Marquez, E. (2007a). SAGE, version 1.21. Retrieved from http://www-personal.umich.edu/~emarquez/morph/.

Marquez, E. (2007b). CORIANDIS version 1.12. Retrieved from http://www-personal.umich.edu/~emarquez/morph/.

Marroig, G., and Cheverud, J. M. (2005). Size as a line of least evolutionary resistance: diet and adaptive morphological radiation in New World monkeys. *Evolution, 59*(5), 1128-1142.

Mayr, E. (1982). *The Growth of Biological Thought: Diversity, Evolution, and Inheritance*. Cambridge, MA: Harvard University Press.

Mitteroecker, P., and Bookstein, F. (2007). The conceptual and statistical relationship between modularity and morphological integration. *Systematic biology, 56*(5), 818-836.

Møller, A. P., and Swaddle, J. P. (1997). *Asymmetry, Developmental Stability, and Evolution*. Oxford, England: Oxford University Press.

Monteiro, L. R., Bonato, V., and Dos Reis, S. F. (2005). Evolutionary integration and morphological diversification in complex morphological structures: mandible shape divergence in spiny rats (Rodentia, Echimyidae). *Evolution and development, 7*(5), 429-439.

Moore, R. C. (1959). *Treatise on Invertebrate Paleontology, Part O, Arthropoda*. Boulder, CO: The Geological Society of America.

Moysiuk, J., and Caron, J. B. (2019). Burgess Shale fossils shed light on the agnostid problem. *Proceedings of the Royal Society B, 286*(1894), 20182314.

Müller, K. J. and Walossek, D. (1987). Morphology, ontogeny and life habit of Agnostus pisiformis from the Upper Cambrian of Sweden. *Fossils and Strata, 19*, 1-124.

Muñoz-Muñoz, F., Carreira, V. P., Martínez-Abadías, N., Ortiz, V., González-José, R., and Soto, I. M. (2016). Drosophila wing modularity revisited through a quantitative genetic approach. *Evolution, 70*(7), 1530-1541.

Naimark, E. B. (2006). Growth and development of agnostids Pentagnostus proanabarensis Fedoseev, 1999. *Paleontological Journal, 40*(5), 541-552.

Naimark, E. B. (2007). Comparative ontogeny of different species of agnostina. *Paleontological Journal, 41*(1), 69-78.

Naimark, E. B. (2008). Morphogenesis in the genus Peronopsis Hawle et Corda (Agnostina). *Paleontological Journal, 42*(4), 389.

Naimark, E. B. (2012). Hundred species of the genus Peronopsis Hawle et Corda, 1847. *Paleontological Journal, 46*(9), 945-1057.

Naimark, E. B. (2014). Revision of Eurudagnostus Lermontova (Agnostida,? Trilobita). *Paleontological Journal, 48*(2), 166-176.

Naimark, E. B., and Pegel, T. V. (2017). Revision of the Cambrian Agnostina (Trilobita?) from Russia. *Paleontological Journal, 51*(11), 1167-1248.

O'Reilly, J. E., Puttick, M. N., Parry, L., Tanner, A. R., Tarver, J. E., Fleming, J., Pisani, D., and Donoghue, P. C. (2016). Bayesian methods outperform parsimony but at the expense of precision in the estimation of phylogeny from discrete morphological data. *Biology Letters, 12*(4), 20160081.

Oksanen, J., Blanchet, F.G., Kindt, R., Legendre, P., O'hara, R.B., Simpson, G.L., Solymos, P., Stevens, M.H.H. and Wagner, H. (2019). Vegan: community ecology package. R package version 2.5-6. Retrieved from https://cran.r-project.org/web/packages/vegan/index.html.

Olson, E. C. and Miller, R. L. (1958). *Morphological Integration*. Chicago, IL: University of Chicago Press.

Öpik, A. A. (1961). The geology and palaeontology of the headwaters of the Burke River, Queensland. *Bureau of Mineral Resources, Bulletin, 53.*

Öpik, A. A. (1963). Early upper Cambrian fossils from Queensland. *Bureau of Mineral Resources, Bulletin 64.*

Öpik, A. A. (1967). The Mindyallan fauna of north-western Queensland. *Bureau of Mineral Resources, Bulletin, 74*.

Öpik, A. A. (1975). Cymbric Vale fauna of New South Wales and Early Cambrian biostratigraphy. *Bureau of Mineral Resources, Bulletin, 159.*

Öpik, A. A. (1979). Middle Cambrian agnostids: systematics and biostratigraphy. *Bureau of Mineral Resources, Bulletin 172(1).*

Padian, K., Hutchinson, J. R., and Holtz, T. R. (1999). Phylogenetic definitions and nomenclature of the major taxonomic categories of the carnivorous Dinosauria (Theropoda). *Journal of Vertebrate Paleontology, 19*(1), 69-80.

Pagel, M. (1994). Detecting correlated evolution on phylogenies: a general method for the comparative analysis of discrete characters. *Proceedings of the Royal Society of London. Series B: Biological Sciences, 255*(1342), 37-45.

Palmer, A. R. (1955). Upper Cambrian Agnostidae of the Eureka District, Nevada. Journal of Paleontology, 86-101.

Palmer, A. R. (1994). Fluctuating asymmetry analyses: a primer. In Markow, T.A. (Ed.) *Developmental instability: its origins and evolutionary implications* (pp. 335-364). Boston, MA: Springer.

Palmer, A. R., and Strobeck, C. (2003). Fluctuating asymmetry analyses revisited. In Polak, M. (ed.), *Developmental) Instability: Causes and Consequences.* (pp. 279-319) Oxford, England: Oxford University Press.

Paterson, J. R., and Edgecombe, G. D. (2006). The Early Cambrian trilobite family Emuellidae Pocock, 1970: systematic position and revision of Australian species. Journal of Paleontology, 80(3), 496-513.

Peng, S., and Robison, R. A. (2000). Agnostoid biostratigraphy across the Middle–Upper Cambrian boundary in Hunan, China. Journal of Paleontology, 74(sp53), 1-105.

Plotnick, R. E., and Wagner, P. J. (2006). Round up the usual suspects: common genera in the fossil record and the nature of wastebasket taxa. Paleobiology, 32(1), 126-146.

Pratt, B. R. (1992). Trilobites of the Marjuman and Steptoean stages (Upper Cambrian), Rabitkettle Formation, southern Mackenzie Mountains, northwest Canada. Paleontographica Canadiana, 9, 179 p.

Puttick, M. N., O'Reilly, J. E., Tanner, A. R., Fleming, J. F., Clark, J., Holloway, L., Lozano-Fernandez, J., Parry, L.A., Tarver, J. E., Pisani, D., and Donoghue, P. C. (2017). Uncertain-tree: discriminating among competing approaches to the phylogenetic analysis of phenotype data. Proceedings of the Royal Society B: Biological Sciences, 284(1846), 20162290.

Pyron, R. A. (2011). Divergence time estimation using fossils as terminal taxa and the origins of Lissamphibia. *Systematic Biology, 60*(4), 466-481.

Rae, T. C. (1998). The logical basis for the use of continuous characters in phylogenetic systematics. *Cladistics, 14*(3), 221-228.

Rambaut, A., and Drummond, A. J. (2018). TreeAnnotator v2.5.2. Institute of Evolutionary Biology, University of Edinburgh. Retrieved from https://beast.community/treeannotator.

Rambaut, A., Suchard, M. A., Xie, D., and Drummond, A. J. (2014). Tracer 1.6. Retrieved from http://tree.bio.ed.ac.uk/software/tracer/.

Rasetti, F. (1945). New Upper Cambrian trilobites from the Lévis conglomerate. *Journal of Paleontology*, 462-478.

Rasetti, F. (1948). Middle Cambrian trilobites from the conglomerates of Quebec (exclusive of the Ptychopariidea). *Journal of Paleontology*, 315-339.

Rasetti, F. (1952). Revision of the North American trilobites of the family Eodiscidae. *Journal of Paleontology*, 434-451.

Raymond, P. E. (1913). Some changes in the names of genera of trilobites. *Ottawa Naturalist, 26*(11), 137-142.

Rego, C., Matos, M., and Santos, M. (2006). Symmetry breaking in interspecific Drosophila hybrids is not due to developmental noise. *Evolution, 60*(4), 746-761.

Renaud, S., Auffray, J. C., and Michaux, J. (2006). Conserved phenotypic variation patterns, evolution along lines of least resistance, and departure due to selection in fossil rodents. *Evolution, 60*(8), 1701-1717.

Revell, L. J. (2012). phytools: an R package for phylogenetic comparative biology (and other things). *Methods in Ecology and Evolution*, *3*(2), 217-223.

Robison, R. A. (1964). Upper middle Cambrian stratigraphy of western Utah. *Geological Society of America Bulletin*, *75*(10), 995-1010.

Robison, R. A. (1984). Cambrian Agnostida of North America and Greenland, Part I, Ptychagnostidae. *The University of Kansas Paleontological Contributions, 109*.

Robison, R.A., Babcock, L.E. and Gunther, V.G. 2015. Exceptional Cambrian Fossils from Utah: A window into the age of trilobites. *Utah Geological Survey, Miscellaneous Publications, 15.*

Rohlf, F. J. (2017). tpsDIG2 2.30. Retrieved from https://life.bio.sunysb.edu/morph/soft-dataacq.html.

Ronquist, F., Klopfstein, S., Vilhelmsen, L., Schulmeister, S., Murray, D. L., and Rasnitsyn, A. P. (2012). A total-evidence approach to dating with fossils, applied to the early radiation of the Hymenoptera. *Systematic Biology, 61*(6), 973-999.

Rozova, A. V. (1960). Upper Cambrian trilobites of Salair. *Trudy Instituta geologii i geofiziki, Sibirskoe otdelenie, 5*, 1-116.

Rushton, A.W.A. (1966). The Cambrian trilobites from the Purley Shales of Warwickshire. *Palaeontographical Society Monographs, 120*.

Salter, J. W. (1864). On some new fossils from the Lingula-flags of Wales. *Quarterly Journal of the Geological Society, 20*(1-2), 233-241.

Schluter, D. (1996). Adaptive radiation along genetic lines of least resistance. *Evolution, 50*(5), 1766-1774.

Sereno, P. C. (1997). The origin and evolution of dinosaurs. *Annual Review of Earth and Planetary Sciences, 25*(1), 435-489.

Sereno, P. C., McAllister, S., and Brusatte, S. L. (2005). TaxonSearch: a relational database for suprageneric taxa and phylogenetic definitions. *PhyloInformatics, 8*(56), 1-25.

Shaw, A. B. (1957). Quantitative trilobite studies II. Measurement of the dorsal shell of non-agnostidean trilobites. *Journal of Paleontology*, *31*(1), 193-207.

Sheets, H.D. (2014) Integrated Morphometrics Package (IMP) 8. Available at http://www.philadb.com/an-behav/imp/.

Shergold, J. H. (1975). Late Cambrian and early Ordovician trilobites from the Burke River structural belt, western Queensland, Australia. *Bureau of Mineral Resources, Bulletin, 153*.

Shergold, J. H. (1977). Classification of the trilobite Pseudagnostus. *Palaeontology, 20*(1), 69-100.

Shergold, J. H., and Laurie, J. R. (1997). Suborder Agnostina Salter, 1864. In Moore, R.C. and Kaesler (Eds.) *Treatise on Invertebrate Paleontology, Part O, Arthropoda.* (pp. 331-383). Lawrence, KS: The University of Kansas.

Shergold, J. H., Laurie, J. R., and Sun, X. (1990). Classification and Review of the Trilobite Order, Agnostida Salter, 1864: An Australian Perspective. *Bureau of Mineral Resources, Bulletin, 296.*

Shergold, J.H. (1991). Protaspis and early meraspis growth stages of the eodiscoid trilobite Pagetia ocellata Jell, and their implications for classification. *Alcheringa, 15*, 65-86.

Slater, G. J. (2013). Phylogenetic evidence for a shift in the mode of mammalian body size evolution at the Cretaceous-Palaeogene boundary. *Methods in Ecology and Evolution, 4*(8), 734-744.

Slater, G. J. (2015). Iterative adaptive radiations of fossil canids show no evidence for diversity-dependent trait evolution. *Proceedings of the National Academy of Sciences, 112*(16), 4897-4902.

Smith, A. B. (1984). Classification of the Echinodermata. *Palaeontology, 27*(3), 431-459.

Smith, A. W., and Stewart Thomson, K. (1994). Systematics and the fossil record: documenting evolutionary patterns. *Nature, 372*(6505), 419-420.

Smith, D. D. (2007). Sequence stratigraphy of the middle Cambrian Marjum Formation: response of sedimentary facies and biota to sea-level changes. (Order No. 1454869,

Utah State University). ProQuest Dissertations and Theses, 156. Retrieved from https://search-proquest-com.proxy.uchicago.edu/docview/304805125?accountid=14657.

Sneath, P. H., and Sokal, R. R. (1973). *Numerical taxonomy. The principles and practice of numerical classification*. New York, NY: W.H. Freeman and Company.

Stadler, T. (2010). Sampling-through-time in birth–death trees. *Journal of Theoretical Biology, 267*(3), 396-404.

Stevens, P. F. (1991). Character states, morphological variation, and phylogenetic analysis: a review. *Systematic botany*, 553-583.

Strait, D. S., Moniz, M. A., and Strait, P. T. (1996). Finite mixture coding: a new approach to coding continuous characters. *Systematic Biology, 45*(1), 67-78.

Streissguth, A. P., Bookstein, F. L., Sampson, P. D., and Barr, H. M. (1993). *The enduring effects of prenatal alcohol exposure on child development: Birth through seven years, a partial least squares solution*. Ann Arbor, MI: The University of Michigan Press.

Strong, E. E., and Lipscomb, D. (1999). Character coding and inapplicable data. *Cladistics, 15*(4), 363-371.

Sundberg, F. A. (2000). Homeotic evolution in Cambrian trilobites. *Paleobiology*, *26*(2), 258-270.

Swafford, D. L. (2002). PAUP*. Phylogenetic analysis using parsimony (* and other models). Version 4.0 b10 for Macintosh. Sunderland, MA: Sinauer Associates Inc. Retrieved from https://paup.phylosolutions.com/

Thiele, K. (1993). The holy grail of the perfect character: the cladistic treatment of morphometric data. *Cladistics, 9*(3), 275-304.

Troedsson, G. T. (1937). On the Cambro-Ordovician faunas of western Quruq tagh, eastern T'ien-shan. *Palaeontologica Sinica, 106*.

Valentine, J. W. (1995). Why no new phyla after the Cambrian? Genome and ecospace hypotheses revisited. *Palaios*, 190-194.

Valen, L. V. (1962). A study of fluctuating asymmetry. *Evolution,* 16(2), 125-142.

Wagner, G. P., and Altenberg, L. 1996. Complex adaptations and the evolution of evolvability. *Evolution, 50,* 967–976

Wagner, G. P., and Laubichler, M. D. (2004). Rupert Riedl and the re-synthesis of evolutionary and developmental biology: body plans and evolvability. *Journal of*

Experimental Zoology Part B: Molecular and Developmental Evolution, 302(1), 92-102.

Wagner, P. J. (1999). The utility of fossil data in phylogenetic analyses: a likelihood example using Ordovician-Silurian species of the Lophospiridae (Gastropoda: Murchisoniina). *American Malacological Bulletin, 15*(1), 1-31.

Walch, J. E. I. (1771). Die Naturgeschichte der Versteinerungen: zur Erläuterung der Knorrischen Sammlung von Merkwürdigkeiten der Natur. *Dritter Theil*, *3*.

Ward Jr, J. H. (1963). Hierarchical grouping to optimize an objective function. *Journal of the American statistical association*, *58*(301), 236-244.

Webster, M. (2007). A Cambrian peak in morphological variation within trilobite species. *Science*, *317*(5837), 499-502.

Webster, M., and M. L. Zelditch. 2011. Evolutionary lability of integration in Cambrian ptychoparioid trilobites. *Evolutionary Biology, 38,* 144-162.

Webster, M., and M. L. Zelditch. 2011. Modularity of a Cambrian ptychoparioid trilobite cranidium. *Evolution and Development 13*(1): 96-109.

Westergård, A. H. (1936). Paradoxides oelandicus beds of Oland. *Sveriges Geologiska Undersokning, Serie C, 394*, 1-66.

Westrop, S. R., Ludvigsen, R., and Kindle, C. H. (1996). Marjuman (Cambrian) agnostoid trilobites of the Cow Head Group, western Newfoundland. *Journal of Paleontology, 70*(5), 804-829.

Whitehouse, F. W. (1936). The Cambrian faunas of northeastern Australia. Parts 1 and 2. *Memoirs of the Queensland Museum, 11*(1), 59-112.

Whittaker, J. (2009). *Graphical models in applied multivariate statistics*. Hoboken, NJ: Wiley Publishing.

Wright, A. M., and Hillis, D. M. (2014). Bayesian analysis using a simple likelihood model outperforms parsimony for estimation of phylogeny from discrete morphological data. *PLoS One, 9*(10), e109210.

Wright, D. F. (2017). Bayesian estimation of fossil phylogenies and the evolution of early to middle Paleozoic crinoids (Echinodermata). *Journal of Paleontology, 91*(4), 799-814.

Wright, D. F., and Stigall, A. L. (2013). Geologic drivers of Late Ordovician faunal change in Laurentia: investigating links between tectonics, speciation, and biotic invasions. *PLoS One, 8*(7), e68353.

Wright, D. F., Ausich, W. I., Cole, S. R., Peter, M. E., and Rhenberg, E. C. (2017). Phylogenetic taxonomy and classification of the Crinoidea (Echinodermata). *Journal of Paleontology, 91*(4), 829-846.

Young, R. L., and Badyaev, A. V. (2006). Evolutionary persistence of phenotypic integration: influence of developmental and functional relationships on complex trait evolution. *Evolution, 60*(6), 1291-1299.

Zelditch, M. L., Swiderski, D. L., Sheets, H. D., and Fink, W. L. (2004). *Geometric morphometrics for biologists: a primer.* Burlington, MA: Elsevier Academic Press.

Zelditch, M. L., Wood, A. R., and Swiderski, D. L. (2009). Building developmental integration into functional systems: function-induced integration of mandibular shape. *Evolutionary Biology, 36*(1), 71-87.

Zelditch, M. L., Wood, A. R., Bonett, R. M., and Swiderski, D. L. (2008). Modularity of the rodent mandible: integrating bones, muscles, and teeth. *Evolution and development, 10*(6), 756-768.

Zhou, Z. and Zhen, Y. (2008), *Trilobite record of China.* Beijing, China: Science Press.